

DEPARTMENT OF PHYSICS AND ASTRONOMY "A. RIGHI"

SECOND CYCLE DEGREE

PHYSICS

DEVELOPMENT OF ERANOS MODULES FOR THE SENSITIVITY ANALYSIS OF THE EFFECTIVE DELAYED NEUTRON FRACTION BEYOND CROSS SECTIONS

Supervisor

Prof. Paolo Finelli

Defended by Luca Damele

Co-supervisor
Donato Maurizio Castelluccio, PhD

Co-supervisor

Ing. Matteo Stanzani



Abstract

The current global energy landscape demands a fundamental reassessment of the primary sources sustaining modern societies. While the imperative of deep decarbonization has elevated the role of renewable energy, their inherent intermittency necessitates reliable, low-emission alternatives capable of ensuring system stability and continuity. Within this framework, nuclear power emerges as a key component, offering firm capacity that enhances both grid resilience and energy security.

The structural limitations of existing nuclear technologies have prompted the advancement of Generation IV reactors, which aim to enhance sustainability, reduce waste, and improve flexibility. Among these, Lead-cooled Fast Reactors (LFRs) stand out for their inherent safety features, high thermal efficiency, and compatibility with closed fuel cycles. In Europe, ENEA is leading the development of ALFRED, the reference demonstrator for LFR technology.

As a Generation IV system, ALFRED integrates technological innovation with an advanced safety philosophy, requiring robust tools to assess the impact of physical and modeling uncertainties on key neutronic parameters.

Sensitivity analysis is essential for both understanding core neutronics and optimizing design safety margins. By quantifying how input parameters affect key outputs, it highlights the components requiring tighter control to ensure stable reactor behavior. It also lays the groundwork for uncertainty analysis, which assesses the impact of data uncertainties on integral quantities and informs regulatory decisions during reactor licensing.

In this framework, the present thesis contributed to the neutronic design activities for ALFRED by extending the ERANOS code system with new computational modules for the sensitivity analysis of the effective delayed neutron fraction, $\hat{\beta}_{\rm eff}$, with respect to nuclear data other than cross sections.

The methodology is based on Generalized Perturbation Theory (GPT), and enables the evaluation of sensitivity coefficients $S(\hat{\beta}_{\mathrm{eff}},\alpha)$, where α represents a generic nuclear parameter. Specifically, the study addressed sensitivities with respect to the average number of delayed and prompt neutrons per fission (ν^{d} , ν^{p}), as well as delayed and prompt fission spectra (χ^{d} , χ^{p}). All new expressions were derived from first principles and implemented by leveraging validated ERANOS functionalities, ensuring internal consistency and preserving the integrity of the existing code framework.

A progressive numerical verification strategy was adopted, starting from an analytically solvable minimal configuration and culminating in a simplified ALFRED-inspired Toy Model featuring a finite cylindrical geometry subdivided into two zones with different fuel compositions.

Verification focused primarily on $\nu^{\rm d}$, chosen for its practical advantages and physical relevance. For this parameter, GPT-based sensitivity coefficients were benchmarked

against reference values obtained via a Direct Perturbation (DP) method. The results demonstrated strong consistency, with relative discrepancies in the total sensitivities remaining below 0.2% across all isotopes and precursor families, confirming the reliability of the GPT-based implementation.

Verification for the remaining parameters (ν^p , χ^d , χ^p) was conducted using progressively complex, simplified models, enabling a controlled assessment of the methodology without compromising validation fidelity.

Overall, the tools produced in this thesis establish a robust foundation for advanced sensitivity and uncertainty analyses of $\hat{\beta}_{\rm eff}$ in realistic reactor models, directly supporting the safety-oriented design and licensing objectives of the ALFRED project.

Contents

Αb	stract		i
Lis	t of Fi	gures	vii
Lis	t of Ta	ables	viii
1	Ener	getic and Technological Context	1
	1.1	Global Energy Scenario	1
		1.1.1 Nuclear Power and Energy Transition	4
	1.2	The Generation IV International Forum (GIF) Initiative	7
		1.2.1 Technological Evolution of Nuclear Reactors	9
		1.2.2 IV Generation: Advanced Reactors	11
	1.3	The European LFR Technology Demonstrator: ALFRED	13
		1.3.1 ALFRED's core	15
		1.3.2 Safety Margins for ALFRED	16
	1.4	Thesis Motivation and Goals	17
2	Thec	oretical Background	20
	2.1	Overview of Nuclear Data and Integral Parameters	20
	2.2	Derivation of Neutron Fluxes from the Boltzmann Transport Equation .	21
	2.3	Role of Delayed Neutrons in Reactor Dynamics	25
	2.4	The Effective Delayed Neutron Fraction $\hat{oldsymbol{eta}}_{ ext{eff}}$	28
		2.4.1 Physical Interpretation of the Delayed Neutron Fraction \hat{eta}_{eff}	28
		2.4.2 Sensitivity Analysis of $\hat{eta}_{ ext{eff}}$	30
	2.5	The Generalized Perturbation Theory	31
		2.5.1 First Order Formulation of the GPT using the Variational Approach	
		2.5.2 GPT application on $\hat{oldsymbol{eta}}_{ ext{eff}}$	35
3	ERAI	NOS: Computational Framework and Implementation Details	38
	3.1	Computational Paradigms in Neutron Transport: Deterministic and Monte	
		Carlo Approaches	38
	3.2	General Architecture and Functional Overview of ERANOS	40
		3.2.1 Computational Workflow and Multi-Level Structure of ERANOS	40
	3.3	The ECCO Cell Code	42
		3.3.1 ECCO-ERANOS Interface	44
	3.4	Neutronic Data Analysis Modules	45
		3.4.1 Module for the Calculation of MACRO EDLs	45
		3.4.2 Modules for the Evaluation of Source Distributions	46

		3.4.3 3.4.4 3.4.5	Module for the Evaluation of Flux Distributions Modules for the Calculation of Integral Quantities	48 51
			tion $\hat{oldsymbol{eta}}_{ ext{eff}}$	53
4		nodolog	ical Framework for the Delayed Neutrons Fraction Sensitivity Anal	
	ysis			55
	4.1		cal Derivation of the Sensitivity Coefficients	55
		4.1.1	Sensitivity Coefficients of the Effective Delayed Neutron Frac-	59
		4.1.2	tion $\hat{eta}_{ m eff,n}$ to the Delayed Neutrons Yield $ u_{ m in}^{ m d}$ Sensitivity Coefficients of the Effective Delayed Neutron Frac-	37
		4.1.2	tion $\hat{eta}_{ m eff,n}$ to the Prompt Neutron Yields $ u^{ m p}_{ m igz}$	65
		4.1.3	Sensitivity Coefficients of the Effective Delayed Neutron Frac-	03
			tion $\hat{eta}_{ m eff,n}$ to the Delayed Neutrons Emission Spectrum $\chi_{ m ng}^{ m d}$	68
		4.1.4	Sensitivity Coefficients of the Effective Delayed Neutron Frac-	
			tion $\hat{eta}_{ m eff,n}$ to the Prompt Neutrons Emission Spectrum $\chi^{ m p}_{ m igz}$	72
	4.2	Implem	nentation of the Quantities Entering Sensitivity Coefficient Ex-	
		pressio		76
		4.2.1	Implementation of Procedures for Sensitivity Coefficient Calcu-	
		4.0.0	lation Using the GPT Approach	84
		4.2.2	Implementation of Procedures for Sensitivity Coefficient Calculation Using the Direct Perturbation (DP) Approach	93
			ration using the direct Perturbation (DP) Approach	93
5	Preli	minary I	Results from the Implemented Sensitivity Analysis Modules	99
	5.1	-	ation with a Minimal Core Configuration and Comparison with	
		Analyti	cal Benchmarks	100
	5.2	Verifica	ation of Sensitivity Modules by GPT and DP Approaches Using a	
		•	ied Core Model	103
		5.2.1	Computational Testbed for the Newly Developed Sensitivity Anal-	
		500	,	103
		5.2.2	Analysis of Sensitivity Results on the Simplified Core Model	106
6	Conc	lusions	and Perspectives	111
	6.1	Conclu	sions	111
	6.2	Perspe	ctives	115
Ac	knowl	ledgeme	ent	119
Аp	pendi	x		120
Α	Neut	ron Flu	x Evaluation with the Discrete Ordinates Method: The BISTRO	
^	Solve			120
	20170		V	

В	ERANOS Implementation of the ALFRED Core for Sensitivity and Uncertainty	,
	Studies	124
Re	eferences	127

List of Figures

1	Historical trends and future projections of total energy and electricity	
	demand	3
2	Global low-emissions electricity generation by source in 2023	5
3	Nuclear power capacity under construction (December 2024)	6
4	Schematic cross-sectional view of the ALFRED reactor core layout	15
5	Graphical representation of the concept of safety margin	18
6	Diagram of the general computational scheme of ERANOS	43
7	Diagram summarizing the terms contributing to the calculation of the	
	sensitivity coefficient $S(\hat{eta}_{ ext{eff},n}, u^{ ext{d}}_{ ext{i'n'}})$ as implemented in ERANOS	87
8	Diagram summarizing the terms contributing to the calculation of the	
	sensitivity coefficient $S(\hat{eta}_{ ext{eff},n}, u^{ ext{p}}_{ ext{i'g'z'}})$ as implemented in ERANOS	90
9	Diagram summarizing the terms contributing to the calculation of the	
	sensitivity coefficient $S(\hat{eta}_{ ext{eff},n},\chi^{ ext{d}}_{ ext{n'g'}})$ as implemented in ERANOS	92
10	Diagram summarizing the terms contributing to the calculation of the	
	sensitivity coefficient $S(\hat{eta}_{ ext{eff},n},\chi^{ ext{p}}_{ ext{i'g'z'}})$ as implemented in ERANOS	94
11	3D representation of the simplified reactor configuration (Toy Model)	
	employed for intermediate-level numerical verification	104
12	Spatial discretization for the discrete ordinates method in the 1D case .	122
13	Schematic representation of the axial characterization process for as-	
	semblies	125
14	Cylindrized representation of the ALFRED core	126

List of Tables

1	Generation IV reactor systems selected by the GIF	13
2	Overview of the advantages and limitations of the Generation IV reactor	
	concepts	14
3	Types of bilinear integrals computable with a dedicated ERANOS module	53
4	Numerical verification of the ERANOS sensitivity modules against ana-	
	lytical reference values	102
5	Main features of the considered core configurations	105
6	Direct contributions to the sensitivity of the delayed neutron fraction	
	associated with a specific precursor family with respect to the average	
	number of delayed neutrons emitted per fission event	107
7	Indirect contributions to the sensitivity of the delayed neutron fraction	
	associated with a given precursor family with respect to the average	
	number of delayed neutrons emitted per fission event	109
8	Sensitivity of the total delayed neutron fraction with respect to the av-	
	erage number of delayed neutrons emitted per fission event	110

1 Energetic and Technological Context

The contemporary global energy landscape is characterized by a complex interplay of factors, such as rising demand, finite resources, environmental responsibilities, and geopolitical instability. Addressing these issues requires a diversified and sustainable energy strategy, where nuclear systems play a crucial role. Given the broad context and the multifaceted nature of nuclear technology, this introduction surveys challenges and frames the role of the nuclear energy as a key player in meeting future requirements.

1.1 Global Energy Scenario

The trajectory of human civilization inevitably leads to a steadily increasing demand for energy.

Although the major economic powers may not exhibit a clear political commitment to reversing this trend, recent data indicate a modest decline in energy consumption across several high-income regions: a development that appears driven more by structural and economic shifts than from deliberate policy choices. [1].

This decline can be attributed to improvements in energy system efficiency, a growing public awareness of the need for more ecological lifestyles (at both individual and systemic scale), implying a gradual shift from fossil fuels to cleaner energy sources and, notably,demographic stagnation.

By contrast, emerging markets and developing economies (EMDEs), which accounts for roughly 85% of the global population, , are now the primary engine of rising energy demand. Over the past decade, these regions have experienced an average annual growth of about 2.6% in energy demand, driven primarily by massive population increases and industrial development [2].

Assuming that the future energy landscape will be shaped by policies currently in place or officially announced by governments, it is possible to define the so called Stated Policies Scenario (STEPS). This scenario represents the "business as usual" case, in which no changes are expected relative to existing strategies, and the future energy trajectory is essentially driven by economic and demographic factors. In addition to STEPS, such projections typically consider two other scenarios based on more committed hypothetical policies aimed at reversing the growth trend in energy consumption. These are the Announced Pledges Scenario (APS) and the Net Zero Emissions by 2050 (NZE) scenario.

Under the APS, it is assumed that, in addition to the current commitments, governments will take action to implement announced plans – although these may not yet be legally binding or fully enacted – regarding energy consumption policies. APS thus offers an intermediate transition outlook, in which declared climate targets shape the development of the global energy trajectory. Under these conditions, total energy demand is expected to peak around 2030, reaching about 3% below current levels by

2035 [3].

The third and most ambitious scenario is NZE, which is formulated in a manner opposite to the previous two: it starts from the objective of eliminating net greenhouse gas emissions by 2050 and then defines the energy policies necessary to achieve this goal. In theory, this ideal scenario is the only one capable of delivering the outcomes envisioned by the Paris Agreement [4], provided that aggressive climate policies are adopted early, technological development in energy systems is strongly promoted, and drastic behavioral changes are implemented on a global scale. The impact of the NZE Scenario extends beyond reductions in total energy demand: it significantly reshapes the global energy system. Under this pathway, global energy-related ${\rm CO}_2$ emissions are projected to decline by approximately 40% between 2020 and 2035, while total energy consumption is expected to decrease by about 7% by 2030 and further decline modestly by 2050 [5].

Figure 1 charts total energy demand and electricity demand, starting from the early 2000s through 2050. Across all scenarios considered, total energy demand either remain broadly flat or rises slightly (STEPS scenario), or it decline progressively (APS and NZE scenarios). Regardless of the path for total energy demand, electricity demand increases in all cases –more sharply in scenarios pursuing more ambitious decarbonization targets [3].

Returning to the current reality, it must be acknowledged that the triad of oil, coal, and natural gas – resources from which a decisive disengagement has yet to occur – is becoming increasingly unsustainable. This has become ever more evident in recent years, as the long-standing challenges associated with fossil fuels (namely greenhouse gas emissions and the depletion of finite terrestrial resources) are now compounded by heightened geopolitical risks. The vulnerability inherent in reliance on a limited number of fossil-fuel suppliers was starkly revealed by the outbreak of the war in Ukraine, which severely disrupted European energy markets and exposed the fragility of the current energy systems.

In this context, where the transition towards sustainable and secure energy systems is imperative, nuclear energy can play a pivotal role in strategies aimed at development of more efficient energy sources, as well as the enhancement of storage systems and the resilience of electrical grids. According to the IEA's *World Energy Outlook 2024* [3], the variable and intermittent nature of predominant renewable energy sources, such as wind and solar, can be effectively balanced and complemented by nuclear energy systems. These nuclear systems combine low greenhouse gas emissions with the ability to provide programmable, baseload electricity over long operational lifespans – features that are essential for ensuring long-term grid stability.

Historically, nuclear power has been a key contributor to global electricity generation since the 1950s, maintaining a prominent role for approximately half a century [6]. Its contribution has fluctuated over time due to a combination of technological ad-

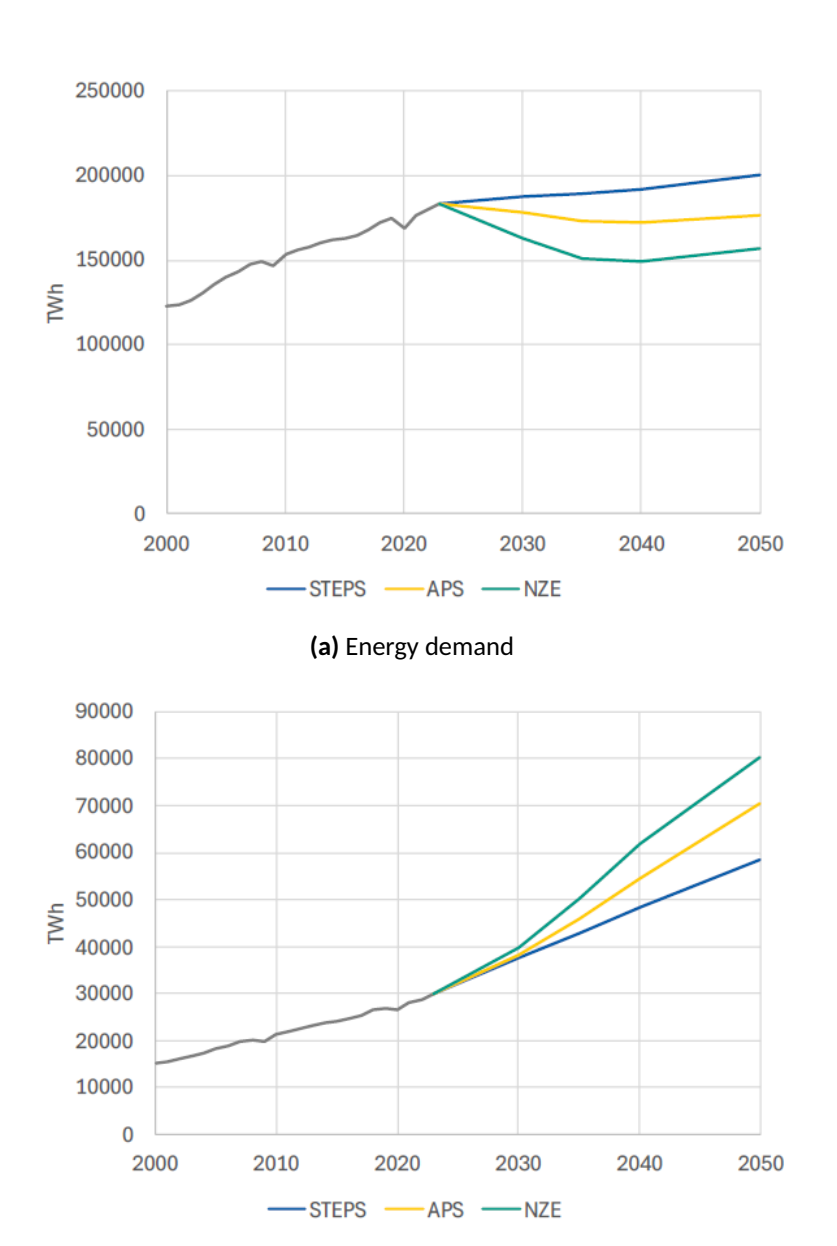


Figure 1: Historical trends and future projections of total energy demand (a) and electricity demand (b) under the STEPS, APS, and NZE scenarios (2000–2050). While total energy demand is expected to remain stable or decline depending on the scenario, electricity demand consistently shows consistent growth across all scenarios, with the most rapid increases occurring in the APS and NZE pathways - reflecting a broadershift toward electrification as a key strategy for achieving climate goals [3].

(b) Electricity demand

vancements, shifts in electricity demand, and political factors. The energy crises of the 1970s, the scaling back of nuclear programs in various countries during the 1980s and 1990s, and the growing emphasis on renewable energy in the 21st century have all significantly influenced the trajectory of nuclear energy development. In particular, the past decade has seen a rapid surge in electricity demand, growing at twice the rate of overall energy demand [7]. This trend has led to the characterization of the current era as the "Age of Electricity", reshaping both the operational landscape and policy framework surrounding nuclear energy.

1.1.1 Nuclear Power and Energy Transition

In 2024, global installed nuclear capacity reached approximately 420 GW, driven by the addition of over 7 GW of new nuclear power capacity. This increase represents a 33% rise in newly installed capacity compared to the amount added in 2023 [2].

Despite this growth, nuclear energy still accounts for approximately 9% of global electricity generation, a significant drop from the historical peak of about 16.6% achieved around the year 2000 [8]. This decline is partly due to the expansion of overall electricity demand, which has outpaced the relative growth of nuclear generation. According to the IEA [3], nuclear energy remains the second largest source of low-carbon electricity¹ globally, providing approximately ($\sim 2600\,\mathrm{TW}$ h) annually. it is surpassed only by hydropower, which contributes around ($\sim 4300\,\mathrm{TW}$ h).

Global nuclear energy production exceeds that from wind by 20%, surpasses solar by approximately 70%, and is nearly four times greater than the energy produced from biomass (see Figure 2).

In terms of CO_2 emissions, currently operating nuclear reactors prevent the release of approximately $1.5~\mathrm{Gt}$ of CO_2 into the atmosphere each year [10]. Cumulatively, over their operational lifetime, it is estimated that nuclear power has avoided the emission of around 72 Gt of $\mathrm{CO}_2{}^2$. In high-income, developed economies, nuclear energy plays a more prominent role than the global average, contributing approximatively 9% of the electricity generation in 2023 [11]. The countries most reliant in nuclear power include France, where it accounts for 65% of the total energy consumption, and Slovakia with 60%. By comparison, in the United States – which hosts the largest fleet of nuclear reactors globally, with 94 operational units – nuclear energy supplies about 20% of total electricity demand.

Shifting the focus to emerging markets and developing economies (EMDEs), a clear contrast emerged in the deployment of nuclear technology. As of 2023, nuclear energy

¹Low-carbon electricity refers to electricity produced from sources that emit little to no CO₂ during generation, such as hydroelectric, nuclear, solar photovoltaic and thermal, wind, and in some cases biomass.

²This quantity represents the amount of CO₂ that would have been emitted if the same quantity of electricity had instead been generated using fossil fuels such as coal, oil, or natural gas.

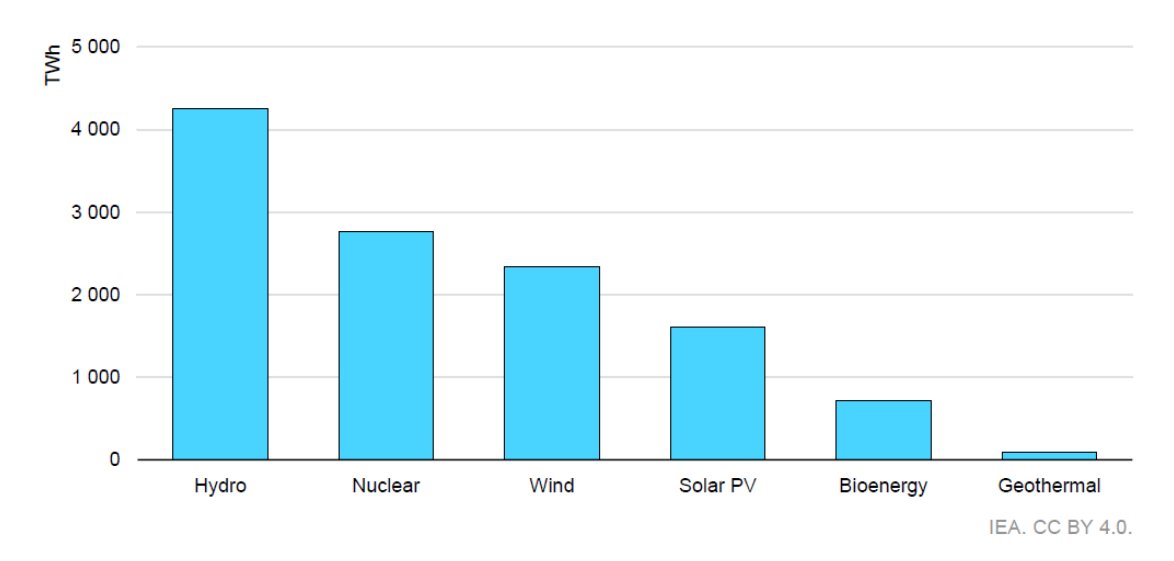


Figure 2: Global low-emissions electricity generation by source in 2023. Energy values are expressed in terawatt-hour. Other low-emissions sources are not shown, as their contribution is comparatively minor. [9]

contributes an average of 5% to electricity generation in these countries. However, there are notable exceptions within this group of countries: in Ukraine, where 50% of electricity comes from nuclear plants, and Belarus, where nuclear power accounts for 35% [11].

Global investments in the nuclear sector has fluctuated over time. Interest increased significantly in the first half of the 1980s, driven by the energy crisis of the previous decade, which had caused a sharp rise in oil prices. At the same time, the sector has also faced severe downturns, most notably in the aftermath of the Chernobyl disaster (1986) [12] and Fukushima (2011) [13] accident. These events prompted the adoption of strict safety principles that underpin current regulatory frameworks, resulting in substantially higher costs and much longer construction times for nuclar plants – often exceeding 10 years – than had previously been the case [14]. Investments in the nuclear sector grew modestly between 2000 and 2010. During this period, most investments were directed toward extending the operational lifetimes of reactors in developed economies, and constructing new plants in China, which was significantly expanding its nuclear capacity. However, in recent years, interest in the sector has been revitalized: in 2024, investments reached approximately USD 80 billion, nearly double the average annual level of the previous decade [3].

A significant paradigm shift has occurred regarding the countries where nuclear projects are being developed: the majority of these activities now take place in EMDEs rather than in advanced economies. China and Russia have emerged as the leading players, both through large-scale domestic construction and by exporting their nuclear

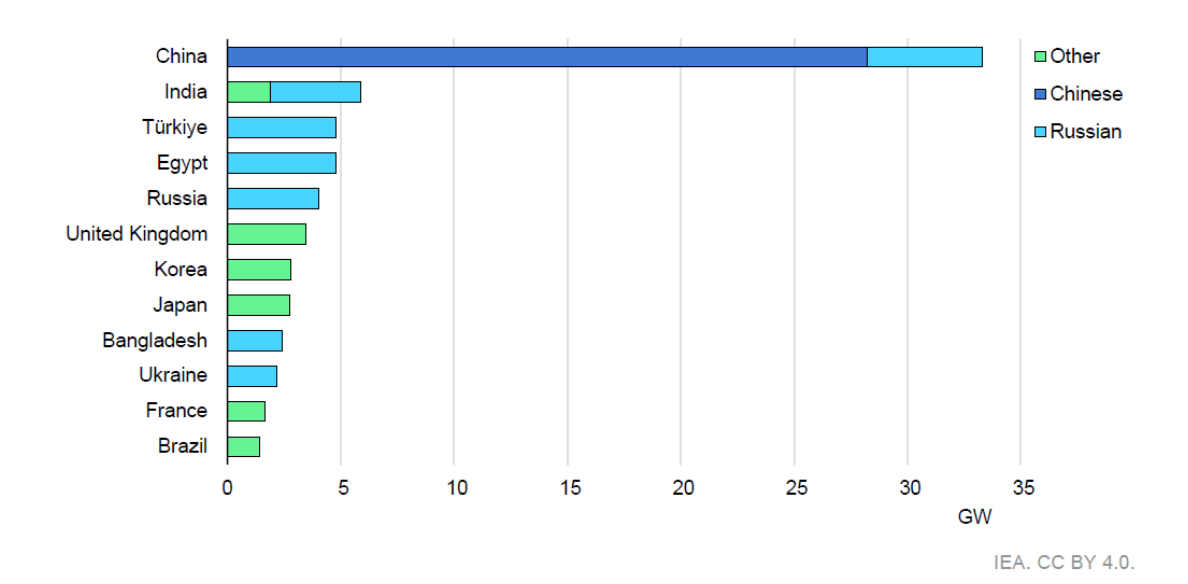


Figure 3: Nuclear power capacity under construction by region and national origin of technology (as of December 2024). [9]

technologies (a trend clearly reflected in Figure 3, which shows the nuclear power capacity under construction by region and national origin of technology as of December 2024). The technical and industrial dominance of these two powers is evident – indeed, over the past five years, every newly launched nuclear construction project has been based on Chinese or Russian designs. As of February 2025, a total of 62 nuclear reactors are under construction across 15 countries, with a total capacity of nearly 70 GW. Almost half of the global nuclear capacity currently under construction is located in China, while advanced economies account for only 9.5 GW, distributed among two reactors in Japan, two in South Korea, two in the United Kingdom, and one in Slovakia [2]. In conclusion of the overview of the global energy landscape and the role of nuclear energy therein, the future outlook projected by the IEA [3] is examined according to the three scenarios previously outlined: STEPS, APS, and the NZE pathway.

steps An increase in nuclear energy capacity is projected from the current 420 GW available at the end of 2024 to an expected 647 GW by 2050. This rate of growth, characterized as moderate and aligned with the general expansion of clean energy technologies – such as wind, solar, and hydro, which are increasingly contributing to the global energy mix – cannot be deemed sufficient to fulfill the requirements of the necessary energy transition. In fact, fossil fuels (oil, gas, coal) would still account for approximately 58% of global energy demand in 2050.

APS Assuming that all countries fully comply with their already declared climate commitments, such as those outlined in the Paris Agreement or in national plans for

climate neutrality, nuclear expansion is promoted more strongly than in the STEPS scenario, with projected nuclear capacity reaching 874 GW by 2050. The future envisioned under this scenario entails a faster and deeper reduction in the use of fossil fuels and a greater deployment and integration of low- or zero-emission energy sources. The energy policies considered would also help limit the increase in global average temperature to approximately 1.7 °C by the end of the century.

NZE Explicitly ambitious, the assumptions underlying this scenario would result in projected nuclear capacity reaching 1017 GW by 2050, highlighting the central role of the nuclear sector in the global decarbonization effort. This outcome represents the minimum required to keep global warming on a trajectory below the $1.5\,^{\circ}$ C limit relative to pre-industrial temperature levels (as it's been set by the Paris Agreement), and would require a reduction in CO_2 emissions by 15% annually starting from today. The technological means currently available would need to undergo drastic development in all areas related to clean energy production and energy efficiency in order to realize such a scenario.

Taking into account the considerations outlined above, the key priorities emphasized by a global institution such as the IEA for revitalizing the nuclear sector within the energy transition process become evident and can be summarized as follows: targeted financial incentives, adequate infrastructure investments, and strong governmental policies. These measures are essential to mitigate (if not eliminate) the economic risks that have historically affected the sector, particularly those associated with construction delays (see the cases of the Vogtle projects [15] in the USA and Olkiluoto [16] in Finland) and the related cost overruns. Ultimately, the successful integration of nuclear power into a low-emission energy systems worldwide will depend on coordinated international efforts and sustained investments to ensure the technologies achieve their full potential.

1.2 The Generation IV International Forum (GIF) Initiative

In the current context of energy instability and mounting concerns over the ongoing climate crisis—primarily driven by excessive reliance on fossil fuels – nuclear energy systems represent a crucial resource. Nuclear power is distinguished by minimal greenhouse gas emissions during operation (and acrosss its entire life cycle) and high reliability, owing to the availability of extractable fuel and the capacity for sustained energy production. However, to fully realize its potential and convincingly demonstrate the benefits of this technology – even to the most critical segments of public opinion – nuclear power must undergo substantial advancements and innovations. In particular, it must become safer and more cost-effective, maximize the efficient use of natural resources, and minimize both the production and long-term radiotoxicity of radioactive waste, thereby surpassing the capabilities of the existing fleet of nuclear reactors, which, at best, belong to the third generation of nuclear systems.

An international collaboration aimed at advancing the research and development of next-generation nuclear energy systems began to take shape around the year 2000: the Generation IV International Forum (GIF). As of today, the Forum include the following member Countries: the People's Republic of China, the Russian Federation, and Australia. Argentina, Brazil, Canada, France, Japan, the Republic of Korea, South Africa, Switzerland, the United Kingdom, the United States, Euratom³. It is important to note that this body is not the unique global initiative concerned with the development of Advanced Reactors (ARs) – the next generation of nuclear energy systems. However, GIF remains the only international organization specifically dedicated to coordinating and integrating all components of the candidate Generation IV systems in a unified framework aimed at meeting established long-term objectives. In addition, the Forum carries out cross-cutting studies addressing key aspects such as safety, security, and technoeconomic performance [17]

In practical terms, the objectives defined by the GIF are expressed by eight essential criteria, which are grouped into four overarching categories: sustainability, economics, safety and reliability, and proliferation resistance and physical protection. As might be expected progress in one area may at times come at the expense of another, and substantial research and development (R&D) efforts are therefore devoted to identifying and implementing optimal trade-offs among these competing priorities.

Sustainability-1 Be capable of delivering the expected amount of energy for the sector while ensuring the long-term availability of systems, in compliance with international agreements on greenhouse gas emissions and fuel material usage.

Sustainability-2 Minimize nuclear waste production and simplify its long-term management, with direct implications for environmental protection and public health.

Economics-1 Offer an advantage in terms of total operating and decommissioning costs compared to other energy sources.

Economics-2 Reduce the financial risks associated with the nuclear energy system to a level comparable with other energy projects of different origin.

Safety and reliability-1 Excel among energy systems in terms of safety and reliability.

Safety and reliability-2 Minimize core damage risks and their severity.

Safety and reliability-3 Eliminate the need for off-site emergency response systems.

³Euratom (European Atomic Energy Community) is an international organization established in 1957 to coordinate the member states' research programs for the peaceful use of nuclear energy and to promote nuclear safety and security within the European Union.

Proliferation resistance and physical protection Reduce attractiveness as a pathway for proliferation or theft of fissile materials for weaponization, and ensure advanced physical protection against terrorist threats.

Based on these criteria, a committee of experts within the GIF, reviewed over 130 reactor concepts, ultimately selecting 6 deemed the most promising for further R&D efforts. The selected technologies are:

- Gas-cooled Fast Reactor (GFR) [18];
- Lead-cooled Fast Reactor (LFR) [19];
- Molten Salt Reactor (MSR) [20];
- SuperCritical Water-cooled Reactor (SCWR) [21];
- Sodium-cooled Fast Reactor (SFR) [22];
- Very-High-Temperature Reactor (VHTR) [23].

To illustrate how these six technologies embody the latest stage in nuclear reactor design, the following sections provide an overview of the historical evolution of nuclear reactor systems across successive generations, with particular emphasis on the innovations and objectives that define Generation IV.

1.2.1 Technological Evolution of Nuclear Reactors

To provide context for the advanced reactor systems discussed above, it is useful to first review the historical development of nuclear reactor technology. This evolution can be broadly classified into three main generations, together with an intermediate stage that marks the most recent advancements bridging current technologies and the forthcoming fourth generation.

Each of these stages is defined by specific technological features and improvements, reflecting continuous efforts to enhance safety, efficiency, and sustainability. The following overview provides a concise summary of the key attributes and milestones that define these successive generations of nuclear reactors.

Generation I This category includes the early prototypes and first-generation power reactors that marked the beginning of nuclear energy applications in the civilian sector. These reactors represented a preliminary technological stage, preceding the development of more powerful, efficient, and reliable systems in later generations. Their prototype nature meant that each project was essentially unique, often characterized by differing technological approaches and experimental configurations.

The operational life of Generation I reactors began in the 1950s and 1960s, typically lasting several decades. As of today, all such reactors have been decommissioned; the last to cease operations was the Wylfa Nuclear Power Station in Wales, which was permanently shut down on December 30, 2015 [24]. Typically, the power delivered by a single reactor was below 300 MW.

Generation II This category comprises the first generation of reactors to achieve technological maturity sufficient for commercially competitive energy production.. The expansion of nuclear R&D programs led to the standardization of several core technologies including pressurized water reactors (PWR), CANada Deuterium Uranium reactors (CANDU), boiling water reactors (BWR), and advanced gas-cooled reactors (AGR) [25]. Ongoing refinements in engineering practices and the accumulation of operational experience enabled a process of continuous improvement in safety performance, further supported by the emergence and consolidation of a genuine nuclear safety culture. Generation II reactors generally rely on traditional active safety systems, which involve mechanical or electrical components and may require manual initiation by an operator.

These reactors form the majority of currently operating nuclear power plants worldwide, with more than 400 commercial PWRs and BWRs in service [26]. Their deployment began in the late 1960s through 1990s, with a typical design lifetime of around 40 years.

The increase in reactor during this era leverages the principle of "economy of scale", wherein fixed costs – such as those for construction – are spread over a larger output, making the energy produced among the most cost-effective in the history of nuclear power. The power output of individual reactors in this generation often exceeds 1000 MW.

Generation III This class of reactors builds upon the technological advancements and operational experience gained from Generation II, introducing significant improvements in several key areas. These include enhanced fuel technology, improved thermal efficiency, and the adoption of standardized designs – a development that enables modular construction, thereby reducing both construction time and associated costs.

A major innovation in Generation III systems is the transition from active to passive safety systems, which rely on natural physical principles (such as gravity, natural circulation, or pressure differentials) rather than operator intervention or powered equipment, enhancing safety in emergency scenarios.

This category includes all reactors currently under construction, with a typical design lifetime of 60 years, which may be significantly expanded through appropriate maintenance and refurbishment programs. In terms of power output

and underlying technologies, Generation III reactors are generally consistent with the best-performing systems from Generation II, continuing to offer high-capacity generation—often around or above 1000 MW per unit.

Generation III+ Reactors in this category represent an evolutionary enhancement of Gen III designs, offering significant improvements, particularly in safety systems. A defining feature is the strong emphasis on passive safety aiming to reduce dependence on human intervention and active mechanical or electrical components. Many Generation III+ designs incorporate passive mechanisms – such as gravity-driven cooling or natural convection – to effectively manage abnormal events and enhance overall safety.

The pronounced inclusion of passive safety measures brings, in turn, economic benefits, accelerating regulatory certification process and shortening construction timelines. A prominent example of Generation III+ reactors is the so-called Small Modular Reactors (SMR) [27]. In thee designs, critical reactor components are where the various key components of the nuclear reactor are integrated into a single compact unit, as opposed to the distributed configuration of conventional-large-scale reactors. This integrated architecture enhances safety, simplifies installation and operation, and reduces construction costs. However, the smaller scale of SMRs limits their ability to benefit from traditional economies of scale, presenting a trade-off between flexibility and cost-efficiency.

1.2.2 IV Generation: Advanced Reactors

Generation IV nuclear reactors were developed within the framework established by the GIF. Despite their differences, these systems share common goals aimed at advancing the global energy landscape:

- optimization of operational efficiency;
- extension of nuclear energy applications beyond electricity (e.g. hydrogen production);
- sustainable strategies for nuclear material management.

Generation IV nuclear technologies encompass a variety of reactor systems designed to address key challenges in sustainability, safety, and efficiency. Among their defining features are the ability of the design to operate at elevated outlet temperatures – thereby enhancing the efficiency of process-heat applications such as hydrogen production – and the adoption of closed fuel cycles, which promote sustainability by enabling the reprocessing and recycling of plutonium, uranium, and minor actinides. Fast neutron spectrum reactors, which employs high-energy neutrons, are particularly effective in

managing minor actinides and improving fuel utilization. By increasing the probability of fission in heavy nuclei, these systems enable the consumption of both fissile and fertile materials, thereby reducing the radiotoxicity, heat load, and volume of nuclear waste. This not only contributes to more favorable waste disposal strategies but also conserves uranium resources through repeated recycling within the fuel cycle. It is important to note that alternative approaches beyond fast neutron spectra and closed fuel cycles can also satisfy key Generation IV criteria even in the absence of recycling. This is exemplified by the VHTRs, which compensate for this limitation through the use of TRI-structural ISOtropic fuel (TRISO) particles⁴. These features provide enhanced proliferation resistance and physical protection, while maintaining strong performance under demanding operating conditions. [28].

Table 1 provides a comparative overview of the six nuclear reactor technologies currently under development within the Generation IV framework. These systems differ in neutron spectrum, coolant type, outlet temperature, fuel cycle approach, and power output, reflecting a diversity of design strategies aligned with varied operational goals. The VHTR is characterized by a thermal neutron spectrum and helium coolant, achieving outlet temperatures up to $1000\,^{\circ}\text{C}$ with an open fuel cycle. The GFR also uses helium but operates with a fast neutron spectrum and a closed fuel cycle, targeting higher fuel efficiency. SFR and LFR utilize liquid metal coolants, with sodium and lead respectively, operating in the fast neutron spectrum and closed fuel cycles, and exhibiting outlet temperatures between approximately $480\,^{\circ}\text{C}$ and $550\,^{\circ}\text{C}$. The MSR employs fluoride salt coolant and can operate in either thermal or fast spectra with a closed fuel cycle. Finally, the SCWR utilizes water at supercritical pressures, operating across thermal and fast spectra, and supports both open and closed fuel cycles depending on the specific design.

This diversity illustrates the multifaceted approaches within Generation IV to optimize reactor performance, safety, and fuel sustainability across different technological pathways.

Based on an evaluation of the advantages and limitations of each technology in terms of performance and short- to medium-term feasibility (as schematically summarized in Table 2) the technology based on Lead-cooled Fast Reactors (LFRs) has been identified as one of the most promising options by ENEA [29], the Italian National Agency for New Technologies, Energy and Sustainable Economic Development. This position is consistent with the strategic direction adopted by several prominent research institutions and international stakeholders, including the European Commission through the Euratom research and training programmes [30]. ENEA's commitment to Lead-cooled Fast Reactor (LFR) technology is further evidenced by its prominent and proactive in-

⁴TRISO fuel particles consist of a uranium-based fuel kernel encapsulated within three successive layers: a porous carbon buffer, an inner pyrolytic carbon layer, and an outer silicon carbide (SiC) layer. This multilayer configuration provides inherent containment of fission products and ensures exceptional structural stability under extreme irradiation and high-temperature conditions.

Fast

Thermal/Fast

Thermal/Fast

LFR

MSR

SCWR

System	Neutron Spectrum	Coolant	Outlet Temp. (°C)	Fuel Cycle	Size (MWe)
VHTR	Thermal	Helium	900-1000	Open	250-300
GFR	Fast	Helium	\sim 850	Closed	∼1200
SFR	Fast	Sodium	500-550	Closed	up to 1500

480-570

700-800

510-625

Closed

Closed

Open/Closed

up to 1200

300-1000

up to 1500

Table 1: Generation IV reactor systems selected by the GIF and their main features. [17]

volvement in the ALFRED project (Advanced Lead Fast Reactor European Demonstrator) [31]. ALFRED currently represents the European reference demonstrator for LFR technology and is conceived as a key milestone toward the future industrial deployment of lead-cooled fast reactors.

1.3 The European LFR Technology Demonstrator: ALFRED

Lead

Fluoride salt

Water

The ALFRED project was initiated with the objective of developing a prototype that faithfully replicates, at full scale, the characteristics of a nuclear reactor intended for industrial energy production. As a technological demonstrator, it is designed to combine a particularly high level of safety with the capability to operate under a wide range of scenarios. These scenarios include both transient and accidental conditions, aiming to simulate situations that reactors of this type might encounter in the future. The site selected for the construction of the reactor is located at the RATEN research center in Mioveni, Romania. RATEN, together with Ansaldo Nucleare and ENEA, is part of the Fostering ALfred CONstruction (FALCON) international consortium, the entity responsible for coordinating all activities related to the reactor's realization. The FALCON consortium carries out its activities following a collaborative approach, involving an increasing number of international research institutions, engineering companies, and manufacturing enterprises. These entities contribute concrete resources to the development of solutions that are technically sound, practically feasible, and economically sustainable. The roadmap of the ALFRED Project aims to achieve, by 2040, a level of technological competitiveness that enables the industrial-scale deployment of LFRs, with particular emphasis on the adopted engineering solutions [33].

Table 2: Overview of the advantages and limitations of selected Generation IV reactor concepts – Very High Temperature Reactor (VHTR), Gas-cooled Fast Reactor (GFR), Sodium-cooled Fast Reactor (SFR), Lead-cooled Fast Reactor (LFR), Molten Salt Reactor (MSR), SuperCritical Water-cooled Reactor (SCWR) - across key evaluation criteria. Positive or potentially favorable characteristics are highlighted in green, negative or potentially limiting aspects are highlighted in red, while technical challenges are highlighted in yellow. [32]

Aspect	VHTR	GFR	SFR	LFR	MSR	SCWR
Fuel cycle	Open	Closed	Closed	Closed	Open/Closed	Once-through
Safety characteristics	Demonstrated high inherent safety	Safety performance not yet validated	Historically associated with safety challenges	Potential for acceptable safety performance	Safety performance under evaluation	Expected to achieve safety standards comparable to LWRs
Economic potential	Targeted economic competitiveness (conceptual stage)	Promising cost profile (preliminary designs available)	Limited economic viability (demonstrated high costs)	Favorable cost assumptions (design proposals exist)	Targeted economic performance (design under development)	Promising cost projections (design concepts exist)
Technology readiness	Early-stage development (leveraging HTR experience)	Conceptual stage, no experimental validation	Mature technology with extensive operational history	Experimental validation in military applications (submarine reactors)	Limited experimental demonstration (single pilot test)	No experimental deployment, but based on LWR technology
Technical challenges	High- temperature materials qualification	Advanced fuel and material development under extreme conditions		Corrosion mitigation in lead environment	Corrosion mitigation in molten salt environment	

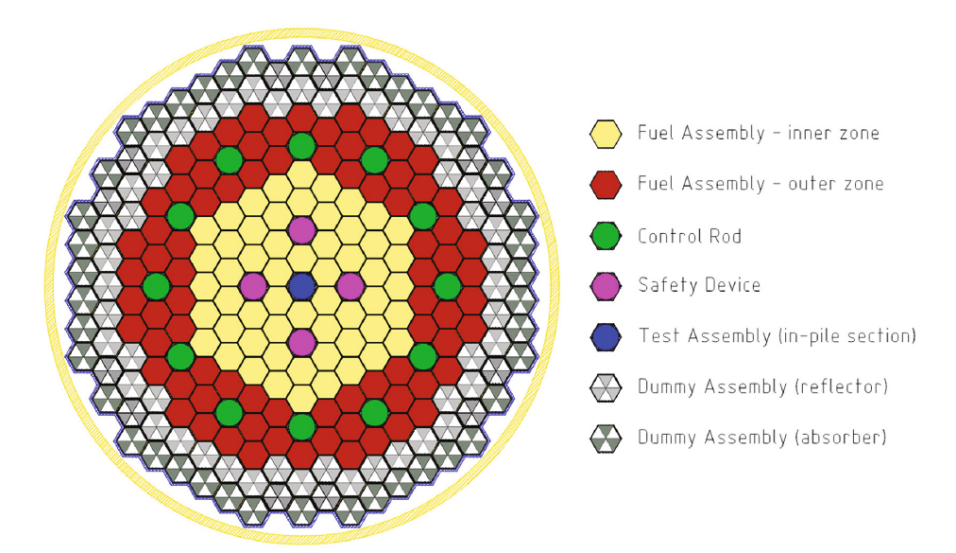


Figure 4: Schematic cross-sectional view of the ALFRED reactor core layout. The configuration includes 134 hexagonal fuel assemblies divided into two radial zones: an inner zone (light yellow) and an outer zone (red). It also features 12 control rods (green), 4 safety devices (purple), and 1 test assembly for in-pile irradiation experiments (blue). The surrounding region contains 102 dummy assemblies, which are further classified as reflector-type (white) and absorber-type (gray). The outermost boundary represents the core barrel and radial shielding structures.

1.3.1 ALFRED's core

The ALFRED core is designed to produce a nominal thermal power of 300 MW_{th} under normal operating conditions, using a MOX fuel, (U, Pu)O_{1.97}, composed of reprocessed Plutonium and depleted Uranium.

The core configuration consists of 134 hexagonally wrapped fuel assemblies, 12 control rods, 4 safety devices, 1 special position for in-pile irradiation experiments, and 102 dummy assemblies. A schematic representation of their arrangement is shown in Figure 4.

Neutronic analyses were performed to define the fuel enrichment level and its corresponding zoning, pursuing three main objectives regarding core design [34]:

- \bullet Ensure criticality during operation while maintaining a target maximum burn-up of 100 MW d kg $^{-1}{}_{\rm HM}$;
- Achieve a uniform power distribution among the fuel rods to avoid localized peaks that could compromise fuel integrity or limit the core lifetime;
- Provide adequate negative reactivity worth from the reactor control and shutdown systems, necessary to safely manage reactivity variations over time and to guarantee reactor shutdown under abnormal or emergency conditions.

The outcome of these studies resulted in the core configuration currently adopted for ALFRED (the one depicted in the Figure 4), featuring two fuel zones – referred to as inner and outer – characterized by MOX fuel with different plutonium enrichments: $20.5\,\mathrm{wt.\%}$ for the 56 FAs in the inner zone, and $26.2\,\mathrm{wt.\%}$ for the remaining 78 in the outer zone.

1.3.2 Safety Margins for ALFRED

Due to its demonstrative nature, the safety objectives defined for the ALFRED reactor extend beyond the general directives issued by the IAEA, incorporating additional guidelines formulated within the framework of the GIF.

According to the IAEA Safety Standards, the fundamental safety objective is to protect people and the environment from the harmful effects of ionizing radiation [35]. This overarching principle is further articulated into the following specific safety goals:

- To control radiation exposure to individuals and the release of radioactive materials into the environment;
- To limit the probability of events that could lead to a loss of control over the reactor core, the chain reaction, or any radioactive source;
- To mitigate the consequences of such events, should they occur.

The safety framework established by the Generation IV initiative contributes to these objectives by introducing the following additional requirements:

- Generation IV systems must demonstrate excellence in both safety and reliability;
- They must exhibit a very low probability and extent of core damage, which necessitates robust analysis tools capable of evaluating uncertainties across a wide spectrum of scenarios;
- They must aim to eliminate the need for off-site emergency response by implementing preventive measures that significantly reduce the potential release of radioactive materials to the environment.

Safety margins, defined as "the difference or ratio in physical units between the limiting value of an assigned parameter, the surpassing of which leads to the failure of a system or component, and the actual value of that parameter in the plant" [36] (as illustrated in Figure 5), are considered adequate as long as all physical barriers comply with safety criteria across the full range of operational states considered in the reactor design, including conditions beyond normal operation.

The purpose of safety analysis is to provide robust evidence that these safety requirements are effectively met – i.e. that sufficient safety margins exist between the

actual operating values of key physical parameters and the threshold values whose exceedance would compromise the structural or functional integrity of barriers designed to contain radioactive materials [37].

For this reason, it is necessary to categorize potential operational and accidental events according to their probability of occurrence and the severity of their consequences – two parameters generally characterized by an inverse correlation.

The classification typically adopted includes the following categories:

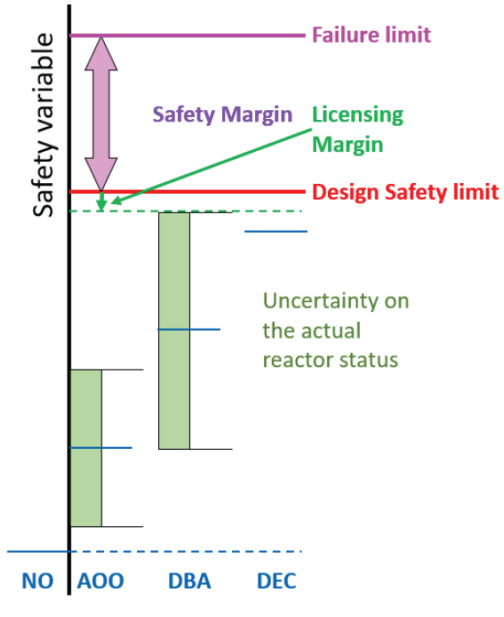
- **Normal Operation (NO):** All operating conditions for which the plant is designed throughout its intended lifetime.
- Anticipated Operational Occurrences (AOOs): Deviations from normal operation that are expected to occur during the reactor's lifetime but do not cause significant damage to safety-related systems or lead to accident scenarios.
- **Design Basis Accidents (DBAs):** Hypothetical accidents for which the plant is explicitly designed, following established engineering criteria and conservative methodologies. In these scenarios, any release of radioactive material must remain within acceptable limits.
- **Design Extension Conditions (DECs):** Low-probability postulated accident conditions not included in the design basis, but still considered during the design process. These may involve either minor fuel degradation or core meltdown. In both cases, the release of radioactive material must be minimized so as not to pose a risk to public health or the environment.

Due to the current limited knowledge regarding the physics of Gen-IV systems, and in alignment with the GIF vision integrated into ALFRED's safety objectives, safety analyses for AOOs, DBAs, and DECs should be conducted using conservative approaches. This includes consideration of uncertainties in data, models, and boundary conditions – an approach known as Best Estimate Plus Uncertainty (BEPU).

1.4 Thesis Motivation and Goals

The studies carried out in support of this work were carried out at the Core Design Laboratory of the ENEA Bologna Research Center, which plays a central role in the development of ALFRED – the European demonstrator of LFR technology – by coordinating the core design activities within the FALCON consortium. In recent years, several studies were conducted by ENEA with the aim of advancing the core design towards a final configuration suitable for licensing. [32, 34, 38].

In this context, neutronic analyses are a key tool for evaluating reactor safety characteristics, and for defining and optimizing design margins.



NO: Normal Operation

AOO: Anticipated Operational Occurrences

DBA: Design-Basis Accidents
DEC: Design Extension Conditions

Figure 5: Graphical representation of the concept of safety margin. In the case of Generation IV reactors, the BEPU methodology is expected to be applied even to DECs, whereas it is not required for the licensing of existing light- and heavy-water-cooled reactors.

This thesis contributes to the core design activities by developing and implementing new computational modules within the ERANOS (European Reactor ANalysis Optimized System) code system, an advanced suite for fast reactor neutronic analysis. These modules enable the calculation of sensitivity coefficients associated with specific neutronic parameters, thereby providing the basis for future studies on the ALFRED core.

Sensitivity analysis investigates how small variations applied to input parameters (e.g., fuel isotopic composition, the cross section of a specific nuclear reaction, the number of neutrons emitted per fission event, etc.) affect the reactor's neutronic behavior, by quantifying the corresponding changes in selected quantities of interest.

The results of sensitivity analysis play a fundamental role in both deepening the physical understanding of core characterization and in optimizing the design safety margins and overall reactor performance. Specifically, beyond providing a detailed mapping of the interdependencies among nuclear parameters, sensitivity analysis guides the design process by identifying which components require more stringent safety margins to avoid notable deviations in the reliable operation of the entire system.

Furthermore, sensitivity analysis is an essential prerequisite for subsequent uncer-

1 ENERGETIC AND TECHNOLOGICAL CONTEXT

tainty analysis, which propagates the uncertainties of input parameters into those of "derived" (integral) quantities. This provides essential information on design reliability and safety margins, supporting regulatory decision-making in the licensing process [37].

2 Theoretical Background

Sensitivity analysis can be carried out by considering perturbations in either the reactor's geometric and structural quantities or in the underlying nuclear data. While sensitivity with respect to structural parameters can directly inform design decisions by identifying the most influential physical dimensions and configurations, sensitivity to nuclear data is equally important – not only for assessing the reliability of neutron transport calculations, but also because uncertainties in these data can propagate to integral reactor parameters in ways that may influence design margins, safety assessments, and operational flexibility.

The perturbations considered in this work are limited to nuclear parameters, such as fission spectra and average neutron multiplicities, which characterize fundamental nuclear processes. The resulting sensitivity analysis is thus aimed at identifying the nuclear parameters that most significantly influence the evaluation of key integral quantities. Moreover, this type of sensitivity coefficients represents a fundamental component for assessing the uncertainties in reactor parameters arising from nuclear data. Indeed, nuclear data have always been among the primary sources of uncertainty in reactor simulations, however, with the progressive refinement of reactor physics tools and the associated reduction of numerical approximations – enabled by advances in computational capabilities – this role has become even more pronounced [39, 40].

In case of Generation IV reactors, uncertainties in nuclear data are particularly critical due to the lack of extensive operational experience with these systems. Unlike previous generations, whose design and optimization benefited by decades of experimental feedback, the development of advanced reactors depends more heavily on predictive modeling, making the reduction of nuclear data uncertainties a fundamental requirement.

2.1 Overview of Nuclear Data and Integral Parameters

The term "nuclear data" covers a broad set of structures and quantities, including reaction cross-sections (typically expressed in differential form, i.e., interaction probabilities per unit energy and solid angle), nuclear masses with their decay modes and parameters, as well as various types of emission spectra.

From the 1950s through the 1990s, extensive experimental campaigns were carried out to characterize fundamental nuclear data [41]. In the following decades, the rapid increase in computational power enabled significant advances in the modeling and simulation of nuclear systems, providing increasingly detailed descriptions of the underlying physical phenomena.

The high level of sophistication achieved by modern numerical tools underscores that uncertainties in cross-section data – together with those introduced by processing

codes - remain the main source of uncertainties.

These tools generate nuclear data libraries by reconstructing the continuous-energy behavior of cross sections across the full energy spectrum of interest, consistently integrating experimental measurements with theoretical model predictions.

The production of increasingly updated and refined nuclear data – both in terms of precision and accuracy – relies on a multi-stage process. Starting from experimental measurements, nuclear data evaluators use theoretical models to reconstruct quantities that either have not yet been measured, cannot be directly measured due to experimental limitations, or have been measured with insufficient precision or accuracy.

The integration of experimental observation with theoretical prediction allows the construction of continuous nuclear data libraries covering the full energy range of interest. These libraries result from a rigorous assessment process, in which specialists (the so-called "evaluators") analyze, compare, and combine all available datasets, select the most reliable ones, and establish a consistent set of standardized reference data, which constitute the nuclear data libraries – e.g. the Evaluated Nuclear Data File (ENDF) [42], mainly developed by the National Nuclear Data Center (NNDC) in the USA, and the Joint Evaluated Fission and Fusion File (JEFF) [43], developed in collaboration by several European countries within the framework of the Organization for Economic Co-operation and Development project of the Nuclear Energy Agency (OECD-NEA) [44].

Once nuclear data libraries are established, their impact on reactor behavior is assessed through a set of derived quantities known as integral parameters. These macroscopic observables (such as reaction rates, multiplication factors, and reactivity coefficients) result from integrating nuclear data over the entire reactor system and its operating conditions, and are essential for characterizing the overall macroscopic behavior of the reactor.

At the core of this process lies the neutron flux, which links the microscopic nuclear data (e.g., cross sections, fission yields) to the macroscopic response of the reactor. The flux describes the spatial, energy, and time-dependent distribution of neutrons within the system, and acts as a weighting function in the computation of integral parameters.

2.2 Derivation of Neutron Fluxes from the Boltzmann Transport Equation

The distribution of neutrons within a reactor, or more generally within any medium, is described by the neutron transport equation. This equation represents a net balance of the neutron population between gains and losses within an infinitesimal volume of the six-dimensional phase space, defined by the spatial coordinates (\vec{r}), the energy (E), and the flight direction ($\hat{\Omega}$).

The neutron transport equation can be derived by considering the time variation of the neutron distribution, described by the neutron density function $N(\vec{r}, E, \hat{\Omega}; t)$. This

function expresses the number of neutrons present at time t within an infinitesimal volume centered at \vec{r} , having kinetic energy E and traveling in the direction $\hat{\Omega}$, per unit volume, energy, and solid angle. For practical purposes, however, it is customary to adopt an alternative quantity for this formulation, namely the angular flux, defined as:

$$\phi(\vec{r}, E, \hat{\Omega}; t) = v(E)N(\vec{r}, E, \hat{\Omega}; t), \tag{1}$$

where the parameter v denotes the neutron velocity.

Neutron transport theory finds a natural application in the field of nuclear reactor design, as the characteristics of the neutron distribution govern the reactor's behavior. To predict these characteristics, the nuclear reactor theory is developed, based on a statistical analysis of neutron dynamics within the materials that constitute the system.

The Boltzmann equation (another term commonly used to refer to the neutron transport equation) provides a framework for determining the neutron distribution at each point within the aforementioned six-dimensional phase space. While neutron-neutron interactions are generally neglected, the dominant interactions between neutrons and the nuclei of the surrounding medium can typically be classified into the categories outlined below.

Elastic Scattering: Reactions in which the neutron changes its flight direction and energy depending on the mass of the target nuclide it collides with, while the total kinetic energy of the two-body system (neutron and nuclide) is conserved.

Inelastic Scattering: Reactions that differ from those described above in terms of total kinetic energy conservation. Following the collision with the neutron, the target nuclide becomes excited and occupies higher energy levels within its configuration, leading to a greater energy loss for the neutron.

Nuclear Capture: Reactions in which the incoming neutron is absorbed by the target nuclide, which transmutes into an isotope with an atomic mass increased by one unit. If the newly formed nuclide is unstable, the capture reaction may subsequently result in the emission of secondary particles (e.g., gammas, alphas).

Nuclear Fission: Reactions in which the incoming neutron is absorbed by the target nuclide, leading to its fission into two or more nuclear fragments, accompanied by the emission of secondary neutrons and the release of a large amount of energy.

Within the Boltzmann equation, the following contributions must therefore be considered:

Transport term: Represents the spatial transport of neutrons through the infinitesimal volume under consideration, including both those entering and those leaving it.

Removal term: Represents the loss of neutrons from the infinitesimal volume due to any type of interaction with the nuclei present.

Scattering term: Represents the *scattering source*, that is, all neutrons which, although entering the infinitesimal spatial volume surrounding the point identified by \vec{r} with different energy and direction, are redirected into the specific infinitesimal volume of interest in phase space following a collision $(\vec{r}, E' \to E, \hat{\Omega}' \to \hat{\Omega})$.

Additional sources: Refers to various terms contributing to neutron generation within the system. These include the contribution from neutrons emitted promptly as a result of fission processes (both neutron-induced and spontaneous), neutrons produced with delay from the decay of so-called precursor nuclides (unstable fission fragments), and finally the contribution of any neutrons introduced into the reactor via external sources.

Incorporating all the considerations outlined above, the neutron transport equation can be expressed in its integro-differential form as follows:

$$\frac{1}{v} \frac{\partial \phi(\vec{r}, E, \vec{\Omega}, t)}{\partial t} + \vec{\Omega} \cdot \vec{\nabla} \phi(\vec{r}, E, \vec{\Omega}, t) + \sum_{i} N_{i}(\vec{r}, t) \sigma_{t,i}(E) \phi(\vec{r}, E, \vec{\Omega}, t) =
= \sum_{i} N_{i}(\vec{r}, t) \int_{0}^{\infty} dE' \int_{(4\pi)} d\Omega' \, \sigma_{s,i}(\vec{r}, E' \to E, \vec{\Omega}' \to \vec{\Omega}, t) \phi(\vec{r}, E', \vec{\Omega}', t) +
+ \frac{\chi_{i}^{p}(E)}{4\pi} \sum_{i} N_{i}(\vec{r}, t) \int_{0}^{\infty} dE' \int_{(4\pi)} d\Omega' \, \nu_{f,i}^{p}(E') \sigma_{f,i}(E') \phi(\vec{r}, E', \vec{\Omega}', t) +
+ \frac{1}{4\pi} \sum_{i} \nu_{sf,i}^{p} \lambda_{sf,i} N_{i}(\vec{r}, t) \chi_{i}^{p}(E) + \frac{1}{4\pi} \sum_{i} \lambda_{d,i} N_{i}(\vec{r}, t) \chi_{i}^{d}(E) + S_{ext}(\vec{r}, E, \vec{\Omega}, t) ,$$
(2)

where $N_{\rm i}(\vec{r},t)$ represents the atomic density of isotope i localized at \vec{r} and time t; $\sigma_{\rm x,i}(E)$ denotes the microscopic cross-section dependent on energy for reaction x associated with nuclide i (where x=s indicates scattering reaction, x=f neutron-induced fission, x=sf spontaneous fission, and x=t total cross-section); $\nu_{\rm y,i}^{\rm p}$ is the average number of promptly emitted secondary neutrons per fission event (y=f for neutron-induced, y=sf for spontaneous) of nuclide i; $\chi_{\rm i}^{\rm z}$ is the energy spectrum of prompt (z=p) or delayed (z=d) secondary neutrons produced by the fission of nuclide i; $\lambda_{\rm w,i}$ is the decay constant of nuclide i corresponding to neutron-emitting reactions (w=d) or spontaneous fission (w=sf); and $S_{\rm ext}(\vec{r},E,\vec{\Omega},t)$ accounts for any additional external neutron source.

Based on the nature of the terms present in the Boltzmann equation in its integro-

differential form, two operators can be identified within it:

$$\mathbf{A}\phi = \vec{\Omega} \cdot \vec{\nabla}\phi(\vec{r}, E, \vec{\Omega}, t) + \sum_{i} N_{i}(\vec{r}, t)\sigma_{t,i}(E)\phi(\vec{r}, E, \vec{\Omega}, t) + \\ - \sum_{i} N_{i}(\vec{r}, t) \int_{0}^{\infty} dE' \int_{(4\pi)} d\Omega' \,\sigma_{s,i}(\vec{r}, E' \to E, \vec{\Omega}' \to \vec{\Omega}, t)\phi(\vec{r}, E', \vec{\Omega}', t) ,$$
(3)

which is the so-called *neutron loss operator*, accounting for the contributions of neutron transport, removal, and scattering phenomena; and

$$\mathbf{F}\phi = \frac{\chi_{i}^{p}(E)}{4\pi} \sum_{i} N_{i}(\vec{r}, t) \int_{0}^{\infty} dE' \int_{(4\pi)} d\Omega' \, \nu_{f,i}^{p}(E') \sigma_{f,i}(E') \phi(\vec{r}, E', \vec{\Omega}', t) + \frac{1}{4\pi} \sum_{i} \nu_{sf,i}^{p} \lambda_{sf,i} N_{i}(\vec{r}, t) \chi_{i}^{p}(E) + \frac{1}{4\pi} \sum_{i} \lambda_{d,i} N_{i}(\vec{r}, t) \chi_{i}^{d}(E) ,$$
(4)

which is the *neutron production operator* associated with the fission source, including prompt and delayed neutrons generated by neutron-induced and spontaneous events.

The Boltzmann equation can therefore be rewritten in the following compact form:

$$\frac{1}{v}\frac{\partial \Psi}{\partial t} = (\mathbf{F} - \mathbf{A})\Psi + S, \qquad (5)$$

which can be further simplified in accordance with the assumptions adopted in this work, namely the steady-state condition (under which the neutron flux is time-independent and the time derivative vanishes) and the absence of external sources (i.e., S=0, which renders the equation homogeneous). It is important to note that, in this formulation, the effective multiplication factor $k_{\rm eff}$ is introduced as a formal eigenvalue of the neutron transport equation. Specifically, by factoring $1/k_{\rm eff}$ in front of the fission source term, the neutron balance equation is recast as an eigenvalue problem. The goal is no longer to simply balance sources and losses for a given flux, but to determine the values of $k_{\rm eff}$ for which a non-trivial neutron flux distribution exists.

Based on these assumptions, the steady-state neutron transport equation takes the form of an eigenvalue problem, known as the Boltzmann eigenvalue equation:

$$\left(\mathbf{A} - \frac{\mathbf{F}}{k_{\text{eff}}}\right)\phi = 0. \tag{6}$$

The eigenvalue problem is assumed to admit a countable infinity of real and positive eigenvalues $k_{\rm eff}$, each associated with a corresponding eigenfunction. Among these, the largest eigenvalue – associated with the zeroth-order harmonic – is referred to as the fundamental multiplication factor, and its corresponding eigenfunction is known as the fundamental flux. This solution characterizes the steady-state behavior of the reactor under critical conditions and is of primary interest in most reactor physics analyses.

The fluxes associated with the eigenvalues of the neutron transport equation (including both the fundamental and higher-order modes) are defined only up to a multiplicative constant: if ϕ_i is a solution of the equation $(\mathbf{A} - \mathbf{F}/k_{\mathrm{eff}})\phi_i = 0$, then any scalar multiple $\lambda\phi_i$, with $\lambda\in\mathbb{R}$, is also a valid solution.

Moreover, each operator involved in the neutron balance equation admits a corresponding adjoint operator. When the transport equation is reformulated using these adjoint operators, the resulting eigenvalues remain unchanged, while the associated eigenfunctions correspond to what is defined as the adjoint flux, denoted by ϕ^{\dagger} .

The time-independent adjoint problem with no external sources can thus be written as:

$$\phi^{\dagger} \left(\mathbf{A}^{\dagger} - \frac{\mathbf{F}^{\dagger}}{k_{\text{eff}}} \right) = 0.$$
 (7)

which represents the adjoint eigenvalue formulation of the Boltzmann transport equation.

The adjoint flux is commonly interpreted as the *importance function*. It quantifies the relative contribution of a neutron (characterized by its position in the seven-dimensional phase space – including spatial coordinates, energy, direction, and time) to a given response function of interest, typically related to reactor performance, such as power generation. Equivalently, the importance function can be understood as the variation in the steady-state neutron flux resulting from the introduction of a single neutron at a specific location \vec{r} , with energy E and direction $\hat{\Omega}$. In this sense, it reflects how significantly that neutron, through its progeny, affects the transition from an initial steady-state flux ϕ_0 to a new steady-state flux ϕ_∞ following a perturbation.

To provide an intuitive illustration, consider two limiting cases: a thermal neutron introduced at the core center, and a fast neutron emitted near the reactor boundary and directed outward. The first neutron is well positioned within the fissile region and has an energy corresponding to high fission cross sections, thereby having a high probability of inducing further fission reactions. Conversely, the second neutron is likely to escape the system almost immediately without interacting, making a negligible contribution to the neutron population. As expected, the thermal neutron introduced at the center has a substantially higher importance than the fast neutron lost at the periphery. In this context, the importance quantifies the expected long-term contribution of a neutron to the asymptotic flux distribution after the system has returned to equilibrium.

2.3 Role of Delayed Neutrons in Reactor Dynamics

It is now appropriate to shift the focus toward integral quantities that encapsulate key physical aspects of reactor behavior. Among these, particular attention is devoted to the *effective delayed neutron fraction*, $\beta_{\rm eff}$, which is the parameter of interest of this thesis. To underscore the crucial role of delayed neutrons in the dynamic behavior and

controllability of nuclear reactors, it is helpful to briefly recall the fundamentals of the fission chain reaction and the conditions required to keep it under operational control.

A power reactor must be configured with appropriate inventories and geometries of fuel, absorbers (and/or moderator), and reflector so that a critical state can be achieved and maintained. In critical conditions the number of neutrons produced in one fission generation equals the number in the next. It is important to note that reactor criticality is not solely a design-based condition. While the geometrical and material configuration of the reactor core – as defined at the design stage – determines the potential to reach a critical state (i.e. an effective multiplication factor $k_{\rm eff}=1$), the actual achievement and maintenance of criticality depend on the instantaneous physical conditions of the reactor. These include fuel composition, temperature, control rod positions, neutron poisoning, and other operational parameters 5 .

Power is regulated by moving control rods within the core. Inserting rods introduces negative reactivity ($\rho < 0$) by increasing neutron absorption and drives the system subcritical: withdrawing rods introduces positive reactivity ($\rho > 0$) and drives it supercritical. A power change is executed quasi-statically by briefly biasing $k_{\rm eff} = 1, \; \rho = 0$ to ramp the neutron population up or down, and then restoring criticality at the new power level. Control rods play a central role not only in short-term reactivity control, but also over longer timescales. During reactor operation, they are continuously adjusted to compensate for reactivity changes caused by fuel burn-up – including fuel depletion and spectral shifts – as well as by the accumulation of neutron poisons 6 , both of which have a significant impact on the neutron economy and, consequently, on the reactor's criticality.

Within this framework the fundamental role of delayed neutrons becomes evident: the controllability margin that distinguishes a stable, power-producing reactor from a prompt-supercritical device depends on the small fraction of fission neutrons emitted with a delay. To provide a more concrete understanding of their impact on the balance of the chain reaction, it is useful to introduce some basic calculations.

A key parameter for characterizing the reactor state is the effective multiplication factor, $k_{\rm eff}$ (for a detailed discussion of its microscopic meaning, see the dedicated chapter in [45]). At the macroscopic level, it is interpreted as the ratio of neutron populations

 $^{^5}$ Formally, a reactor is said to be critical when $k_{
m eff}=1$, meaning that each fission event causes, on average, exactly one subsequent fission, sustaining a steady-state chain reaction. However, in practice, a reactor that is shut down is no longer critical, despite its configuration potentially allowing for criticality. This is because, in the absence of sufficient neutron population and adequate operating conditions, the chain reaction cannot be maintained.

⁶Neutron poisons are nuclides with high neutron absorption cross-sections that build up during reactor operation, such as ¹³⁵Xe and ¹⁴⁹Sm. Their presence reduces the neutron population and thus the reactivity of the core. This phenomenon is particularly significant in thermal reactors, such as light water reactors, where these isotopes strongly absorb thermal neutrons. In fast reactors, although the same nuclides are produced, their impact is considerably less pronounced due to the much lower absorption cross-sections in the fast energy range.

in successive generations:

$$k_{\text{eff}} = \frac{N_{\text{i+1}}}{N_{\text{i}}},\tag{8}$$

where $(N_{\rm i+1})$ and $(N_{\rm i})$ denote the numbers of neutrons in two consecutive fission generations. As its name suggests, the effective multiplication factor $k_{\rm eff}$ represents the factor by which the neutron population changes from one generation to the next: when $k_{\rm eff}$ = 1 (i.e., the neutron population remains, on average, constant in time), the reactor is in a critical state. For values $k_{\rm eff} < 1$, the reactor is subcritical, while for $k_{\rm eff} > 1$, it is supercritical.

Introducing the mean generation time τ , the prompt-only kinetics balance can be written as [46]:

$$\frac{dN}{dt} = N \frac{k_{\text{eff}} - 1}{\tau} \,, \tag{9}$$

where $k_{\rm eff}-1$ represents the excess reproduction beyond the single neutron per generation required to sustain the chain reaction in critical balance. The solution of this first-order homogeneous differential equation is given by:

$$N = N_0 e^{(k_{\text{eff}} - 1)t/\tau}$$
, (10)

where N_0 is the neutron density at the reference time t_0 , and N its value at t. The reactor time constant is defined as $T_{\rm R} = \tau/(k_{\rm eff}-1)$.

For practical reactor operation, $k_{\rm eff}$ is very close to unity; deviations are commonly expressed in terms of "per cent mille" (pcm), i.e. $\frac{\Delta k_{\rm eff}}{k_{\rm eff}} \times 10^{-5}$. To illustrate the impact of small supercritical conditions, consider a reactor with

To illustrate the impact of small supercritical conditions, consider a reactor with an effective multiplication factor of $k_{\rm eff}=1.001$. According to Equation 10, and assuming a typical prompt neutron mean generation time $\tau\sim 0.1\,\rm ms$, as in a thermal reactor, the neutron population would increase by more than four orders of magnitude within one second. Such a rapid increase would make the reactor effectively uncontrollable. In a fast reactor, where the prompt mean generation time is significantly shorter ($\tau\sim 0.1\,\mu s$), the same reactivity would result in an exponential increase of the neutron population by a factor of e^{10000} over one second – a physically unrealistic and operationally unacceptable scenario.

Fortunately, the reality is less severe. Alongside prompt neutrons, a small number of neutron-rich fission products are produced during each fission event. These unstable isotopes, known as precursors, undergo beta decay after a characteristic delay, eventually emitting delayed neutrons. For modeling purposes, these precursors are not treated individually, but are grouped into a finite number of families (typically six or eight) based on their average decay constants. This classification is not physically fundamental, but rather a practical simplification that allows the complex spectrum of decay times to be represented by a small set of representative kinetic parameters, averaged over contributing nuclides.[47]

The presence of delayed neutrons affects the average neutron lifetime, which in thermal reactors reaches values on the order of 0.01 s. This is sufficient to ensure that, over a time interval of one second, in a core with $k_{\rm eff}=1.001$, the neutron population increases by approximately 1%, a value that is generally manageable. It is evident that, for fast reactors, these rates of increase become significantly more pronounced. This is one of the main reasons why such systems inherently require critical safety measures, which often translate into stringent design constraints.

In practice, reactors (of any type) are designed to operate in a subcritical configuration when considering only the prompt neutron component. The reactor becomes critical (or supercritical, if operationally required) when the contribution of delayed neutrons is also included. This state is sometimes referred to as the delayed critical condition. To provide an idea of the range within which reactor reactivity can be controlled, a fundamental quantity needs to be defined: the reactivity

$$\rho = \frac{k_{\rm eff} - 1}{k_{\rm eff}} \,. \tag{11}$$

It should be noted that in thermal reactors the delayed neutron fraction typically contributes to a reactivity of approximately $650-700\,\mathrm{pcm}$, whereas in fast reactors this value is limited to about $200-300\,\mathrm{pcm}$.

2.4 The Effective Delayed Neutron Fraction $\hat{\beta}_{\text{eff}}$

The parameter β , commonly referred to as *delayed neutron fraction*, denotes the fraction of fission neutrons emitted with a delay, following the decay of specific fission products, rather than being released promptly at the moment of fission. It is a physical parameter that depends solely on the fissioning isotopes. On the other hand, the *effective delayed neutron fraction*, denoted as $\hat{\beta}_{\rm eff}$ (which constitutes the central focus of this thesis), incorporates both the production of delayed neutrons and their *importance* in the reactor system economy – i.e their contribution to the nuclear chain reaction. Although its difference from the parameter β may initially appear subtle, it is, in fact, of fundamental significance. In fact, $\hat{\beta}_{\rm eff}$ is not a fixed nuclear constant, but a reactorand configuration-dependent quantity that captures the spatial, spectral, and temporal characteristics of the neutron field.

2.4.1 Physical Interpretation of the Delayed Neutron Fraction $\hat{eta}_{ ext{eff}}$

The effective delayed neutron fraction associated with a specific *precursor family* (Section 2.3), denoted by $\hat{\beta}_{\text{eff,n}}$ – where the subscript n is consistently used throughout this work to identify a particular family – can be formally defined as [48]:

$$\hat{\beta}_{\text{eff,n}} = \frac{\int_{V} \int dE' \, \phi^{\dagger}(\vec{r}, E') \chi_{\text{n}}^{\text{d}}(E') \, \sum_{\text{i}} \int dE \, \beta_{\text{in}} \nu_{\text{i}}(E) \Sigma_{\text{f,i}}(\vec{r}, E) \phi(\vec{r}, E) \, d\vec{r}}{\int_{V} \int dE' \, \phi^{\dagger}(\vec{r}, E') \chi(E') \, \sum_{\text{j}} \int dE \, \nu_{\text{j}}(E) \Sigma_{\text{f,j}}(\vec{r}, E) \phi(\vec{r}, E) \, d\vec{r}} \,, \qquad (12)$$

where the macroscopic fission cross section Σ_f is defined as:

$$\Sigma_{\rm f}(\vec{r},E) = \sum_{\rm i} N_{\rm i}(\vec{r}) \sigma_{\rm f,i}(E) \,, \tag{13}$$

and an isotropic medium is assumed (thus eliminating the angular dependence of the flux and cross sections with respect to $\hat{\Omega}$).

By introducing a notation reminiscent of the Bra-Ket formalism, the integration over the full phase space can be compactly expressed using the angled brackets $\langle \ , \ \rangle$, where the comma separates two distinct energy variables (E' and E). This allows Equation 12 to be written in a more concise form:

$$\hat{\beta}_{\text{eff,n}} = \frac{\langle \phi^{\dagger} \chi_{\text{n}}^{\text{d}}, \, \beta_{\text{n}} \nu \Sigma_{\text{f}} \phi \rangle}{\langle \phi^{\dagger} \chi, \, \nu \Sigma_{\text{f}} \phi \rangle} = \frac{\langle \phi^{\dagger}, \mathbf{F}_{\text{d,n}} \phi \rangle}{\langle \phi^{\dagger}, \mathbf{F} \phi \rangle} \,. \tag{14}$$

The final equality introduces the *delayed neutron production operator* $\mathbf{F}_{d,n}$, which differs from the total fission source operator in that it includes only the delayed component associated with precursor family n, by considering the spectrum χ_n^d , and including the multiplicative factor β_n applied to the prompt fission source term $\nu \Sigma_f \phi$.

In order to clarify the physical meaning of the delayed neutron fraction $\hat{\beta}_{\rm eff,n}$, a step-by-step interpretation of the individual terms appearing in its definition is presented below, following an incremental approach:

- ν Average number of neutrons emitted per fission event Represents the mean number of secondary neutrons emitted during a single fission event.
- $\nu\Sigma_{\rm f}$ Fission neutron source Represents the total source of neutrons (both prompt and delayed) produced per unit length.
- $\beta_{\mathbf{n}}\nu\Sigma_{\mathbf{f}}$ Delayed neutron source from family n Denotes the portion of the total neutron source that originates from the precursors of family n.
- $\langle \phi^\dagger \chi_{\rm n}^{\rm d}, \, \beta_{\rm n} \nu \Sigma_{\rm f} \phi \rangle$ **Delayed fission source** This constitutes the numerator of the expression and represents the effective production (per unit of volume and time) of delayed neutrons from family n, weighted by the adjoint flux ϕ^\dagger , which encodes the importance of neutrons in phase space.
- $\langle \phi^{\dagger} \chi, \, \nu \Sigma_{\rm f} \phi \rangle$ **Total fission source** This forms the denominator and accounts for the total effective neutron production in the system, again weighted by the importance ϕ^{\dagger} .

 $\hat{eta}_{ ext{eff,n}}$ - **Complete expression** The overall ratio defines the effective delayed neutron fraction associated with precursor family n. It quantifies the relative contribution of that family to the system's reactivity. This metric accounts not only for the quantity of delayed neutrons produced (through the parameter β_n), but also for their energy and spatial distributions, as well as their overall importance within the reactor's economy.

2.4.2 Sensitivity Analysis of \hat{eta}_{eff}

As discussed in Section 2.3, the effective delayed neutron fraction, $\hat{\beta}_{\rm eff}$, plays a pivotal role in the analysis of reactor safety and control. This parameter becomes particularly critical in the context of advanced reactor systems (such as ALFRED) which employ MOX fuels. In such designs, reactor control tends to be more challenging due to the substantial presence of actinides, particularly plutonium isotopes, which are characterized by significantly lower values of $\hat{\beta}_{\rm eff}$.

The relevance of this parameter extends well beyond its nominal value. In fact, quantities such as $\hat{\beta}_{\text{eff}}$ are often directly involved in the definition of design safety margins, through their sensitivity and uncertainty (S/U) analysis performed during the stage of reactor design development [40].

However, the task of conducting sensitivity analysis for $\hat{\beta}_{\text{eff}}$ presents notable challenges, stemming from the greater physical and mathematical complexity involved in its definition, especially when compared to a quantity like the multiplication factor k_{eff} , which is more amenable from an S/U perspective.

While sensitivity analyses for $k_{\rm eff}$ can be effectively performed using the Standard Perturbation Theory (SPT) [40], this formalism does not extend naturally to more complex response functions such as $\hat{\beta}_{\rm eff}$. As shown in Equation 14, the effective delayed neutron fraction is defined as the ratio of two functionals, each dependent on the neutron flux ϕ , the importance ϕ^{\dagger} , and a combination of nuclear parameters. This structure renders SPT inapplicable for a rigorous evaluation of the delayed neutronfraction sensitivities, as it can be used for sensitivity calculation only if the observable considered is an eigenvalue (i.e. only for the effective multiplication factor $k_{\rm eff}$).

In such cases, the Generalized Perturbation Theory (GPT) [48] must be adopted. GPT extends the capabilities of standard sensitivity methods to response functions that are non-linear or non-homogeneous in the flux⁷, such as $\hat{\beta}_{\text{eff}}$, making it the only suitable theoretical framework for this kind of analysis.

⁷A functional is said to be *linear* if its response scales proportionally with the flux (i.e., $R(\phi_1+\phi_2)=R(\phi_1)+R(\phi_2)$), and homogeneous of first order if scaling the flux by a constant factor α yields $R(\alpha\phi)=\alpha R(\phi)$.

2.5 The Generalized Perturbation Theory

The techniques introduced by perturbation theories in the field of reactor physics play a central role in all aspects of sensitivity analysis. The strength of this mathematical tool lies in its remarkable versatility, understood as the ability to be applied to a wide variety of physical systems, ranging from cosmology to quantum mechanics. In fact, the fundamental problem addressed by perturbative approaches is exceptionally general in nature: to evaluate the variations of a quantity of interest induced by small perturbations applied to the variables of the system under consideration. Several formulations of perturbation theory have been developed, each tailored to address specific needs dictated by the characteristics of the problem at hand. The most relevant factors concern the nature of the parameter of interest to be analyzed and the approximations allowed by the type of perturbation being considered.

This work focuses on a perturbation approach classified as "first-order," consistent with the computational tools employed. This refers to the assumption that the perturbations introduced are sufficiently small so that the resulting variation in the output quantity can be evaluated solely on the basis of the unperturbed system and the magnitude of the perturbation. This avoids the need to explicitly compute perturbed states, resulting in a potentially significant reduction in computational cost.

When the first-order approximation is no longer valid – for instance, when perturbations are not small – higher-order formulations of perturbation theory must be used. These require knowledge of both perturbed and unperturbed states, and more detailed discussions of such methods can be found in [49].

From a mathematical standpoint, perturbation theories can generally be classified into three categories:

Differential Methods: based on the Taylor series expansion of the quantity of interest with respect to the input parameters, evaluating each partial derivative at the nominal point [50];

Variational Approaches: based on the optimization (typically minimization) of a response functional associated with the quantity of interest, subject to constraints usually derived from the governing physical equations [51];

Heuristic Approaches: based on the principle of the neutron importance conservation [52].

Although these three approaches are formally equivalent under appropriate assumptions, the variational method is adopted in this work, in accordance with the implementation of perturbation theories within the ERANOS code system.

2.5.1 First Order Formulation of the GPT using the Variational Approach

The perturbation (and thus the sensitivity) of quantities such as ratios of reaction rates or importance-weighted reaction rates with respect to state variables cannot be obtained through standard theory [48].

For simplicity (and in line with the assumptions adopted in the ERANOS calculations performed in this work), the reactor is assumed to operate under steady-state conditions, without external neutron sources, and to be critical. This assumption allows the use the Boltzmann equations in the form given by Equation 6 and Equation 7, and enables the calculation of sensitivities with respect to nuclear data of homogeneous functionals of degree zero with respect of the direct and adjoint fluxes. An example of such parameter is:

$$f = f(\sigma, \phi, \phi^{\dagger}) = \frac{\langle \phi^{\dagger}, \sigma_1 \phi \rangle}{\langle \phi^{\dagger}, \sigma_2 \phi \rangle},$$
 (15)

where, for convenience, σ denotes a set of input nuclear data σ_1 , σ_2 , etc., for which the following property holds:

$$f(\sigma, \lambda \phi, \mu \phi^{\dagger}) = f(\sigma, \phi, \phi^{\dagger}),$$
 (16)

for any scalar coefficients λ and μ . This property characterizes almost all linear and bilinear ratios typically encountered in critical reactor analysis.

Under these premises, the infinitesimal variation of this functional can be expressed as:

$$df = \langle \frac{\partial f}{\partial \sigma}, d\sigma \rangle + \langle \frac{\partial f}{\partial \phi}, d\phi \rangle + \langle \frac{\partial f}{\partial \phi^{\dagger}}, d\phi^{\dagger} \rangle. \tag{17}$$

As can be observed, besides the terms proportional to $d\sigma$, additional contributions arise that depend on the variations of both the direct neutron flux ($d\phi$) and the importance ($d\phi^{\dagger}$). This dependence is undesirable, as the goal of sensitivity analysis is to evaluate the response of integral reactor parameters solely as a function of perturbations in the input nuclear data, without requiring knowledge of how the fluxes themselves change under such perturbations.

Thus, the central idea behind the development of the GPT is to eliminate, at the mathematical level, the explicit dependence on flux variations, both direct or adjoint. Achieving this requires introducing a set of constraints equal in number to the terms that must be removed. For the physical system considered, these constraints correspond to the direct and adjoint Boltzmann equations, respectively:

$$(\mathbf{A} - \mathbf{F}/k_{\text{eff}})\phi = 0$$
 and $(\mathbf{A}^{\dagger} - \mathbf{F}^{\dagger}/k_{\text{eff}})\phi^{\dagger} = 0$. (18)

Under the imposed constraints, the Lagrange multipliers Ψ and Ψ^{\dagger} are introduced. Since they share the same dimensionality as the direct and adjoint fluxes ϕ and ϕ^{\dagger} ,

they are referred to as the generalized direct flux and generalized adjoint flux, or more generally as *generalized importances*.

On this basis, the constrained response functional R is defined, preserving the same physical interpretation as the original parameter of interest:

$$R = f(\sigma, \phi, \phi^{\dagger}) - \langle \Psi^{\dagger}, (\mathbf{A} - \frac{\mathbf{F}}{k_{\text{eff}}}) \phi \rangle - \langle \Psi, (\mathbf{A}^{\dagger} - \frac{\mathbf{F}^{\dagger}}{k_{\text{eff}}}) \phi^{\dagger} \rangle. \tag{19}$$

The subsequent step involves computing the differential of this constrained response functional:

$$dR = \langle \frac{\partial f}{\partial \sigma}, d\sigma \rangle + \langle \frac{\partial f}{\partial \phi}, d\phi \rangle + \langle \frac{\partial f}{\partial \phi^{\dagger}}, d\phi^{\dagger} \rangle +$$

$$- \langle \Psi^{\dagger}, d(\mathbf{A} - \frac{\mathbf{F}}{k_{\text{eff}}})\phi \rangle - \langle \Psi^{\dagger}, (\mathbf{A} - \frac{\mathbf{F}}{k_{\text{eff}}})d\phi \rangle +$$

$$- \langle \Psi, d(\mathbf{A}^{\dagger} - \frac{\mathbf{F}^{\dagger}}{k_{\text{eff}}})\phi^{\dagger} \rangle - \langle \Psi, (\mathbf{A}^{\dagger} - \frac{\mathbf{F}^{\dagger}}{k_{\text{eff}}})d\phi^{\dagger} \rangle$$

$$= \langle \frac{\partial f}{\partial \sigma}, d\sigma \rangle + \langle \frac{\partial f}{\partial \phi} - (\mathbf{A} - \frac{\mathbf{F}}{k_{\text{eff}}})\Psi^{\dagger}, d\phi \rangle +$$

$$+ \langle \frac{\partial f}{\partial \phi^{\dagger}} - (\mathbf{A}^{\dagger} - \frac{\mathbf{F}^{\dagger}}{k_{\text{eff}}})\Psi, d\phi^{\dagger} \rangle +$$

$$- \langle \Psi^{\dagger}, (d\mathbf{A} - \frac{d\mathbf{F}}{k_{\text{eff}}})\phi \rangle - \langle \Psi, (d\mathbf{A}^{\dagger} - \frac{d\mathbf{F}^{\dagger}}{k_{\text{eff}}})\phi^{\dagger} \rangle +$$

$$- \frac{dk_{\text{eff}}}{k_{\text{eff}}^2} \left(\langle \Psi^{\dagger}, \mathbf{F}\phi \rangle + \langle \Psi, \mathbf{F}^{\dagger}\phi^{\dagger} \rangle \right) .$$
(20)

Given the interpretation of the generalized fluxes Ψ and Ψ^{\dagger} as Lagrange multipliers, their value can be determined according to the computational requirements, provided that the *compatibility conditions* (see Equation 23 below) between the imposed perturbation and the physical behavior of the system are fulfilled.

By exploiting the degrees of freedom introduced by the generalized fluxes, these fluxes are required to satisfy the following equations:

$$\left(\mathbf{A}^{\dagger} - \frac{\mathbf{F}^{\dagger}}{k_{\text{eff}}}\right) \Psi^{\dagger} = \frac{\partial f}{\partial \phi} \,, \tag{21}$$

and

$$\left(\mathbf{A} - \frac{\mathbf{F}}{k_{\text{eff}}}\right)\Psi = \frac{\partial f}{\partial \phi^{\dagger}}.$$
 (22)

The compatibility conditions that must be satisfied, which are directly related to neutron balance in the system, are given by:

$$\left\langle \frac{\partial f}{\partial \phi}, \phi \right\rangle = 0 \quad \text{and} \quad \left\langle \frac{\partial f}{\partial \phi^{\dagger}}, \phi^{\dagger} \right\rangle = 0 \,, \tag{23}$$

and are associated respectively with Equation 21 and Equation 22. The terms on the right-hand side of these last two equations, namely $\frac{\partial f}{\partial \phi^{\dagger}}$ and $\frac{\partial f}{\partial \phi}$, are referred to as the generalized forward flux source Q and the generalized adjoint flux source Q^{\dagger} , respectively:

$$Q=rac{\partial f}{\partial \phi^{\dagger}}$$
 and $Q^{\dagger}=rac{\partial f}{\partial \phi}$ (24)

Among the advantages of considering the functional f, which is homogeneous of degree zero with respect to the fluxes, is that the compatibility conditions mentioned above are automatically satisfied as a direct consequence of Euler's theorem on homogeneous functions [48]. Specifically, for a generic homogeneous function of degree n (i.e. $f(\lambda x) = \lambda^n f(x)$), it holds that

$$\langle \frac{\partial f}{\partial x}, x \rangle = nf$$
 (25)

Having established this property, attention must be directed towards the non-uniqueness of the generalized fluxes Ψ and Ψ^{\dagger} . Indeed, for arbitrary scalars λ and λ^{\dagger} , the solutions to Equations 21 and 22 are not unique, since they admit the infinite family of solutions given by $(\Psi - \lambda \phi)$ and $(\Psi^{\dagger} - \lambda^{\dagger} \phi^{\dagger})$, respectively.

The adopted approach to uniquely determine these generalized fluxes consists of first selecting particular solutions Ψ_0 and Ψ_0^{\dagger} , and then fixing λ and λ^{\dagger} so as to enforce orthogonality of the generalized fluxes with respect to the fluxes ϕ^{\dagger} and ϕ , namely:

$$\langle \Psi^\dagger, {\bf F} \phi \rangle = 0 \quad \text{and} \quad \langle \Psi, {\bf F}^\dagger \phi^\dagger \rangle = 0 \,. \tag{26}$$

This procedure removes the perturbation term proportional to $dk_{\rm eff}$ from the differential expression dR (see Equation 20). Accordingly, the generalized fluxes are defined as:

$$\Psi = \Psi_0 - \lambda \phi$$
, such that $\langle \Psi, \mathbf{F}^{\dagger} \phi^{\dagger} \rangle = 0 \Rightarrow \lambda = \frac{\langle \phi^{\dagger}, \mathbf{F}^{\dagger} \Psi_0 \rangle}{\langle \phi^{\dagger}, \mathbf{F} \phi \rangle}$ (27)

and

$$\Psi^\dagger = \Psi_0^\dagger - \lambda^\dagger \phi^\dagger \,, \quad \text{such that} \quad \langle \Psi^\dagger, \mathbf{F} \phi \rangle = 0 \quad \Rightarrow \lambda = \frac{\langle \Psi_0^\dagger, \mathbf{F} \phi \rangle}{\langle \phi^\dagger, \mathbf{F} \phi \rangle} \tag{28}$$

Building on these arguments, the infinitesimal variation of the homogeneous functional $f(\sigma,\phi,\phi^{\dagger})$, which is of degree zero with respect to the fluxes ϕ and ϕ^{\dagger} and subject to the constraints imposed by the Boltzmann equations $(\mathbf{A} - \mathbf{F}/k_{\mathrm{eff}})\phi = 0$ and

 $(\mathbf{A}^{\dagger} - \mathbf{F}^{\dagger}/k_{\text{eff}})\phi^{\dagger} = 0$, can be expressed as follows:

$$\begin{cases} df = \langle \frac{\partial f}{\partial \sigma}, d\sigma \rangle - \langle \Psi^{\dagger}, (d\mathbf{A} - d\mathbf{F}/k_{\text{eff}})\phi \rangle - \langle \Psi, (d\mathbf{A}^{\dagger} - d\mathbf{F}^{\dagger}/k_{\text{eff}})\phi^{\dagger} \rangle \\ \left(\mathbf{A}^{\dagger} - \frac{\mathbf{F}^{\dagger}}{k_{\text{eff}}} \right) \Psi^{\dagger} = \frac{\partial f}{\partial \phi}, & \text{with} \quad \langle \Psi^{\dagger}, \mathbf{F}\phi \rangle = 0 \\ \left(\mathbf{A} - \frac{\mathbf{F}}{k_{\text{eff}}} \right) \Psi = \frac{\partial f}{\partial \phi^{\dagger}}, & \text{with} \quad \langle \Psi, \mathbf{F}^{\dagger}\phi^{\dagger} \rangle = 0 \end{cases}$$
(29)

Here, the equivalence between dR and df has been employed to write the expression in the first line of the system. The first term on the right-hand side of the same equation is referred to as the *direct sensitivity term*, while the remaining two terms represent the *indirect terms*.

Despite the mathematical abstraction underlying the present formulation, interpreting the results summarized in Equation 29 from a physical perspective is straightforward. In particular, it can be observed that:

- the direct term represents the component of the perturbation of the parameter of interest caused solely by the small variation of an input parameter;
- the **indirect term** exclusively reflects the perturbation of the parameter of interest due to the side effects experienced by the system (e.g. the variations induced in the flux and the importance) as a consequence of the same small variation of the considered input parameter.

The use of GPT offers numerous advantages, particularly in terms of efficiency and interpretability, when compared to other perturbation techniques (see for example the one discussed in Section 4.2.2).

The fundamental basis of this enhanced computational efficiency is the introduction of generalized fluxes. Physically, these mathematical constructs are analogous to neutron importance functions, but are defined within the sensitivity framework: a locally high generalized flux indicates that a perturbation in that region has a strong impact on the response. The key advantage of generalized fluxes lies in their computational reuse; once calculated, they enable the evaluation of the effects of multiple perturbations without necessitating repeated full system resolutions.

2.5.2 GPT application on $\hat{eta}_{ ext{eff}}$

The objective of applying the GPT to the effective delayed neutron fraction, $\hat{\beta}_{\rm eff}$, is to derive a formally consistent expression for its sensitivity coefficients with respect to a generic input parameter α . This approach is particularly advantageous, as GPT provides a unified mathematical framework that yields multiple sensitivity coefficients from a

single transport solution, significantly reducing computational cost while enhancing the interpretability and traceability of the results.

The aim is to establish a general formulation that provides the foundation for the development of parameter-specific expressions tailored to the various input quantities considered in this work. To this end, the analysis begins by examining the perturbation of the effective delayed neutron fraction associated with a single precursor family, $\hat{\beta}_{\rm eff,n}$, as defined in Equation 14. The corresponding response functional, subject to the constraints imposed by the direct and adjoint Boltzmann equations, can be written as:

$$R = \hat{\beta}_{\text{eff,n}} - \langle \Psi^{\dagger}, \left(\mathbf{A} - \frac{\mathbf{F}}{k_{\text{eff}}} \right) \phi \rangle - \langle \Psi, \left(\mathbf{A}^{\dagger} - \frac{\mathbf{F}^{\dagger}}{k_{\text{eff}}} \right) \phi^{\dagger} \rangle$$
 (30)

Imposing the independence of R from the fluxes ϕ and ϕ^{\dagger} leads to the stationarity conditions:

$$rac{\partial R}{\partial \phi}=0 \quad {
m and} \quad rac{\partial R}{\partial \phi^\dagger}=0 \, .$$
 (31)

Focusing on the first of these conditions, and substituting the definition of R from Equation 30, yields:

$$\frac{\partial \hat{\beta}_{\text{eff,n}}}{\partial \phi} - \left(\mathbf{A}^{\dagger} - \frac{\mathbf{F}^{\dagger}}{k_{\text{eff}}} \right) \Psi^{\dagger} = 0. \tag{32}$$

After normalization with respect to $\hat{\beta}_{\mathrm{eff},n}$ and rearrangement of terms, the relation becomes:

$$\left(\mathbf{A}^{\dagger} - \frac{\mathbf{F}^{\dagger}}{k_{\text{eff}}}\right) \tilde{\Psi}_{n}^{\dagger} = \frac{1}{\hat{\beta}_{\text{eff,n}}} \frac{\partial \hat{\beta}_{\text{eff,n}}}{\partial \phi}, \tag{33}$$

where the definition $\tilde{\Psi}_n^\dagger = \Psi^\dagger/\hat{\beta}_{eff,n}$ has been introduced. By computing the derivative on the right-hand side of the equation, the expression for the source term of the generalized adjoint flux is obtained, namely:

$$\left(\mathbf{A}^{\dagger} - \frac{\mathbf{F}^{\dagger}}{k_{\text{eff}}}\right) \tilde{\Psi}_{n}^{\dagger} = \frac{\left[\phi^{\dagger} \chi_{n}^{\text{d}}\right] \beta_{n} \nu \Sigma_{f}}{\left\langle \phi^{\dagger} \chi_{n}^{\text{d}}, \beta_{n} \nu \Sigma_{f} \phi \right\rangle} - \frac{\left[\phi^{\dagger} \chi\right] \nu \Sigma_{f}}{\left\langle \phi^{\dagger} \chi, \nu \Sigma_{f} \phi \right\rangle}, \tag{34}$$

where the convention has been introduced that square brackets $[\cdot]$ denote integration over the entire energy spectrum. In a completely analogous manner, the expression for the source term of the generalized forward flux is derived, which takes the form:

$$\left(\mathbf{A} - \frac{\mathbf{F}}{k_{\text{eff}}}\right)\tilde{\Psi}_{n} = \frac{\chi_{n}^{d} \left[\beta_{n} \nu \Sigma_{f} \phi\right]}{\left\langle \phi^{\dagger} \chi_{n}^{d}, \beta_{n} \nu \Sigma_{f} \phi\right\rangle} - \frac{\chi \left[\nu \Sigma_{f} \phi\right]}{\left\langle \phi^{\dagger} \chi, \nu \Sigma_{f} \phi\right\rangle}, \tag{35}$$

where the definition $\tilde{\Psi}_n = \Psi/\hat{\beta}_{\mathrm{eff},n}$ has been used. Under these assumptions, the sensitivity coefficient of the parameter $\hat{\beta}_{\mathrm{eff},n}$ with respect to a generic input parameter

 α can be defined as:

$$S\left(\hat{\beta}_{\rm eff,n},\alpha\right) = \frac{\alpha}{\hat{\beta}_{\rm eff,n}} \frac{\delta \hat{\beta}_{\rm eff,n}}{\delta \alpha} \simeq \frac{\alpha}{\hat{\beta}_{\rm eff,n}} \frac{\partial R}{\partial \alpha}, \tag{36}$$

where the variation ratio $\delta\hat{\beta}_{\mathrm{eff,n}}/\delta\alpha$ is approximated by the partial derivative of the constrained response functional R with respect to the parameter α . By substituting into this definition the expression of R given in Equation 30, the sensitivity coefficient can then be evaluated in terms of the generalized fluxes Ψ and Ψ^{\dagger} and the perturbation of the operators with respect to α :

$$S\left(\hat{\beta}_{\text{eff,n}},\alpha\right) = \frac{\alpha}{\hat{\beta}_{\text{eff,n}}} \left\{ \frac{\partial \hat{\beta}_{\text{eff,n}}}{\partial \alpha} - \langle \Psi^{\dagger}, \left(\frac{\partial \mathbf{A}}{\partial \alpha} - \frac{1}{k_{\text{eff}}} \frac{\partial \mathbf{F}}{\partial \alpha}\right) \phi \right\} - \langle \Psi, \left(\frac{\partial \mathbf{A}^{\dagger}}{\partial \alpha} - \frac{1}{k_{\text{eff}}} \frac{\partial \mathbf{F}^{\dagger}}{\partial \alpha}\right) \phi^{\dagger} \rangle \right\}.$$
(37)

The resulting expression clearly shows that the general formula for the sensitivity coefficients (in this case, relative sensitivities, due to the normalization with respect to $\hat{\beta}_{\mathrm{eff,n}}$) consists of three distinct contributions: a direct term and two indirect terms. These components correspond to those introduced and discussed in Section 2.5.1, and collectively describe how the perturbation of the input parameter α propagates through both the direct and adjoint physical models to influence the delayed neutrons fraction $\hat{\beta}_{\mathrm{eff,n}}$.

It should be noted that, at this stage, the initial objective of deriving an expression for the sensitivity coefficients of $\hat{\beta}_{\text{eff}}$ with respect to the generic parameter α can be considered as effectively accomplished. Indeed, the total sensitivity coefficient can be expressed in terms of the previously derived quantities $S(\hat{\beta}_{\text{eff.n}}, \alpha)$ as follows:

$$S(\hat{\beta}_{\text{eff}}, \alpha) = \frac{\alpha}{\hat{\beta}_{\text{eff}}} \frac{\delta \hat{\beta}_{\text{eff}}}{\delta \alpha} = \frac{\alpha}{\hat{\beta}_{\text{eff}}} \sum_{n} \frac{\delta \hat{\beta}_{\text{eff,n}}}{\delta \alpha} = \sum_{n} \frac{\hat{\beta}_{\text{eff,n}}}{\hat{\beta}_{\text{eff}}} S(\hat{\beta}_{\text{eff,n}}, \alpha),$$
(38)

where, to obtain the last equality, Equation 36 was used to express the ratio $\delta \hat{\beta}_{\rm eff,n}/\delta \alpha$. As can be readily observed, the total sensitivity coefficient is obtained as a weighted sum of the individual contributions associated with each precursor family n, where the weighting factor $\hat{\beta}_{\rm eff,n}/\hat{\beta}_{\rm eff}$ represents the relative contribution of each family to the total effective delayed neutron fraction. This decomposition highlights the role of each precursor family in the overall sensitivity of $\hat{\beta}_{\rm eff}$ to the input parameter α , and emphasizes how the family-wise sensitivities $S(\hat{\beta}_{\rm eff,n},\alpha)$ collectively determine the global response.

3 ERANOS: Computational Framework and Implementation Details

Within the GPT framework, fundamental nuclear data such as cross sections, neutron sources, flux distributions, integral quantities, and kinetic parameters constitute the essential input for the evaluation of system response variations and sensitivity coefficients. The European Reactor ANalysis Optimized System (ERANOS) provides dedicated computational modules for the generation and storage of these quantities, organizing them into Evaluated Data Libraries (EDLs) to ensure consistent access and integration within the broader calculation chain.

In the context of the present work, particular emphasis is placed on the calculation of the effective delayed neutron fraction, $\hat{\beta}_{\rm eff}$, a key kinetic parameter that plays a crucial role in reactor safety and dynamic behavior. Accurate sensitivity analysis of $\hat{\beta}_{\rm eff}$ requires a consistent and detailed description of the underlying nuclear data and model parameters. Therefore, understanding how ERANOS generates, structures, and stores such data is a prerequisite for ensuring the reliability of subsequent perturbation-based evaluations.

This section provides an overview of the procedures used within ERANOS to generate and manage these quantities, with particular emphasis on the aspects most relevant to GPT-based analyses and their application to the sensitivity characterization of the effective delayed neutron fraction $\hat{\beta}_{\rm eff}$ in reactor systems.

3.1 Computational Paradigms in Neutron Transport: Deterministic and Monte Carlo Approaches

The study of the sensitivity of the delayed neutron fraction $\hat{\beta}_{\text{eff}}$ necessarily involves the resolution of the neutron transport equation (Equation 2), which describes the behavior of neutrons within a medium.

Due to the high level of complexity inherent in this equation – as can be seen from its integro-differential form presented in Section 2.2 – an analytical solution is only feasible in highly simplified cases. Therefore, its application to realistic reactor configurations requires the adoption of numerical methods.

To this end, various computational codes have been developed, which can be classified into two main categories depending on their nature:

Deterministic Codes: These codes solve the neutron transport equation using numerical methods based on the discretization of the 6-dimensional phase space, consisting of spatial, energy, and angular variables.

This involves subdividing the reactor volume into discrete mesh elements defined by a spatial grid; discretizing the energy domain (typically going from 0 to 20 MeV) into spectral intervals optimized to capture the system's integral behavior; reducing the angular domain to a finite set of discrete directions.

The simplified nuclear system obtained from this approximation can then be solved using several techniques, the most common of which include:

- the discrete ordinates method, commonly referred to as the $S_{\rm N}$ method where S denotes angular segmentation and the subscript N specifies the number of discrete directions used. This is the approach adopted in this work for neutron flux calculations; further details are provided in Appendix A;
- the spherical harmonics expansion (P_N), which is based on the projection of the angular flux on spherical harmonics, and the approximation of that expansion by limiting it to the first N harmonics [51];
- the diffusion approximation to the transport equation [53].

These codes yield a deterministic average solution, i.e. a continuous estimate of the variables of interest, free from statistical noise. The accuracy of the solution strongly depends on the discretization choices, such as the number of energy groups, angular directions, and spatial resolution.

Stochastic Codes: In contrast, stochastic codes solve the transport problem using probabilistic simulations based on the Monte Carlo method [54].

In this approach, neutron transport is modeled by simulating the trajectories of a large number of individual neutrons, each of which interacts with the material according to probabilistic laws derived from nuclear data.

This strategy allows the neutron transport equation to be solved regardless of the geometric complexity of the model, without requiring energy group condensation or angular discretization, and enabling the use of pointwise nuclear data.

However, the statistical nature of the method introduces stochastic noise into the results, which can only be reduced by increasing the number of simulated particles, leading to increased computational time.

In the context of this thesis, deterministic codes (in particular, ERANOS) are preferred over their stochastic counterparts, as they are better suited for systematic studies, such as design optimization or sensitivity analysis of nuclear systems. This preference stems from their numerical stability and computational efficiency.

3.2 General Architecture and Functional Overview of ERANOS

Jointly developed by the major European nuclear research institutions as a comprehensive computational suite for reactor physics, the strengths of the deterministic code ERANOS lie in its high degree of modularity and operational flexibility [55].

It encompasses a wide range of applications, including core operation simulation, the effects of refueling and of control and safety devices, as well as neutron shielding analysis and advanced analyses performed on computed flux and reaction rate distributions – such as sensitivity analysis, which is the focus of this study.

These characteristics allow, on the one hand, for the flexible evolution of the code over time through the integration of new functionalities, and on the other hand, they provide users with the ability to overcome the intrinsic code limitations by employing dedicated routines developed in the ERANOS metalinguistic interface "LU" (Language Utilisateur). These user-defined routines make it possible to configure and interconnect modules in various ways, enabling the construction of specific analytical sequences as required. Thanks to these features, ERANOS is particularly well suited for performing neutronic characterization of nuclear reactor cores under both static and transient conditions.

Considering the latest version of ERANOS (version 2.3N), the code provides a comprehensive framework for reactor physics analysis, supporting a wide range of neutronic calculations including core modeling, fuel cycle studies, shielding evaluations, and perturbation-based methods for sensitivity and uncertainty analysis. It also includes the European Cell COde (ECCO [55]), designed for detailed cell-level calculations. These consist in the accurate modeling of individual fuel or structural cells within a reactor lattice, typically involving the solution of the neutron transport equation over a representative geometry to produce homogenized cross sections for use in subsequent reactor physics calculations.

ECCO processes evaluated nuclear data libraries using a high-resolution energy grid, with up to 1968 energy groups, in order to accurately resolve resonance structures and generate group-wise cross sections. The resulting condensed and self-shielded cross sections serve as input for reactor-scale transport or diffusion calculations, commonly referred to as core-level analyses, where the spatial and spectral behavior of the neutron flux is evaluated over the entire reactor geometry.

3.2.1 Computational Workflow and Multi-Level Structure of ERANOS

Due to the intrinsic complexity of solving the neutronic transport equation, it is essential to find a compromise between result accuracy and computational costs in terms of time and resources. To address this need, the general computational sequence of ERANOS can be described as developed in three levels (see the schematic illustration in Figure 6), which are distinguished from one another based on the following characteristics:

Nuclear data level

This stage involves processing nuclear data from evaluated libraries by condensing continuousenergy cross sections into a standardized, problem-independent multi-group format (see the concluding part of Section 3.2). This discretization facilitates the efficient treatment of nuclear interactions in subsequent reactor physics calculations, ensuring an accurate representation of energy-dependent phenomena while preserving computational feasibility.

It constitutes the foundational step for all subsequent computational operations, as the nuclear data libraries contain the complete information on neutron-isotope interactions.

The primary objective at this level is to transform the nuclear data extracted from evaluated libraries into a format compatible with ERANOS. To this end, the processed data are organized according to the ECCOLIB [56] format, a dedicated library structure designed to store multi-group cross sections alongside the probability tables necessary for the sub-group method employed at the cell level by ECCO. This conversion process encompasses not only data reformatting but also essential transformations, such as collapsing continuous-energy data into discrete energy groups and generating the relevant probability tables. Therefore, specialized processing codes [57, 58] are utilized to guarantee that the resulting ECCOLIB libraries faithfully represent microscopic nuclear interactions in a form suitable for reactor physics calculations within ERANOS.

Cell level

This stage begins with the definition of elementary cells representing fuel assemblies, aimed at accurately capturing the key physical effects arising from the heterogeneous structure of the system under investigation. The evaluated nuclear data, previously processed into multi-group libraries, provide the input for these cell-level calculations. At this point, the ECCO module performs detailed neutron transport simulations within each cell, producing microscopic and macroscopic cross sections that account for spatial and material heterogeneities.

Following the generation of these cross sections, the structural details of each cell are homogenized, and the ultra-fine energy discretization is collapsed into a coarser group structure, yielding effective cross sections suitable for subsequent core-level analyses. Throughout the condensation and homogenization processes, physical consistency is maintained by ensuring the preservation of global reaction rates.

The primary purpose of this intermediate step is therefore to reduce the complexity inherent in continuous-energy data and heterogeneous geometries, while preserving

⁸Although the original nuclear data libraries provide physical data over a continuous energy spectrum, ERANOS operates exclusively with multi-group representations.

the essential physical information required for accurate core-level calculations. Further details on ECCO can be found in Section 3.3.

Core level

At this stage, the entire reactor core is modeled, with heterogeneity considered only at the level of different assembly types. The neutron transport equation is solved by associating the macroscopic cross-section data derived at the cell level with the corresponding homogeneous regions defined within a user-specified spatial mesh representing the reactor geometry. This approach enables an efficient yet accurate simulation of neutron flux distribution across the core.

Specialized modules are incorporated to build a comprehensive system model that faithfully reproduces the reactor's physical behavior under operational conditions. These modules account for important phenomena such as Doppler broadening of resonance cross sections, core thermal expansion, changes in isotopic composition due to fuel burn-up, control rod insertion effects, and feedback mechanisms influencing reactivity and power distribution over time.

Furthermore, this level supports sensitivity and uncertainty analyses, allowing the assessment of how variations in nuclear data, operating parameters, or modeling assumptions impact key reactor performance indicators. By integrating these effects, the corelevel calculations provide reliable predictions of reactor behavior essential for safety analysis, fuel management, and operational planning. The specific modules employed in this work are described in detail in Section 3.4.

3.3 The ECCO Cell Code

ECCO is used to perform cell-level calculations aimed at producing homogenized and condensed cross-section libraries tailored to a specific system, starting from fine-group nuclear data sources (e.g., JEFF or ENDF/B via ECCOLIB). These cell calculations are typically applied to assemblies or representative portions thereof, enabling efficient reactor-scale analysis.

A cell calculation in ECCO involves two key operations:

• Energy group condensation: Fine-group microscopic cross sections are collapsed into a coarse multi-group structure using flux weighting. For example, a macroscopic cross section in broad group G is computed as:

$$\Sigma_{\mathbf{x},\mathbf{z}}^{\mathbf{G}} = \frac{\sum_{\mathbf{g} \in \mathbf{G}} \Sigma_{\mathbf{x},\mathbf{z}}^{\mathbf{g}} \phi_{\mathbf{z}}^{\mathbf{g}}}{\sum_{\mathbf{g} \in \mathbf{G}} \phi_{\mathbf{z}}^{\mathbf{g}}}$$
(39)

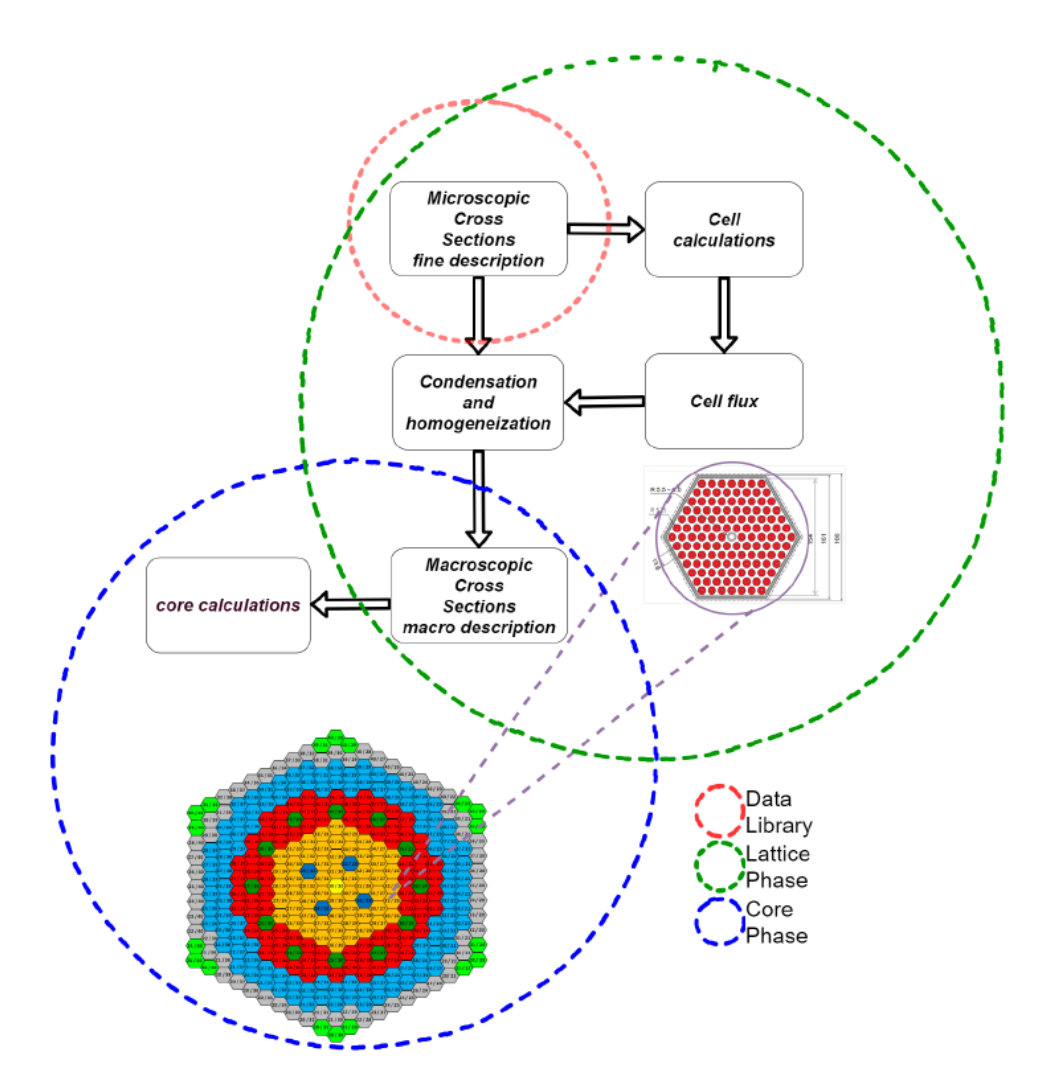


Figure 6: Representation of the general computational scheme of ERANOS, highlighting the three calculation phases and their intersections. [37]

where the indices x,i, and z indicate respectively the reaction type, the isotope, and the cell region considered; g identifies a specific group in the fine energy structure contained within the broad energy group labeled with G; ϕ denotes the flux, and in particular it holds that $\phi_{\rm z}^{\rm G} = \sum_{{\rm g} \in {\rm G}} \phi_{\rm z}^{\rm g}$, which represents the formula adopted for flux condensation.

 Material homogenization: Material compositions and number densities across subregions are combined into homogenized values under the coarse-group flux distribution. For example, a microscopic cross section for reaction x of isotope i in broad energy group G can be homogenized as:

$$\sigma_{\mathrm{x,i}}^{\mathrm{G}} = \frac{\sum_{\mathrm{z}} \sigma_{\mathrm{x,iz}}^{\mathrm{g}} V_{\mathrm{z}} N_{\mathrm{iz}} \phi_{\mathrm{z}}^{\mathrm{g}}}{\left(\sum_{\mathrm{z}} V_{\mathrm{z}} \phi_{\mathrm{z}}^{\mathrm{g}}\right) \left(\sum_{\mathrm{z}} V_{\mathrm{z}} N_{\mathrm{iz}} / \sum_{\mathrm{z}} V_{\mathrm{z}}\right)} \tag{40}$$

where the volume V, the homogenized flux $\phi^{\rm g}=\sum_{\rm z}V_{\rm z}\phi^{\rm g}_{\rm z}/V$, and the homogenized number density $N_{\rm i}=\sum_{\rm z}V_{\rm z}N_{\rm iz}/V$ are defined.

The calculation methods adopted by ECCO for determining the flux differ depending on the type of cell considered (homogeneous or heterogeneous), and would require an in-depth discussion that lies beyond the scope of this work. For further details, the reader is referred to the ECCO manual [59].

ECCO supports different geometric cell descriptions using a hierarchical "link" structure. Links may be OD, 1D, or 2D with appropriate base geometries (e.g. homogeneous, planar, cylindrical, square, hexagonal lattices). Materials are defined at specified temperature, with options for temperature effects. Boundary conditions – such as vacuum or reflection – are applied at the outer surfaces of the cell as needed.

Reactor-scale calculations utilize the homogenized and condensed cross sections to reduce computational cost and enhance numerical stability. This approach is particularly well-suited for deterministic methods – such as $S_{\rm N}$ or $P_{\rm N}$ – which inherently require the definition of energy groups. Moreover, the use of a reduced number of energy groups contributes to greater numerical stability, as the fine-scale fluctuations of the cross sections are already accounted for during the nuclear data processing stage. Specifically, phenomena such as Doppler broadening and self-shielding are incorporated into the generation of multi-group cross-section libraries, effectively smoothing out energy-dependent variations and ensuring consistent behavior in the reactor-scale calculations. These considerations also justify the homogenization of the material properties within the unit cell model.

3.3.1 ECCO-ERANOS Interface

This section provides an overview of the function responsible for generating the three fundamental EDLs from an ECCO file. The function, designated BASIC_EDL_CREATION_

STARTING_FROM_ECCO_FILE⁹, serves as the critical interface between cell-level and core-level calculations, producing the essential data required for all subsequent ERA-NOS computations.

The module outputs three distinct types of EDLs, described as follows:

MICRO: Contains microscopic cross-section data σ (expressed in barns, where $1~b=10^{-24}~\rm cm^2$), defined for each isotope, energy group, reactor or core zone, and reaction type.

MACRO: Contains macroscopic cross-section data Σ , as defined in Section 2.4.1. Within ERANOS, Σ is expressed in units of cm⁻¹ for each combination of energy group, spatial zone, and reaction.

MEDIUM: Contains material composition and related information necessary for the definition of the system.

During the generation of these outputs, the user must specify the list of reactions to be considered from the ECCO files. Consequently, the data produced correspond to the so-called *sections* of both the MICRO and MACRO libraries. These sections include, but are not limited to, total, capture, and fission cross-sections, the product of the average neutron yield per fission and the fission cross-section ($\nu\Sigma_{\rm f}$), as well as the fission spectrum (normalized to unity).

3.4 Neutronic Data Analysis Modules

The ERANOS neutronic calculation suite provides a broad set of validated computational modules for reactor core analysis. Within the context of this thesis, particular attention is devoted to a subset of these modules that enable the evaluation of integral quantities derived from the neutron flux and reaction rate distributions, such as those involved in sensitivity analysis. Therefore, this section focuses on describing the specific ERANOS modules that were directly employed or extended in the development of the computational procedures presented in this work (as comprehensively detailed in Chapter 4). For a complete and exhaustive description of all ERANOS functionalities, the reader is referred to the official documentation of version 2.3 [48].

3.4.1 Module for the Calculation of MACRO EDLs

The module MACRO_CALCULATION can be employed for the following purposes:

⁹In this work, ERANOS module names are consistently typeset in monospace font to distinguish them from the surrounding text.

- to generate a MACRO EDL starting from a MICRO EDL, provided in input together with a medium EDL (or a concentration EDL containing burn-up data), from which the initial isotopic concentrations are extracted;
- to update an existing MACRO EDL by supplying a consistent set of macroscopic and concentration data;
- to produce partial MACRO EDLs limited to a user-defined subset of isotopes.

Macroscopic cross-sections are generally calculated using Equation 13, which is reproduced below for convenience:

$$\Sigma_{\rm g} = \sum_{\rm i} N_{\rm i} \, \sigma_{\rm i,g} \,, \tag{41}$$

where $N_{\rm i}$ denotes the atomic density of isotope i, and $\sigma_{\rm i,g}$ represents the corresponding microscopic cross-section in energy group g.

In particular, the macroscopic fission spectrum $\chi_{\rm gz}$ in region z is evaluated through the following relation:

$$\chi_{\rm gz} = \frac{\sum_{\rm i} \chi_{\rm igz} \sum_{\rm g} (\nu \sigma_{\rm f})_{\rm igz} N_{\rm iz} \phi_{\rm gz}}{\sum_{\rm g} (\nu \Sigma_{\rm f})_{\rm gz} \phi_{\rm gz}}, \tag{42}$$

where χ_{igz} denotes the microscopic fission spectrum of isotope i in region z, $(\nu\sigma_f)_{igz}$ is the product of the average number of neutrons emitted per fission and the microscopic fission cross-section, and $(\nu\Sigma_f)_{gz}$ is its macroscopic equivalent. The quantities N_{iz} and ϕ_{gz} represent, respectively, the atomic density of isotope i and the group-wise neutron flux in region z, the latter obtained during the cell-level calculation and stored for each medium in the MICRO set.

The sections included in the resulting MACRO will match those present in the corresponding MICRO (with the necessary differences discussed in Section 3.3.1) or in the MACRO provided as input, unless the user explicitly specifies a list of sections to be considered. A similar selection mechanism is available for the isotopes to be included in the MACRO generation: unless explicitly defined by the user, all isotopes present in the input MICRO will be considered. Concentrations, on the other hand, are selected from the medium EDL, or selected in the concentration EDL if such a set is provided.

3.4.2 Modules for the Evaluation of Source Distributions

Prior to introducing the module responsible for generating source distributions employed in generalized importance calculations – namely, IMPORTANCE_CALCULATION_ SOURCE_CREATION – it is essential to clarify the nature and role of source terms already embedded within the flux EDLs, which accompany the stored neutron flux data.

Specifically, for each spatial volume element m with volume $V_{
m m}$, the flux EDL contains a quantity denoted as the total source, whose definition depends on whether the calculation is performed in the forward or adjoint mode:

$$V_{
m m} \sum_{
m g=1}^{
m G}
u \Sigma_{
m f,g} \phi_{
m g} \,, \quad {
m for the forward calculation} \,; \qquad \qquad (43)$$

$$\sum_{
m g=1}^{
m G} \chi_{
m g} \phi_{
m g}^{\dagger} \,, \quad {
m for the adjoint calculation} \,, \qquad \qquad (44)$$

$$\sum_{\mathrm{g}=1}^{\mathrm{G}} \chi_{\mathrm{g}} \phi_{\mathrm{g}}^{\dagger} \,, \quad ext{for the adjoint calculation} \,,$$

where G is the total number of energy groups, $\phi_{\rm g}$ and $\phi_{\rm g}^{\dagger}$ denote the forward and adjoint neutron fluxes in group g, respectively, $\nu\Sigma_{\rm f,g}$ is the product of the average number of neutrons produced per fission and the macroscopic fission cross-section in group g, and $\chi_{\rm g}$ is the corresponding fission neutron spectrum.

In the forward case (Equation 43), the total source is scaled by the volume of the spatial element, thus having units of neutrons per second. This unit convention is consistent with the source terms generated by the IMPORTANCE_CALCULATION_SOURCE_ CREATION module, discussed subsequently. Conversely, the adjoint source (Equation 44) is stored as a dimensionless quantity, since no volumetric scaling is applied.

This distinction between the sources associated with forward and adjoint fluxes enables ERANOS to efficiently compute bilinear integrals involving products of forward and adjoint flux functions (see Section 3.4.4), using these total sources directly extracted from the corresponding fluxes, without requiring explicit geometric information of the reactor configuration [48].

The sources generated via the IMPORTANCE_CALCULATION_SOURCE_CREATION module are constructed by combining neutron flux distributions with relevant cross-section data. 10 Input data consist of flux EDLs (either forward or adjoint) and cross-section data, which can be obtained directly from a MACRO EDL, derived from a MICRO EDL combined with a medium EDL, or specified manually by the user through explicit numerical values.

As previously noted, the resulting source terms are expressed in physical units of neutrons per second (n/s). This arises because the source values represent the product of the source density (in $n/s/cm^3$) and the volume of each spatial mesh element (in cm³). It is important to highlight that the source EDLs generated by this procedure share the same structural format as the flux EDLs, but store group-wise source values by default. Furthermore, when accessed from their respective data segments within the EDL, the arrays containing source values and scalar fluxes possess identical dimensionality, corresponding to the number of spatial volume elements defined by the computational mesh.

¹⁰The term "cross-section" is understood broadly here to include other section-like quantities present in the MICRO and MACRO EDLs, such as the fission neutron spectrum.

3.4.3 Module for the Evaluation of Flux Distributions

When computing a flux with the procedure RECTANGULAR_SN_TRANSPORT_ITERATION, ERANOS outputs two distinct quantities:

Angular flux $\phi_{\rm n}(\vec{r}, E, \vec{\Omega}_{\rm n})$ represents the number of neutrons at position \vec{r} , with energy E, and traveling in the direction $\vec{\Omega}_{\rm n}$, which belongs to a discrete set of vectors used to approximate the solid angle as described in Appendix A.

Scalar Flux $\phi(\vec{r},E)$ corresponds to the weighted sum of the discrete angular fluxes, and is given by:

$$\phi(\vec{r}, E) = \sum_{\rm n=1}^{\rm N} w_{\rm n} \phi_{\rm n}(\vec{r}, E, \vec{\Omega}_{\rm n}),$$
 (45)

where the coefficients w_{n} are those defined in Equation 167.

The role of these quantities in sensitivity analysis, particularly when conducted within frameworks such as GPT, is both diverse and fundamental. The classification of fluxes considered in this context distinguishes two categories: direct (ϕ) and adjoint (ϕ^\dagger) fluxes, which are solutions to homogeneous Boltzmann equations; and generalized importances $(\tilde{\Psi}_n$ and $\tilde{\Psi}_n^\dagger)$, obtained from solutions to non-homogeneous Boltzmann equations. Accordingly, the methodology employed by ERANOS for computing these quantities is presented separately for each case, both of which are characterized by iterative solution processes.

Homogeneous calculation The direct and adjoint fluxes computed in ERANOS are the result of an iterative process whose essence can be analytically expressed by the following system:

$$\begin{cases} S_{i} = \frac{\mathbf{F}\phi_{i}}{k_{\text{eff,i}}} \\ \mathbf{A}\phi_{i+1} = S_{i} \\ k_{\text{eff,i+1}} = \frac{\langle \mathbf{F}\phi_{i+1} \rangle}{\langle \mathbf{A}\phi_{i+1} \rangle} \end{cases}$$
(46)

This computational cycle is composed of what are referred to as "outer iterations". In fact, as can be observed, the relation appearing at the center of the system

$$\mathbf{A}\phi_{i+1} = S_i \,, \tag{47}$$

is itself iterative and involves what are known as "inner iterations". The convergence of the iterative process is assessed according to two criteria. The first is a global, integral criterion:

$$\left| \frac{k_{\text{eff,i+1}}}{k_{\text{eff,i}}} - 1 \right| < \epsilon_{\text{I}}, \tag{48}$$

and the second is a local criterion, expressed as:

$$\max \left| 1 - \frac{\phi_{\rm i}(\vec{r}, g)}{\phi_{\rm i+1}(\vec{r}, g)} \right| < \epsilon_{\rm P} \,. \tag{49}$$

Using this methodology, the flux converges to the solution of the Boltzmann equation associated with the fundamental eigenvalue $k_{\rm eff}$. However, it remains possible to perform the calculation for any harmonic n by employing a procedure similar to the one previously described, provided that the harmonics (fluxes and eigenvalues) of orders ranging from zero to n-1 are known in both the direct and adjoint cases.

For what concern the algorithm for the calculation of adjoint fluxes, the only difference with respect to what has been described so far for the direct case, is that the fluxes and operators in the presented equations are replaced by their dual counterparts (i.e. $\phi \to \phi^{\dagger}$, ${\bf F} \to {\bf F}^{\dagger}$, ${\bf A} \to {\bf A}^{\dagger}$).

Inhomogenous calculation — As previously introduced in Section 2.5.1, the GPT formalism relies on the definition of suitable generalized importances (denoted in the present work as $\tilde{\Psi}_n$ and $\tilde{\Psi}_n^{\dagger}$) that quantify the sensitivity of a given integral quantity with respect to local variations in system parameters. These generalized importances are solutions of an inhomogeneous transport equation, whose structure depends on the specific functional under consideration.

To illustrate this concept, consider the following example of an adjoint Boltzmann equation, which represents a typical formulation used to compute generalized importances within the GPT framework:

$$\left(\mathbf{A}^{\dagger} - \mathbf{F}^{\dagger}/k_{\text{eff}}\right)\Psi^{\dagger} = S^{\dagger}.$$
 (50)

Continuing with this example, the existence of a solution Ψ^{\dagger} implies that the condition $\langle S^{\dagger}, \phi \rangle = 0$ must necessarily be satisfied. Indeed:

$$\langle S^{\dagger}, \phi \rangle = \langle \left(\mathbf{A}^{\dagger} - \frac{\mathbf{F}^{\dagger}}{k_{\text{eff}}} \right) \Psi^{\dagger}, \phi \rangle = \langle \Psi^{\dagger}, \left(\mathbf{A} - \frac{\mathbf{F}}{k_{\text{eff}}} \right) \phi \rangle = 0.$$
 (51)

The ERANOS code is nonetheless capable of providing a solution to the adjoint equation even when the theoretical condition $\langle S^\dagger, \phi \rangle = 0$ is not satisfied. In other words, a result is still obtained even if the adjoint source term S^\dagger is not orthogonal to the fundamental direct flux ϕ . It follows that the solution produced under such conditions does not strictly correspond to that of the original theoretical problem, since ERANOS is, in practice, solving a modified form of the equation required for the computation of generalized importances.

This deviation arises from an internal orthogonalization procedure implemented during the outer iteration cycle. At each step, ERANOS adjusts the adjoint solution to enforce orthogonality with respect to the fission source – thus indirectly ensuring orthogonality to the direct fundamental mode ϕ . As a result, the system being solved is no longer the original one, but rather a projected version that satisfies the imposed orthogonality constraint.

The key steps and mathematical properties of this iterative orthogonalization process are described below. At iteration i+1, a raw (non-orthogonalized) solution $\tilde{\Psi}_{i+1}^{\dagger}$ is obtained using the adjoint fission source constructed from the previously orthogonalized solution Ψ_{i}^{\dagger} . This intermediate solution is then orthogonalized with respect to the direct fission source associated with the fundamental flux (i.e. the solution of the zeroth-order harmonic calculation) according to the following scheme:

$$\begin{cases} \mathbf{A}^{\dagger} \tilde{\Psi}_{1}^{\dagger} = S^{\dagger} \\ \dots \\ \mathbf{A}^{\dagger} \tilde{\Psi}_{i+1}^{\dagger} = S^{\dagger} + \frac{\mathbf{F}^{\dagger}}{k_{\text{eff}}} \Psi_{i}^{\dagger} \\ \dots \end{cases}$$
(52)

where, for each iteration i, the following holds:

$$\Psi_{i}^{\dagger} = \tilde{\Psi}_{i}^{\dagger} - \frac{\langle \tilde{\Psi}_{i}^{\dagger}, \mathbf{F}\phi \rangle}{\langle \phi^{\dagger}, \mathbf{F}\phi \rangle} \phi^{\dagger} , \qquad (53)$$

In analogy with what was previously obtained in Equation 28.

If the iterative process converges, then Ψ_i^{\dagger} and $\tilde{\Psi}_i^{\dagger}$ respectively tend to the functions Ψ^{\dagger} and $\tilde{\Psi}^{\dagger}$, for which the following relations can be demonstrated [48]:

$$\begin{cases} \mathbf{A}^{\dagger} \tilde{\Psi}^{\dagger} = S^{\dagger} + \frac{\mathbf{F}^{\dagger}}{k_{\text{eff}}} \Psi^{\dagger} \\ \Psi^{\dagger} = \tilde{\Psi}^{\dagger} - \frac{\langle \tilde{\Psi}^{\dagger}, \mathbf{F} \phi \rangle}{\langle \phi^{\dagger}, \mathbf{F} \phi \rangle} \phi^{\dagger} \\ \langle \Psi^{\dagger}, \mathbf{F} \phi \rangle = 0 \\ \langle \tilde{\Psi}^{\dagger}, \mathbf{F} \phi \rangle = k_{\text{eff}} \langle S^{\dagger}, \phi \rangle \end{cases}$$
(54)

First of all, it is noted that the generalized importances Ψ^\dagger and $\tilde{\Psi}^\dagger$ differ only by a component proportional to ϕ^\dagger , which, as previously recalled, is itself a solution of the adjoint Boltzmann equation (see Equation 7). As a consequence, both quantities satisfy the following equation:

$$\left(\mathbf{A}^{\dagger} - \frac{\mathbf{F}^{\dagger}}{k_{\text{eff}}}\right) \Psi^{\dagger} = S^{\dagger} - \langle S^{\dagger}, \phi \rangle \frac{\mathbf{F}^{\dagger} \phi^{\dagger}}{\langle \phi^{\dagger}, \mathbf{F} \phi \rangle} = \Sigma^{\dagger}.$$
 (55)

This is the form effectively solved by ERANOS for the computation of generalized importances, in which the source term Σ^{\dagger} (constructed to satisfy the orthogonality condition $\langle \Sigma^{\dagger}, \phi \rangle = 0$) replaces the original S^{\dagger} appearing in Equation 50.

An important aspect to consider when computing generalized importances from sources that exhibit sign changes is that the resulting fluxes will also display sign variations. This is strictly related with their pointwise convergence, which is not achievable (according to the method used for its verification) in most cases. This occurs because ERANOS checks the maximum of the pointwise relative discrepancies between the solutions obtained at the two latest inner iterations within the same outer iteration. However, these relative differences can become very large at points where the solution is close to zero, regardless of how small the absolute variation between the two iterations is, since one encounters a quantity of the form

$$\lim_{x_{\rm n}\to 0} \left| \frac{x_{\rm n+1} - x_{\rm n}}{x_{\rm n}} \right| = \infty. \tag{56}$$

Nevertheless, these apparently large relative differences have no real impact on the calculated physical quantities (such as perturbation integrals, Section 3.4.4), because they are localized at points in phase space where the generalized importance has zero or negligible value (otherwise convergence would not fail).

3.4.4 Modules for the Calculation of Integral Quantities

ERANOS includes a set of dedicated modules for the evaluation of integral quantities. For a comprehensive overview of the available functionalities, the reader is referred to the official user manual [48]. The present discussion is limited to the two categories of integrals relevant to the computation of sensitivity coefficients: perturbation integrals and generalized integrals.

Perturbation Integrals In the context of neutronic analysis, perturbation integrals are mathematical tools used to estimate the impact of small local variations in reactor parameters – such as macroscopic cross-sections or geometric/material properties – on global neutronic quantities of interest, including the effective multiplication factor $k_{\rm eff}$ or spatially integrated reaction rates. These methods enable fast and computationally efficient evaluations, without the need to recompute the entire flux field for each perturbation scenario.

Two dedicated ERANOS modules are available for the calculation of such integrals:

- DIFFUSION_PERTURBATION_INTEGRAL, which uses fluxes obtained from diffusion theory;
- TRANSPORT_PERTURBATION_INTEGRAL, which instead relies on transport-theory-based flux solutions.

In this work, only the transport-based formulation is employed, in accordance with the transport model consistently adopted throughout all flux calculations.

The integration domain corresponds to those regions of the reactor core for which the macroscopic cross-sections (hence, their perturbations) can be considered spatially uniform. These regions are defined in the MACRO EDL, which must be provided to the module alongside the flux and importance EDLs.

The perturbation integrals relevant to this study, and consistent with the internal ERANOS nomenclature, are given below:

the contribution of the direct flux in group g to the adjoint source:

$$SIAP_{g} = \int_{V} \phi_{g} \left(\sum_{g'=1}^{G} \chi_{g'} \phi_{g'}^{\dagger} \right) dV, \qquad (57)$$

• the contribution of the adjoint flux in group *g* to the forward source:

$$SIDP_{g} = \int_{V} \phi_{g}^{\dagger} \left(\sum_{g'=1}^{G} \nu \Sigma_{f,g'} \phi_{g'} \right) dV, \qquad (58)$$

• a global bilinear integral quantifying the coupling between forward and adjoint fluxes via the fission source and spectrum.

$$VIMPOR = \int_{V} \left(\sum_{g'=1}^{G} \chi_{g'} \, \phi_{g'}^{\dagger} \right) \left(\sum_{g=1}^{G} \nu \Sigma_{f,g} \, \phi_{g} \right) \, dV \,. \tag{59}$$

These integrals play a central role in the formulation of generalized perturbation theory (GPT) and are used extensively in ERANOS for sensitivity and importance analyses.

Generalised Integrals Linear and bilinear integrals are computed using the ERANOS module GENERALIZED_INTEGRAL. The specific type of linear integral evaluated depends on the keyword provided in the corresponding directive. The available options include the following:

- explicitly requesting that no source term be used (WITHOUT): $\langle \phi \rangle$;
- providing an EDL source S in the directive: $\langle S, \phi \rangle$;
- requesting the use of the source term stored in the EDL flux (TOTAL, see Section 3.4.2): $\langle \nu \Sigma_{\rm f} \phi \rangle$ or $\langle \chi \phi^{\dagger} \rangle$, depending on the nature of the flux specified in the module call.

Table 3: Types of bilinear integrals computable via the GENERALIZED_INTEGRAL module. The adopted notation assumes that the integration is performed with respect to the variables indicated in the subscript, specifically energy (E) and spatial coordinate (\vec{r}) .

Case	Integral	Directive SOURCE for the forward flux	Directive SOURCE for the adjoint flux
1	$\langle \phi^\dagger, \phi \rangle_{ ilde{\mathbf{r}}, \mathrm{E}}$	WITHOUT	WITHOUT
2	$\langle \phi^{\dagger}, \nu \Sigma_{\mathrm{f}} \phi \rangle_{\tilde{\mathrm{r}}, \mathrm{E}}$	TOTAL	WITHOUT
3	$\langle \phi^{\dagger}, S \phi \rangle_{\tilde{\mathbf{r}}, \mathbf{E}}$	(flux source EDL S)	WITHOUT
4	$\langle \phi^{\dagger} \chi, \phi \rangle_{\tilde{\mathbf{r}}, \mathbf{E}}$	WITHOUT	TOTAL
5	$\langle \phi^{\dagger} S^{\dagger}, \phi \rangle_{\tilde{\mathbf{r}}, \mathbf{E}}$	WITHOUT	(flux source EDL S^{\dagger})
6	$\langle\langle S^{\dagger}\phi^{\dagger}\rangle_{\rm E}, \langle S\phi\rangle_{\rm E}\rangle_{\rm \tilde{r}}$	(flux source EDL S^{\dagger})	(flux source EDL S)
7	$\langle \phi^\dagger, \mathbf{F} \phi angle_{ ilde{\mathrm{r}}, \mathrm{E}}$	TOTAL	TOTAL

The various types of bilinear integrals that can be computable are listed in Table 3. Therefore, when the module performs the calculation of a generalized integral, a product is carried out between:

- the adjoint part, which is treated as a pointwise function, i.e. a quantity defined per unit volume;
- the forward part, which is already multiplied by the volume of the element.

To correctly perform the calculation of a bilinear integral using two source EDLs (as in Case 6 reported in Table 3), the values from one of them must be divided by the element volume. This is necessary because source EDLs already contain volume-integrated values, and multiplying them directly would double-count the volumetric contribution. The same principle applies if the source is constructed as the product of two source EDLs: in such a case, one of them must first be normalized with respect to the volume, thereby converting it from an integrated value to a density and ensuring the physical consistency of the result.

3.4.5 Module for the Evaluation of the Effective Delayed Neutron Fraction \hat{eta}_{eff}

The module of interest is called BETA_EFFECTIVE_CALCULATION and is used to compute and store as LU variables the values of the effective delayed neutron fraction $\hat{\beta}_{\rm eff}$. To configure this module, the following data must be specified in the appropriate

directive:

 the average number of delayed neutrons emitted per fission event, provided for each fissile isotope included in the core model and for every precursor nuclide family;

- the decay constants associated with each precursor family;
- the energy spectrum of delayed neutrons for each precursor family.

These data are obtained through dedicated LU procedures distributed with ERA-NOS. These procedures extract the required values from a selected evaluated nuclear data library and process them to generate the input data in the appropriate format for use within the module. These procedures enable the generation of delayed neutron spectra for any energy group structure, provided that its boundaries correspond to a subset of those defined in the standard 1968-group structure.

The formula used by the module to evaluate the effective delayed neutron fraction is analogous to that introduced in Equation 14 and is expressed in the multi-group form as:

$$\hat{\beta}_{\text{eff}} = \frac{\langle \phi^{\dagger}, \mathbf{F}_{\text{d}} \phi \rangle}{\langle \phi^{\dagger}, \mathbf{F} \phi \rangle} = \frac{\int_{V} d^{3}r \sum_{i=1}^{I} \sum_{n=1}^{N} \beta_{in} \left(\sum_{g=1}^{G} \chi_{ng}^{\text{d}} \phi_{g}^{\dagger} \right) \left(\sum_{g=1}^{G} (\nu \Sigma_{f})_{ig} \phi_{g} \right)}{\int_{V} d^{3}r \left(\sum_{g=1}^{G} \chi_{g} \phi_{g}^{\dagger} \right) \left(\sum_{g=1}^{G} (\nu \Sigma_{f})_{g} \phi_{g} \right)}, \quad (60)$$

where:

- i = 1, ..., I denotes the isotopes considered in the calculation domain;
- $n = 1, \dots, N$ identifies the delayed neutron precursor families;
- $g=1,\ldots,G$ represents the discrete energy groups used in the multi-group formulation;
- β_{in} is the delayed neutron fraction associated with isotope i and precursor family n:
- $\chi_{\rm g}$ denotes the total fission neutron spectrum, normalized to unity, in energy group q:
- χ_{ng}^{d} represents the delayed neutron emission spectrum for precursor family n in energy group g;
- $\phi_{\rm g}$ and $\phi_{\rm g}^{\dagger}$ denote the direct and adjoint neutron fluxes, respectively, in energy group g;
- $(\nu \Sigma_{\rm f})_{\rm ig}$ is the product of the average number of neutrons emitted per fission event by isotope i and the corresponding macroscopic fission cross section, both evaluated in energy group g.

4 Methodological Framework for the Delayed Neutrons Fraction Sensitivity Analysis

4.1 Analytical Derivation of the Sensitivity Coefficients

The delayed neutrons fraction ($\hat{\beta}_{\text{eff}}$) is an integral parameter that depends on multiple quantities, as previously shown in Equation 60 and reported below:

$$\hat{\beta}_{\text{eff}} = \frac{\int_{V} d^{3}r \sum_{i=1}^{I} \sum_{n=1}^{N} \beta_{in} \left(\sum_{g=1}^{G} \chi_{ng}^{d} \phi_{g}^{\dagger} \right) \left(\sum_{g=1}^{G} (\nu \Sigma_{f})_{ig} \phi_{g} \right)}{\int_{V} d^{3}r \left(\sum_{g=1}^{G} \chi_{g} \phi_{g}^{\dagger} \right) \left(\sum_{g=1}^{G} (\nu \Sigma_{f})_{g} \phi_{g} \right)}.$$
 (61)

The implementation of dedicated modules within ERANOS for the computation of sensitivity coefficients of $\hat{\beta}_{\rm eff}$ with respect to input parameters (α), namely the coefficients generally denoted in Section 2.5.2 as $S(\hat{\beta}_{\rm eff},\alpha)$, is required to evaluate the impact of nuclear data uncertainties on the delayed neutron fraction. This approach enables the identification of which input dependencies are more or less significant, and contributes – within a broader scope – to a sensitivity analysis aimed at the neutronic characterization of ALFRED, in order to assess both performance optimization and the adequacy of the imposed safety margins.

The set of parameters α considered in this work includes all nuclear quantities that enters the formulation of $\hat{\beta}_{\text{eff}}$, with the exception of those for which ERANOS already provides dedicated modules to calculate the corresponding sensitivity coefficients.

In line with Section 2.5.2, the sensitivity coefficients of the total effective delayed neutrons fraction are derived from the expression given in Equation 38, which can be written as:

$$S(\hat{\beta}_{\text{eff}}, \alpha) = \sum_{n} \frac{\hat{\beta}_{\text{eff},n}}{\hat{\beta}_{\text{eff}}} S(\hat{\beta}_{\text{eff},n}, \alpha).$$
 (62)

As a result, the parameters of primary interest in most of the calculations are the effective delayed neutron fractions associated with each family $(\hat{\beta}_n)$, whose mathematical definition is provided in Equation 14.

The analytical development of the expression for the $S(\hat{\beta}_n,\alpha)$ coefficients, as given in Equation 37, is carried out with the objective of reducing it to a combination of terms that can be evaluated using functions already implemented in the ERANOS suite. This approach enables the use of methods that have already undergone both *verification* and *validation*. Verification ensures that the implemented methods accurately reproduce the underlying mathematical and numerical models, while validation confirms

that the results are consistent with experimental data or reference benchmarks [60]. These verification and validation processes are not only considered good practice, but also represent a requirement imposed by safety authorities, as they provide the necessary confidence in the reliability of the results used during the reactor design phase. Together, these processes confirm that the physical and numerical models are capable of adequately represent real systems.

In order to derive the analytical expressions of the various sensitivity coefficients $S(\hat{\beta}_{\text{eff}}, \alpha)$, it is necessary to introduce the definition of some fundamental parameters:

• The average number of neutrons emitted per fission event, ν_{igz} , which is defined as the sum of its prompt and delayed components:

$$\nu_{\rm igz} = \nu_{\rm igz}^{\rm p} + \sum_{\rm n} \nu_{\rm in}^{\rm d} \,. \tag{63}$$

The total values ν_{igz} can be directly extracted from the MICRO and MACRO EDLs, while the delayed neutron yields ν_{in}^d are obtained using a dedicated procedure already implemented in ERANOS, which provides their values for each precursor family (thus, their contribution is expressed as a sum over all such families). The prompt component ν_{igz}^p , which represents the average number of neutrons emitted during the nuclear fission process, is not directly available and must be determined by subtracting the delayed contribution from the total.

• The fission spectrum χ_{igz} , that is similarly composed of prompt and delayed contributions:

$$\chi_{\rm igz} = (1 - \beta) \chi_{\rm igz}^{\rm p} + \sum_{\rm n} \beta_{\rm n} \chi_{\rm ng}^{\rm d}, \qquad (64)$$

where the total spectrum χ_{igz} is available from the MICRO and MACRO EDLs (see Section 3.3.1), the delayed fission spectra χ_{ng}^d are derived, for each delayed neutron family, through a specific ERANOS routine and the prompt spectrum χ_{igz}^p is not directly accessible and must be reconstructed by appropriately combining the total and delayed components. Each contribution is weighted by the corresponding delayed neutron fraction, ensuring consistency with the actual neutron emission profile.

• The quantity β_{in} , which represents the fraction of delayed neutrons associated with isotope i and family n:

$$\beta_{\rm in} = \frac{\sum_{\rm z} \left(\sum_{\rm g,\,m\in z} \nu_{\rm in}^{\rm d} N_{\rm iz} \sigma_{\rm f,igz} \phi_{\rm gm} V_{\rm m}\right)}{\sum_{\rm z,\,j} \left(\sum_{\rm g,\,m\in z} \left(\nu_{\rm jgz}^{\rm p} + \sum_{\rm n} \nu_{\rm jn}^{\rm d}\right) N_{\rm jz} \sigma_{\rm f,jgz} \phi_{\rm gm} V_{\rm m}\right)}.$$
 (65)

This operational definition of $\beta_{\rm in}$ expresses the ratio between the production rate of delayed neutrons from a given precursor family and isotope, and the total neutron production rate. The numerator accounts of delayed neutron from family n

of isotope i, summed over all zones, whereas the denominator includes the combined prompt and delayed contributions from all isotopes and precursor families.

For the definitions provided above, the subscript n denotes the delayed neutron family under consideration, the index i (or j) refers to the fissile isotope, g indicates the energy group, z the reactor zone, and m the mesh element within the specified zone. Notice that, throughout the discussion, the absence of certain subscripts (where they would ordinarily be expected) implies that summation over the corresponding index is assumed. For instance, the total fraction of delayed neutrons associated with family n is expressed as $\beta_{\rm n} = \sum_i \beta_{\rm in}$.

In deriving the expressions for the sensitivity coefficients, and in line with the strategy of relying on modules already available in the current ERANOS release, the nomenclature conventionally adopted within the code environment is preserved in the analytical formulations. Accordingly, the perturbation integrals introduced in Section 3.4.4 are consistently referred to by their standard names, namely ${\rm SIAP}$ (Equation 57), ${\rm SIDP}$ (Equation 58), and ${\rm VIMPOR}$ (Equation 59). In addition to these, the following quantity is introduced:

VIMPOR_n^d =
$$\langle \phi^{\dagger} \chi_{n}^{d}, \nu \Sigma_{f} \phi \rangle = \frac{\hat{\beta}_{\text{eff,n}}}{\beta_{n}} \text{VIMPOR},$$
 (66)

which differs from the parameter VIMPOR solely by the use of the delayed emission spectrum (χ_{ng}^d) instead of the fission spectrum (χ_{ingz}^d).

With regard to the spectral quantities discussed above, including the prompt neutron emission spectrum $\chi^{\rm p}_{\rm igz}$, particular care must be paid to their normalization. In general, emission spectra that satisfy the condition

$$\sum_{g} \chi_{g} = 1 \tag{67}$$

are referred to as "constrained". In ERANOS, this condition applies to all emission and fission spectra [61]. As a result, any perturbation must preserve the normalization constraint, a requirement that has direct implications for the derivation of the sensitivity coefficient expressions $S(\hat{\beta}, \alpha)$. The effect of this constraint on the spectral shape is analyzed below in the case of a localized perturbation affecting a specific energy group.

Let us consider a perturbation applied to the emission spectrum in a specific energy group g'. Taking into account the normalization condition in Equation 67, which requires that the integral of a spectrum over its entire energy domain equals unity, the following relation is obtained:

$$\sum_{g} (\chi_{g} + \Delta \chi_{g'} \delta_{gg'}) = 1 + \Delta \chi_{g'}.$$
 (68)

Dividing both sides by the right-hand term yields:

$$\sum_{\mathbf{g}} \frac{\chi_{\mathbf{g}} + \Delta \chi_{\mathbf{g}'} \delta_{\mathbf{g}\mathbf{g}'}}{1 + \Delta \chi_{\mathbf{g}'}} = 1.$$
 (69)

On this basis, a perturbed emission spectrum can be defined as:

$$\chi_{\rm g}' = \frac{\chi_{\rm g} + \Delta \chi_{\rm g'} \delta_{\rm gg'}}{1 + \Delta \chi_{\rm g'}},\tag{70}$$

so that the corresponding variation is given by

$$\Delta\chi_{\rm g}=\chi_{\rm g}'-\chi_{\rm g}=\frac{\chi_{\rm g}+\Delta\chi_{\rm g'}\delta_{\rm gg'}}{1+\Delta\chi_{\rm g'}}-\chi_{\rm g}=\frac{(\delta_{\rm gg'}-\chi_{\rm g})\,\Delta\chi_{\rm g'}}{1+\Delta\chi_{\rm g'}}\,. \tag{71}$$

From this relation, the infinitesimal variation of the spectrum is obtained as:

$$d\chi_{\rm g} = \lim_{\Delta\chi_{\rm g'} \to d\chi_{\rm g'}} \Delta\chi_{\rm g} = (\delta_{\rm gg'} - \chi_{\rm g}) d\chi_{\rm g'} \,, \tag{72}$$

which directly leads to the expression for the derivative of the emission spectrum:

$$\frac{d\chi_{\rm g}}{d\chi_{\rm g'}} = (\delta_{\rm gg'} - \chi_{\rm g}). \tag{73}$$

This relation is of key importance in the derivation of the analytical expressions of the sensitivity coefficients, as it is applied in cases where the perturbed input parameter is an emission spectrum. In particular, the derivative in Equation 73 reflects the effect of the normalization constraint: a perturbation in one energy group g' inherently induces compensatory variations in all other groups $g \neq g'$, in order to preserve the total integral of the spectrum. As a consequence, it is not possible to perturb a single component of the spectrum independently of the others. The action on $\chi_{g'}$ modifies the spectral shape rather than the total source intensity, emphasizing that the sensitivity being computed is with respect to the spectral form. This gives rise to additional terms in the sensitivity expressions, that would not appear in the absence of the normalization constraint.

An additional aspect of primary importance in the analytical development of the sensitivity coefficient expressions $S(\hat{\beta},\alpha)$ concerns the interdependencies among the quantities that enter the definition of the parameter $\hat{\beta}_{\rm eff,n}$. Indeed, perturbations applied to quantities such as the average number of neutrons emitted (whether considering only the prompt or delayed component, see Equation 63) have a direct physical impact on the delayed neutron fraction β (see Equation 65). A perturbation applied to β modifies the weighting factors that determine the relative contributions of the prompt and delayed components in the total fission spectrum, as described in Equation 64. This alteration propagates further by affecting the neutron fluxes that solve the forward and adjoint neutron transport equations, since the Boltzmann operator itself is perturbed (see Equations 6 and 7). At first glance, the structure of the parametric dependencies might suggest the emergence of an infinite loop: the perturbed value of β alters the spectrum, which modifies the fluxes, which in turn re-enters the definition of β , and so

on. However, this recursive behavior is only apparent. From a physical standpoint, β is a fundamental nuclear quantity determined exclusively by the fission yields and delayed neutron emission probabilities. Consequently, the fluxes appearing in the numerator and denominator of its definition serve merely as weighting functions. These fluxes are conceptually distinct from the physical neutron flux, which is subject to change under perturbation.

In what follows, a detailed treatment is given of the calculations performed to obtain the sensitivity coefficients $S(\hat{\beta}_n, \alpha)$. It should be recalled that the sensitivity characterization of the total effective delayed neutrons fraction can be derived from the relation given in Equation 38, reported here for convenience:

$$S(\hat{\beta}_{\text{eff}}, \alpha) = \sum_{n} \frac{\hat{\beta}_{\text{eff},n}}{\hat{\beta}_{\text{eff}}} S(\hat{\beta}_{\text{eff},n}, \alpha).$$
 (74)

The derivation of the fundamental expressions underpinning this sensitivity analysis was presented in Section 2.5.2, where the theoretical framework of the GPT was introduced. Building on that basis, the sensitivity formulation maps perturbations of the physical parameters into explicit, computable, sensitivity expressions.

4.1.1 Sensitivity Coefficients of the Effective Delayed Neutron Fraction $\hat{eta}_{\rm eff,n}$ to the Delayed Neutrons Yield $u_{\rm in}^{\rm d}$

The derivation of the sensitivity coefficients of the effective delayed neutron fraction to the delayed neutron yields, $S(\hat{\beta}_{\text{eff},n}, \nu^{\text{d}}_{\text{i'n'}})$, starts from the expression obtained through GPT calculations in Section 2.5.2, namely:

$$S(\hat{\beta}_{\text{eff,n}}, \nu_{i'n'}^{\text{d}}) = \frac{(\hat{\beta}_{\text{eff,n}})_{\nu_{i'n'}^{\text{d}}}}{\hat{\beta}_{\text{eff,n}}} - \langle \tilde{\Psi}_{\text{n}}^{\dagger}, (\mathbf{A} - \frac{\mathbf{F}}{k_{\text{eff}}})_{\nu_{i'n'}^{\text{d}}} \phi \rangle - \langle \tilde{\Psi}_{\text{n}}, (\mathbf{A}^{\dagger} - \frac{\mathbf{F}^{\dagger}}{k_{\text{eff}}})_{\nu_{i'n'}^{\text{d}}} \phi^{\dagger} \rangle,$$
(75)

where it has been introduced the notation

$$(X)_{\alpha} = \alpha \frac{\partial X}{\partial \alpha} \tag{76}$$

in which X denotes a generic parameter (within the scope of this study, it will refer to either $\hat{\beta}_n$ or, possibly, $\hat{\beta}$), and α represents an input parameter.

It can be observed that the right-hand side of Equation 75 consists of three contributions:

• direct term: accounting for the explicit effect of the considered variation

$$(\hat{\beta}_{\mathrm{eff,n}})_{\nu^{\mathrm{d}}_{\mathrm{i'n'}}}/\hat{\beta}_{\mathrm{eff,n}};$$
 (77)

• **first indirect term:** representing the implicit effect due to the corresponding change in the direct flux

$$\langle \tilde{\Psi}_{\rm n}^{\dagger}, \left(\mathbf{A} - \frac{\mathbf{F}}{k_{\rm eff}} \right)_{\nu_{i'n'}^{\rm d}} \phi \rangle ;$$
 (78)

• **second indirect term:** associated with the implicit effect induced by the variation in the adjoint flux

$$\langle \tilde{\Psi}_{\rm n}, \left(\mathbf{A}^{\dagger} - \frac{\mathbf{F}^{\dagger}}{k_{\rm eff}} \right)_{\nu_{i'n'}^{\rm d}} \phi^{\dagger} \rangle$$
 (79)

The physical interpretation of these contributions is discussed in the final part of the dedicated Section 2.5.1.

As a first step, the computation of the direct term will be developed. Therefore, the numerator is explicitly expressed with the aim of reducing its final form to a combination of basic parameters, whose values can be directly obtained from ERANOS through predefined modules, or modules developed based on them:

$$(\hat{\beta}_{\text{eff,n}})_{\nu_{i'n'}^{d}} = \nu_{i'n'}^{d} \frac{\partial \hat{\beta}_{\text{eff,n}}}{\partial \nu_{i'n'}^{d}}$$

$$= \nu_{i'n'}^{d} \frac{\partial \beta_{n}}{\partial \nu_{i'n'}^{d}} \cdot \frac{\hat{\beta}_{\text{eff,n}}}{\beta_{n}} +$$

$$+ \nu_{i'n'}^{d} \beta_{i'n} \left[\frac{\frac{\partial}{\partial \nu_{i'n'}^{d}} \langle \phi^{\dagger} \chi_{n}^{d}, \nu \Sigma_{f} \phi \rangle}{\langle \phi^{\dagger}, \mathbf{F} \phi \rangle} + \right]$$

$$- \frac{\langle \phi^{\dagger} \chi_{n}^{d}, \nu \Sigma_{f} \phi \rangle \cdot \frac{\partial}{\partial \nu_{i'n'}^{d}} \langle \phi^{\dagger} \chi, \nu \Sigma_{f} \phi \rangle}{\langle \phi^{\dagger}, \mathbf{F} \phi \rangle^{2}} .$$
(80)

Note that the development of this expression involves the computation of the two derivatives contained within the square brackets, concerning:

- the delayed fission source $\langle \phi^{\dagger} \chi_{\rm n}^{\rm d}, \nu \Sigma_{\rm f} \phi \rangle$;
- the total fission source $\langle \phi^{\dagger} \chi, \nu \Sigma_{\rm f} \phi \rangle$.

The dependence of these fission sources on the average number of delayed neutrons emitted per fission event ($\nu_{\rm in}^{\rm d}$) is manifested in accordance with the definitions of the

parameters ν_{igz} and χ_{igz} , respectively provided in Equation 63 and Equation 64. In particular, it is noted that:

$$\begin{cases} \frac{\partial \nu}{\partial \nu_{\rm in}^{\rm d}} = 1 \\ \frac{\partial \chi}{\partial \nu_{\rm in}^{\rm d}} = \frac{\partial \beta}{\partial \nu_{\rm in}^{\rm d}} \chi^{\rm p} + \sum_{\rm n} \frac{\partial \beta_{\rm n}}{\partial \nu_{\rm in}^{\rm d}} \chi_{\rm n}^{\rm d} \end{cases}$$
 (81)

The first relation, depicting the derivative of the average number of emitted neutrons per fission event (ν) with respect to its delayed component, highlights the trivial connection between the average neutron yield per fission and its delayed component alone, namely that an increase in the delayed component by a certain amount results in an equivalent increase in the total yield.

The second relation (the one involving the emission spectrum χ), on the other hand, holds because of the assumption that the shapes of the prompt ($\chi^{\rm p}$) and delayed ($\chi^{\rm d}_{\rm n}$) fission spectra are independent of the average number of delayed neutrons emitted. However, the perturbation of a certain $\nu^{\rm d}_{\rm in}$ does not leave the overall fission spectrum unchanged, which undergoes variations in the weighting coefficients (β and $\beta_{\rm n}$) with which the prompt and delayed components are combined. The derivative of the spectrum shown in the system of Equation 81 thus translates into a linear combination of χ^p and the various $\chi^{\rm d}$ associated with each family, each weighted by the derivative of $\beta_{\rm n}$ or β with respect to the parameter $\nu^{\rm d}_{\rm in}$. Consequently, it is necessary to introduce the

development of these derivatives just mentioned:

$$\begin{split} \frac{\partial \beta_{\mathbf{n}}}{\partial \nu_{\mathbf{i'n'}}^{\mathbf{d}}} &= \frac{\displaystyle\sum_{\mathbf{z}} \left(\displaystyle\sum_{\mathbf{g},\mathbf{m}} \delta_{\mathbf{nn'}} N_{\mathbf{i'z}} \sigma_{\mathbf{f},\mathbf{i'gz}} \phi_{\mathbf{gm}} V_{\mathbf{m}} \right)}{\left[\displaystyle\sum_{\mathbf{j},\mathbf{z}} \displaystyle\sum_{\mathbf{g},\mathbf{m}} \left(\nu_{\mathbf{jgz}}^{\mathbf{p}} + \displaystyle\sum_{\mathbf{n}} \nu_{\mathbf{jn}}^{\mathbf{d}} \right) N_{\mathbf{jz}} \sigma_{\mathbf{f},\mathbf{jgz}} \phi_{\mathbf{gm}} V_{\mathbf{m}} \right]} \times \\ &\times \frac{\displaystyle\sum_{\mathbf{j},\mathbf{z}} \left(\displaystyle\sum_{\mathbf{g},\mathbf{m}} \left(\nu_{\mathbf{jgz}}^{\mathbf{p}} + \displaystyle\sum_{\mathbf{n}} \nu_{\mathbf{jn}}^{\mathbf{d}} \right) N_{\mathbf{jz}} \sigma_{\mathbf{f},\mathbf{jgz}} \phi_{\mathbf{gm}} V_{\mathbf{m}} \right)}{\left[\displaystyle\sum_{\mathbf{j},\mathbf{z}} \displaystyle\sum_{\mathbf{g},\mathbf{m}} \left(\nu_{\mathbf{jgz}}^{\mathbf{p}} + \displaystyle\sum_{\mathbf{n}} \nu_{\mathbf{jn}}^{\mathbf{d}} \right) N_{\mathbf{jz}} \sigma_{\mathbf{f},\mathbf{jgz}} \phi_{\mathbf{gm}} V_{\mathbf{m}} \right]} + \\ &- \frac{\displaystyle\sum_{\mathbf{i},\mathbf{z}} \left(\displaystyle\sum_{\mathbf{g},\mathbf{m}} \nu_{\mathbf{in}}^{\mathbf{d}} N_{\mathbf{iz}} \sigma_{\mathbf{f},\mathbf{igz}} \phi_{\mathbf{gm}} V_{\mathbf{m}} \right)}{\left[\displaystyle\sum_{\mathbf{j},\mathbf{z}} \displaystyle\sum_{\mathbf{g},\mathbf{m}} \left(\nu_{\mathbf{jgz}}^{\mathbf{p}} + \displaystyle\sum_{\mathbf{n}} \nu_{\mathbf{jn}}^{\mathbf{d}} \right) N_{\mathbf{jz}} \sigma_{\mathbf{f},\mathbf{jgz}} \phi_{\mathbf{gm}} V_{\mathbf{m}} \right]} \times \\ &\times \frac{\displaystyle\sum_{\mathbf{z}} \left(\displaystyle\sum_{\mathbf{g},\mathbf{m}} N_{\mathbf{i'z}} \sigma_{\mathbf{f},\mathbf{i'gz}} \phi_{\mathbf{gm}} V_{\mathbf{m}} \right)}{\left[\displaystyle\sum_{\mathbf{j},\mathbf{z}} \displaystyle\sum_{\mathbf{g},\mathbf{m}} \left(\nu_{\mathbf{jgz}}^{\mathbf{p}} + \displaystyle\sum_{\mathbf{n}} \nu_{\mathbf{jn}}^{\mathbf{d}} \right) N_{\mathbf{jz}} \sigma_{\mathbf{f},\mathbf{jgz}} \phi_{\mathbf{gm}} V_{\mathbf{m}} \right]} \\ &= \frac{\beta_{\mathbf{i'n'}}}{\nu_{\mathbf{i'n'}}^{\mathbf{d}}} \delta_{\mathbf{nn'}} + \\ &- \frac{\beta_{\mathbf{i'n'}}}{\nu_{\mathbf{i'n'}}^{\mathbf{d}}} \cdot \sum_{\mathbf{j},\mathbf{z}} \displaystyle\sum_{\mathbf{g},\mathbf{m}} \left(\nu_{\mathbf{jgz}}^{\mathbf{p}} + \displaystyle\sum_{\mathbf{n}} \nu_{\mathbf{jn}}^{\mathbf{d}} \right) N_{\mathbf{jz}} \sigma_{\mathbf{f},\mathbf{jgz}} \phi_{\mathbf{gm}} V_{\mathbf{m}} \right) \\ &= \frac{\beta_{\mathbf{i'n'}}}{\nu_{\mathbf{i'n'}}^{\mathbf{d}}} \left(\delta_{\mathbf{nn'}} - \beta_{\mathbf{n}} \right) , \qquad (82) \end{split}$$

in which the final equality is obtained by recognizing, within the second term on the right-hand side of the previous step, the definition of the parameter β_n , expressed as

a summation over the considered isotopes of the definition of $\beta_{\rm in}$ provided in Equation 65.

From this, the expression for the derivative of the total delayed neutron fraction (β) can be readily deduced:

$$\frac{\partial \beta}{\partial \nu_{\mathbf{i'n'}}^{\mathbf{d}}} = \sum_{\mathbf{n}} \frac{\partial \beta_{\mathbf{n}}}{\partial \nu_{\mathbf{i'n'}}^{\mathbf{d}}} = \frac{\beta_{\mathbf{i'n'}}}{\nu_{\mathbf{i'n'}}^{\mathbf{d}}} (1 - \beta). \tag{83}$$

By substituting this result into Equation 80 and performing a straightforward rearrangement of the terms, the following expression is obtained:

$$(\hat{\beta}_{\text{eff,n}})_{\nu_{i'n'}^{d}} = \beta_{i'n'} (\delta_{nn'} - \beta_{n}) \frac{\hat{\beta}_{\text{eff,n}}}{\beta_{n}} +$$

$$+ \nu_{i'n'}^{d} \beta_{i'n} \left[\frac{\langle \phi^{\dagger} \chi_{n}^{d}, \Sigma_{f,i'} \phi \rangle}{\langle \phi^{\dagger}, \mathbf{F} \phi \rangle} -$$

$$- \langle \phi^{\dagger} \chi_{n}^{d}, \nu \Sigma_{f} \phi \rangle \left(\frac{\langle \phi^{\dagger} \chi, \Sigma_{f,i'} \phi \rangle}{\langle \phi^{\dagger}, \mathbf{F} \phi \rangle^{2}} + \frac{\langle \phi^{\dagger} \frac{\partial \chi}{\partial \nu_{i'n'}^{d}}, \nu \Sigma_{f} \phi \rangle}{\langle \phi^{\dagger}, \mathbf{F} \phi \rangle^{2}} \right) \right].$$
(84)

In order to complete the calculation for the direct term, the equation must be normalized with respect to $\hat{\beta}_{\rm eff,n}$, hence:

$$\frac{(\hat{\beta}_{\text{eff,n}})_{\nu_{i'n'}^{d}}}{\hat{\beta}_{\text{eff,n}}} = \frac{\beta_{i'n'}}{\beta_{n}} \left(\delta_{nn'} - \beta_{n}\right) + \\
+ \nu_{i'n'}^{d} \frac{\beta_{i'n}}{\beta_{n}} \left[\frac{\beta_{n}}{\hat{\beta}_{\text{eff,n}}} \frac{\langle \phi^{\dagger} \chi_{n}^{d}, \Sigma_{f,i'} \phi \rangle}{\langle \phi^{\dagger}, \mathbf{F} \phi \rangle} - \frac{\langle \phi^{\dagger} \chi, \Sigma_{f,i'} \phi \rangle}{\langle \phi^{\dagger}, \mathbf{F} \phi \rangle} - \frac{\langle \phi^{\dagger} \frac{\partial \chi}{\partial \nu_{i'n'}^{d}}, \nu \Sigma_{f} \phi \rangle}{\langle \phi^{\dagger}, \mathbf{F} \phi \rangle} \right] \\
= \frac{\beta_{i'n}}{\beta_{n}} \left[\left(\delta_{nn'} - \beta_{n}\right) + \\
+ \frac{\beta_{n}}{\hat{\beta}_{\text{eff,n}}} \frac{\langle \phi^{\dagger} \chi_{n}^{d}, \nu_{i'n'}^{d} \Sigma_{f,i'} \phi \rangle}{\langle \phi^{\dagger}, \mathbf{F} \phi \rangle} - \frac{\langle \phi^{\dagger} \chi, \nu_{i'n'}^{d} \Sigma_{f,i'} \phi \rangle}{\langle \phi^{\dagger}, \mathbf{F} \phi \rangle} - \frac{\langle \phi^{\dagger} \tilde{\chi} (\nu_{i'n'}^{d}), \nu \Sigma_{f} \phi \rangle}{\langle \phi^{\dagger}, \mathbf{F} \phi \rangle} \right], \tag{85}$$

where a new quantity has been defined (for further details on how its value is computed, refer to Section 4.2):

$$\tilde{\chi}(\nu_{\rm in}^{\rm d}) = \nu_{\rm in}^{\rm d} \frac{\partial \chi}{\partial \nu_{\rm in}^{\rm d}},$$
 (86)

which represents the component of the total fission spectrum that depends on the average number of delayed neutrons emitted per fission event.

As for the indirect terms in the starting GPT Equation 75, the following results are obtained:

$$\langle \tilde{\Psi}_{\mathbf{n}}^{\dagger}, \left(\mathbf{A} - \frac{\mathbf{F}}{k_{\text{eff}}}\right)_{\nu_{\mathbf{i'n'}}^{\mathbf{d}}} \phi \rangle = -\frac{\langle \tilde{\Psi}_{\mathbf{n}}^{\dagger} \nu_{\mathbf{i'n'}}^{\mathbf{d}} \frac{\partial \chi}{\partial \nu_{\mathbf{i'n'}}^{\mathbf{d}}}, \nu \Sigma_{\mathbf{f}} \phi \rangle}{k_{\text{eff}}} - \frac{\langle \tilde{\Psi}_{\mathbf{n}}^{\dagger} \chi, \nu_{\mathbf{i'n'}}^{\mathbf{d}} \Sigma_{\mathbf{f}, \mathbf{i'}} \phi \rangle}{k_{\text{eff}}}$$

$$= -\frac{\langle \tilde{\Psi}_{\mathbf{n}}^{\dagger} \tilde{\chi}(\nu_{\mathbf{i'n'}}^{\mathbf{d}}), \nu \Sigma_{\mathbf{f}} \phi \rangle}{k_{\text{eff}}} - \frac{\langle \tilde{\Psi}_{\mathbf{n}}^{\dagger} \chi, \nu_{\mathbf{i'n'}}^{\mathbf{d}} \Sigma_{\mathbf{f}, \mathbf{i'}} \phi \rangle}{k_{\text{eff}}}$$
(87)

and

$$\langle \phi^{\dagger}, \left(\mathbf{A} - \frac{\mathbf{F}}{k_{\text{eff}}}\right)_{\nu_{i'n'}^{\text{d}}} \tilde{\Psi}_{\text{n}} \rangle = -\frac{\langle \phi^{\dagger} \nu_{i'n'}^{\text{d}} \frac{\partial \chi}{\partial \nu_{i'n'}^{\text{d}}}, \nu \Sigma_{\text{f}} \tilde{\Psi}_{\text{n}} \rangle}{k_{\text{eff}}} - \frac{\langle \phi^{\dagger} \chi, \nu_{i'n'}^{\text{d}} \Sigma_{\text{f},i'} \tilde{\Psi}_{\text{n}} \rangle}{k_{\text{eff}}}$$

$$= -\frac{\langle \phi^{\dagger} \tilde{\chi}(\nu_{i'n'}^{\text{d}}), \nu \Sigma_{\text{f}} \tilde{\Psi}_{\text{n}} \rangle}{k_{\text{eff}}} - \frac{\langle \phi^{\dagger} \chi, \nu_{i'n'}^{\text{d}} \Sigma_{\text{f},i'} \tilde{\Psi}_{\text{n}} \rangle}{k_{\text{eff}}}.$$
(88)

As can be observed, the terms appearing on the right-hand sides of these recently derived equations originate from the dependence of the neutron production operator ${\bf F}$ on the parameter $\nu_{\rm in}^d$, whereas the neutron loss operator ${\bf A}$ (whose expression is written in Equation 3) plays no role in the composition of the indirect terms, as it is note dependent in any manner on the input parameter $\nu_{\rm in}^d$.

At this stage, all the necessary information is available to formulate the sensitivity coefficient of the effective fraction of delayed neutrons belonging to a specific family n with respect to the average number of delayed neutrons belonging to family n' emitted per fission event of a given isotope i'. The expression is as follows:

$$S(\hat{\beta}_{\text{eff,n}}, \nu_{i'n'}^{\text{d}}) = \frac{\beta_{i'n}}{\beta_{n}} \left[(\delta_{nn'} - \beta_{n}) + \frac{\beta_{n}}{\hat{\beta}_{\text{eff,n}}} \frac{\langle \phi^{\dagger} \chi_{n}^{\text{d}}, \nu_{i'n'}^{\text{d}} \Sigma_{f,i'} \phi \rangle}{\langle \phi^{\dagger}, \mathbf{F} \phi \rangle} + \frac{-\frac{\langle \phi^{\dagger} \chi, \nu_{i'n'}^{\text{d}} \Sigma_{f,i'} \phi \rangle}{\langle \phi^{\dagger} \mathbf{F}, \phi \rangle} - \frac{\langle \phi^{\dagger} \tilde{\chi} (\nu_{i'n'}^{\text{d}}), \nu \Sigma_{f} \phi \rangle}{\langle \phi^{\dagger}, \mathbf{F} \phi \rangle} \right] + \frac{1}{k_{\text{eff}}} \left[\langle \tilde{\Psi}_{n}^{\dagger} \tilde{\chi} (\nu_{i'n'}^{\text{d}}), \nu \Sigma_{f} \phi \rangle + \langle \tilde{\Psi}_{n}^{\dagger} \chi, \nu_{i'n'}^{\text{d}} \Sigma_{f,i'} \phi \rangle + + \langle \phi^{\dagger} \tilde{\chi} (\nu_{i'n'}^{\text{d}}), \nu \Sigma_{f} \tilde{\Psi}_{n} \rangle + \langle \phi^{\dagger} \chi, \nu_{i'n'}^{\text{d}} \Sigma_{f,i'} \tilde{\Psi}_{n} \rangle \right]$$

$$(89)$$

where all the terms involved can be derived within ERANOS by means of already implemented modules or through a combination thereof.

4.1.2 Sensitivity Coefficients of the Effective Delayed Neutron Fraction $\hat{eta}_{\rm eff,n}$ to the Prompt Neutron Yields $u_{ m igz}^{ m p}$

The formulation of the sensitivity coefficients of $\hat{\beta}_{eff,n}$ with respect to the average number of prompt neutrons emitted per fission event ν_{igz}^{p} can be expressed (consistently with the results obtained from the calculations performed by applying the GPT to the parameter $\hat{\beta}_{eff,n}$) as follows:

$$S(\hat{\beta}_{\text{eff,n}}, \nu_{i'g'z'}^{\text{p}}) = \frac{(\hat{\beta}_{\text{eff,n}})_{\nu_{i'g'z'}^{\text{p}}}}{\hat{\beta}_{\text{eff,n}}} + \frac{\hat{\beta}_{\text{eff,n}}}{\hat{\beta}_{\text{eff,n}}} - \langle \tilde{\Psi}_{\text{n}}^{\dagger}, \left(\mathbf{A} - \frac{\mathbf{F}}{k_{\text{eff}}}\right)_{\nu_{i'g'z'}^{\text{p}}} \phi \rangle - \langle \tilde{\Psi}_{\text{n}}, \left(\mathbf{A}^{\dagger} - \frac{\mathbf{F}^{\dagger}}{k_{\text{eff}}}\right)_{\nu_{i'g'z'}^{\text{p}}} \phi^{\dagger} \rangle.$$
(90)

The right-hand side of the equation consists, in order, of the direct sensitivity term followed by two indirect contributions.

In analogy with the procedure followed in the derivation of the previous sensitivity coefficient, the focus is first placed on the direct term, represented by the quantity $(\hat{\beta}_{\mathrm{eff,n}})_{\nu^{\mathrm{p}}_{i'a'a'}}/\hat{\beta}_{\mathrm{eff,n}}$. Developing the numerator yields:

$$(\hat{\beta}_{\text{eff,n}})_{\nu_{i'g'z'}^{P}} = \nu_{i'g'z'}^{P} \frac{\partial \hat{\beta}_{\text{eff,n}}}{\partial \nu_{i'g'z'}^{P}}$$

$$= \nu_{i'g'z'}^{P} \frac{\partial \beta_{n}}{\partial \nu_{i'g'z'}^{P}} \frac{\hat{\beta}_{\text{eff,n}}}{\beta_{n}}$$

$$+ \nu_{i'g'z'}^{P} \beta_{i'n} \left[\frac{\partial \langle \phi^{\dagger} \chi_{n}^{d}, \nu \Sigma_{f} \phi \rangle}{\partial \nu_{i'g'z'}^{P}} \cdot \frac{1}{\langle \phi^{\dagger}, \mathbf{F} \phi \rangle} + \right.$$

$$\left. - \langle \phi^{\dagger} \chi_{n}^{d}, \nu \Sigma_{f} \phi \rangle \cdot \frac{\partial \langle \phi^{\dagger} \chi, \nu \Sigma_{f} \phi \rangle}{\partial \nu_{i'g'z'}^{P}} \cdot \frac{1}{\langle \phi^{\dagger}, \mathbf{F} \phi \rangle^{2}} \right]$$

$$(91)$$

As in the previous case, the development of the direct term requires accounting for the dependence of the fission sources (represented by the integral terms written in Bra–Ket notation) on the parameter $\nu_{\rm igz}^{\rm p}$. This dependence arises through both ν and χ , as defined in Equation 63 and Equation 64. The derivatives to this calculation are:

$$\begin{cases}
\frac{\partial \nu}{\partial \nu_{\text{igz}}^{\text{p}}} = 1 \\
\frac{\partial \chi}{\partial \nu_{\text{igz}}^{\text{p}}} = \frac{\partial \beta}{\partial \nu_{\text{igz}}^{\text{p}}} \chi^{\text{p}} + \sum_{n} \frac{\partial \beta_{n}}{\partial \nu_{\text{igz}}^{\text{p}}} \chi_{n}^{\text{d}}
\end{cases}$$
(92)

The same physical considerations discussed for the relations in Equation 81 also apply here. In particular, the shapes of the prompt (χ^p) and delayed (χ^d_n) fission spectra are

assumed to be independent of the average number of prompt neutrons emitted, and the derivative of the delayed neutron fraction associated with each family with respect to the parameter $\nu_{\text{igz}}^{\text{p}}$ must be developed:

$$\frac{\partial \beta_{n}}{\partial \nu_{i'g'z'}^{p}} = -\frac{\sum_{i,z} \left(\sum_{g,m} \nu_{in}^{d} N_{iz} \sigma_{f,igz} \phi_{g,m} V_{m}\right) \sum_{m \in z'} N_{i'z'} \sigma_{f,i'g'z'} \phi_{g',m} V_{m}}{\left(\sum_{j,z} \sum_{g,m} \left(\nu_{jgz}^{p} + \sum_{n} \nu_{jn}^{d}\right) N_{jz} \sigma_{f,jgz} \phi_{g,m} V_{m}\right)^{2}}$$

$$= -\beta_{n} \frac{\sum_{m \in z'} N_{i'z'} \sigma_{f,i'g'z'} \phi_{g',m} V_{m}}{\sum_{j,z} \sum_{g,m} \left(\nu_{jgz}^{p} + \sum_{n} \nu_{jn}^{d}\right) N_{jz} \sigma_{f,jgz} \phi_{g,m} V_{m}}$$

$$= -\beta_{n} \frac{\beta_{i'ng'z'}}{\nu_{i'n}^{d}},$$
(93)

where the following quantity has been defined:

$$\beta_{\text{ingz}} = \frac{\sum_{m \in \mathbf{z}} \nu_{\text{in}}^{\text{d}} N_{\text{iz}} \sigma_{\text{f,igz}} \phi_{\text{g,m}} V_{\text{m}}}{\sum_{\text{j,z}} \sum_{\text{g,m}} \left(\nu_{\text{jgz}}^{\text{p}} + \sum_{\text{n}} \nu_{\text{in}}^{\text{d}} \right) N_{\text{jz}} \sigma_{\text{f,jgz}} \phi_{\text{g,m}} V_{\text{m}}},$$
(94)

representing the fraction of delayed neutrons associated with a given isotope i, belonging to a specific temporal family n, characterized by an energy corresponding to the group q, and located in a zone z of the core.

From Equation 93, the expression for the derivative of the total delayed neutron fraction can be readily as the sum of the contributions from all families:

$$\frac{\partial \beta}{\partial \nu_{i'g'z'}^{P}} = -\sum_{n} \beta_{n} \frac{\beta_{i'ng'z'}}{\nu_{i'n}^{d}}.$$
 (95)

At this stage, all the necessary ingredients are available to construct the direct term of the sensitivity coefficient under consideration. By substituting the above relations into Equation 91, one obtains:

$$(\hat{\beta}_{\text{eff,n}})_{\nu_{i'g'z'}^{P}} = -\nu_{i'g'z'}^{P} \hat{\beta}_{\text{eff,n}} \frac{\beta_{i'ng'z'}}{\nu_{i'n}^{d}} + \nu_{i'g'z'}^{P} \hat{\beta}_{\text{eff,n}} \left[\frac{\sum_{f,i'g'z'} \int_{V_{z'}} \phi_{g'} \left(\sum_{g} \chi_{ng}^{d} \phi_{g}^{\dagger} \right) dV}{\langle \phi^{\dagger}, \mathbf{F} \phi \rangle} + \frac{\hat{\beta}_{\text{eff,n}}}{\beta_{i'n}} \left(\frac{\sum_{f,i'g'z'} \int_{V_{z'}} \phi_{g'} \left(\sum_{g} \chi_{g} \phi_{g}^{\dagger} \right) dV}{\langle \phi^{\dagger}, \mathbf{F} \phi \rangle} + \frac{\langle \phi^{\dagger}, \frac{\partial \chi}{\partial \nu_{i'g'z'}^{P}}, \nu \Sigma_{f} \phi \rangle}{\langle \phi^{\dagger}, \mathbf{F} \phi \rangle} \right) \right].$$

$$(96)$$

which, at this stage, only requires normalization with respect to the effective delayed neutron fraction of the same family appearing in the sensitivity coefficient under consideration:

$$\frac{(\hat{\beta}_{\text{eff,n}})_{\nu_{i'g'z'}^{P}}}{\hat{\beta}_{\text{eff,n}}} = -\nu_{i'g'z'}^{p} \frac{\beta_{i'ng'z'}}{\nu_{i'n}^{d}} + \frac{\beta_{i'n}}{\hat{\beta}_{\text{eff,n}}} \frac{(\nu^{p}\Sigma_{f})_{i'g'z'} \operatorname{SIAP}_{ng'z'}^{d}}{\operatorname{VIMPOR}} - \frac{(\nu^{p}\Sigma_{f})_{i'g'z'} \operatorname{SIAP}_{g'z'}}{\operatorname{VIMPOR}} - \frac{\langle \phi^{\dagger}\tilde{\chi}(\nu_{i'g'z'}^{P}), \nu\Sigma_{f}\phi \rangle}{\operatorname{VIMPOR}}.$$
(97)

where the definitions of the perturbation integrals introduced in Equation 59 (VIMPOR) and Equation 57 (SIAP) are applied, and the following quantities are introduced¹¹:

$$SIAP_{ngz}^{d}(\phi^{\dagger}, \phi) = \int_{V_{z}} d\vec{r} \,\phi_{g} \left(\sum_{g'=1}^{G} \chi_{ng'}^{d} \phi_{g'}^{\dagger} \right) , \qquad (98)$$

which differs from the perturbation integral SIAP by employing the emission spectrum of delayed neutrons from family n (χ_{ng}^d) instead of the total fission spectrum (χ_g), and

$$\tilde{\chi}(\nu_{i'g'z'}^{p}) = \nu_{i'g'z'}^{p} \frac{\partial \chi}{\partial \nu_{i'g'z'}^{p}}, \tag{99}$$

which denotes the component of the fission spectrum that explicitly depends on the average number of prompt neutrons emitted per fission event.

The focus can now be shifted to the indirect terms, which are expressed as:

$$\langle \tilde{\Psi}_{\mathbf{n}}^{\dagger}, \left(\mathbf{A} - \frac{\mathbf{F}}{k_{\text{eff}}}\right)_{\nu_{\mathbf{i'g'z'}}^{\mathbf{p}}} \phi \rangle = -\frac{\langle \tilde{\Psi}_{\mathbf{n}}^{\dagger} \nu_{\mathbf{i'g'z'}}^{\mathbf{p}} \frac{\partial \chi}{\partial \nu_{\mathbf{i'g'z'}}^{\mathbf{p}}}, \nu \Sigma_{\mathbf{f}} \phi \rangle}{k_{\text{eff}}} - (\nu^{\mathbf{p}} \Sigma_{\mathbf{f}})_{\mathbf{i'g'z'}} \frac{\int_{V_{\mathbf{z'}}} \phi_{\mathbf{g'}} \left(\sum_{\mathbf{g}} \chi_{\mathbf{g}} \tilde{\Psi}_{\mathbf{ng}}^{\dagger}\right) dV}{k_{\text{eff}}}$$

$$= -\frac{\langle \tilde{\Psi}_{\mathbf{n}}^{\dagger} \tilde{\chi}(\nu_{\mathbf{i'g'z'}}^{\mathbf{p}}), \nu \Sigma_{\mathbf{f}} \phi \rangle}{k_{\text{eff}}} - (\nu^{\mathbf{p}} \Sigma_{\mathbf{f}})_{\mathbf{i'g'z'}} \frac{\mathrm{SIAP}_{\mathbf{g'z'}} (\tilde{\Psi}_{\mathbf{n}}^{\dagger}, \phi)}{k_{\text{eff}}}$$

$$(100)$$

¹¹Throughout this discussion, whenever perturbation integrals are evaluated using generalized fluxes, this is explicitly indicated in the argument. Otherwise, the calculation is assumed to be carried out using the reference flux and importance.

and

$$\langle \phi^{\dagger}, \left(\mathbf{A} - \frac{\mathbf{F}}{k_{\text{eff}}}\right)_{\nu_{i'g'z'}^{\text{P}}} \tilde{\Psi}_{\text{n}} \rangle = -\frac{\langle \phi^{\dagger} \nu_{i'g'z'}^{\text{P}} \frac{\partial \chi}{\partial \nu_{i'g'z'}^{\text{P}}}, \nu \Sigma_{\text{f}} \tilde{\Psi}_{\text{n}} \rangle}{k_{\text{eff}}} - (\nu^{\text{P}} \Sigma_{\text{f}})_{i'g'z'} \frac{\int_{V_{z'}} \tilde{\Psi}_{\text{n},g'}} \left(\sum_{\text{g}} \chi_{\text{g}} \phi_{\text{g}}^{\dagger}\right) dV}{k_{\text{eff}}} - \frac{\langle \phi^{\dagger} \tilde{\chi}(\nu_{i'g'z'}^{\text{P}}), \nu \Sigma_{\text{f}} \tilde{\Psi}_{\text{n}} \rangle}{k_{\text{off}}} - (\nu^{\text{P}} \Sigma_{\text{f}})_{i'g'z'} \frac{\text{SIAP}_{g'z'}}{k_{\text{off}}} \left(\phi^{\dagger}, \tilde{\Psi}_{\text{n}}\right)}{k_{\text{off}}}.$$

$$(101)$$

As observed earlier (and consistently with the discussion of the indirect terms in the previous sensitivity coefficient derivation), no contribution to the indirect terms originates from the loss operator \mathbf{A} , since it does not depend on $\nu^{\mathrm{p}}_{\mathbf{i}'\mathbf{g}'\mathbf{z}'}$.

By substituting into Equation 90 the expressions derived for both the direct and indirect terms, the analytical formula is derived for the sensitivity coefficient of the effective delayed neutrons fraction belonging to a specific family n with respect to the average number of prompt neutrons emitted per fission event of a given isotope i', in energy group g' and located in a spatial region z' of the core:

$$\begin{split} S(\hat{\beta}_{\text{eff,n}}, \nu_{i'g'z'}^{\text{p}}) &= -\nu_{i'g'z'}^{\text{p}} \frac{\beta_{i'ng'z'}}{\nu_{i'n}^{\text{d}}} + \\ &+ \frac{\beta_{i'n}}{\hat{\beta}_{\text{eff,n}}} \frac{(\nu^{\text{p}}\Sigma_{\text{f}})_{i'g'z'}\text{SIAP}_{ng'z'}^{\text{d}}}{\text{VIMPOR}} + \\ &- \frac{(\nu^{\text{p}}\Sigma_{\text{f}})_{i'g'z'}\text{SIAP}_{g'z'}}{\text{VIMPOR}} - \frac{\langle \phi^{\dagger}\tilde{\chi}(\nu_{i'g'z'}^{\text{p}}), \nu\Sigma_{\text{f}}\phi \rangle}{\text{VIMPOR}} + \\ &+ \frac{1}{k_{\text{eff}}} \left[\langle \tilde{\Psi}_{n}^{\dagger}\tilde{\chi}(\nu_{i'g'z'}^{\text{p}}), \nu\Sigma_{\text{f}}\phi \rangle + (\nu^{\text{p}}\Sigma_{\text{f}})_{i'g'z'}\text{SIAP}_{gz'}(\tilde{\Psi}_{n}^{\dagger}, \phi) + \right. \\ &+ \left. \langle \phi^{\dagger}\tilde{\chi}(\nu_{i'g'z'}^{\text{p}}), \nu\Sigma_{\text{f}}\tilde{\Psi}_{n} \rangle + (\nu^{\text{p}}\Sigma_{\text{f}})_{i'g'z'}\text{SIAP}_{gz'}(\phi^{\dagger}, \tilde{\Psi}_{n}) \right] \end{split}$$

which satisfies the initial requirement set for the development of the analytical expressions of the sensitivity coefficients, namely that they be composed exclusively of terms directly available from ERANOS functions or from suitable combinations thereof.

4.1.3 Sensitivity Coefficients of the Effective Delayed Neutron Fraction $\hat{eta}_{\rm eff,n}$ to the Delayed Neutrons Emission Spectrum $\chi_{\rm ng}^{\rm d}$

The purpose of the following calculation is to derive a formulation for the sensitivity coefficients of $\hat{\beta}_{\text{eff.n}}$ with respect to the delayed neutron emission spectrum of given

family n', evaluated at the energy corresponding to group h. The starting expression, based on the result obtained with GPT calculations in Equation 38, is given by:

$$S(\hat{\beta}_{\text{eff,n}}, \chi_{\text{n'h}}^{\text{d}}) = \frac{(\hat{\beta}_{\text{eff,n}})_{\chi_{\text{n'h}}^{\text{d}}}}{\hat{\beta}_{\text{eff,n}}} - \langle \tilde{\Psi}_{\text{n}}^{\dagger}, \left(\mathbf{A} - \frac{\mathbf{F}}{k_{\text{eff}}}\right)_{\chi_{\text{n'h}}^{\text{d}}} \phi \rangle - \langle \tilde{\Psi}_{\text{n}}, \left(\mathbf{A}^{\dagger} - \frac{\mathbf{F}^{\dagger}}{k_{\text{eff}}}\right)_{\chi_{\text{n'h}}^{\text{d}}} \phi^{\dagger} \rangle.$$
(103)

As a first step, the direct term is evaluated, represented by the quantity $(\hat{\beta}_{\text{eff,n}})_{\chi_{n'h}^d}/\hat{\beta}_{\text{eff,n}}$, whose numerator can be expressed as:

$$(\hat{\beta}_{\text{eff,n}})_{\chi_{n'h}^{d}} = \chi_{n'h}^{d} \frac{\partial \hat{\beta}_{\text{eff,n}}}{\partial \chi_{n'h}^{d}}$$

$$= \chi_{n'h}^{d} \left\{ \frac{\int_{V} d\vec{r} \sum_{g'=1}^{G} \phi_{g'}^{\dagger} \left(\frac{\partial \chi_{ng'}^{d}}{\partial \chi_{n'h}^{d}} \right) \sum_{g=1}^{G} \beta_{n} \nu_{g} \sum_{f,g} \phi_{g}}{\langle \phi^{\dagger}, \mathbf{F} \phi \rangle} - \hat{\beta}_{\text{eff,n}} \frac{\int_{V} d\vec{r} \sum_{g'=1}^{G} \phi_{g'}^{\dagger} \left(\frac{\partial \chi_{g'}}{\partial \chi_{n'h}^{d}} \right) \sum_{g=1}^{G} \nu_{g} \sum_{f,g} \phi_{g}}{\langle \phi^{\dagger}, \mathbf{F} \phi \rangle} \right\}.$$

$$(104)$$

To proceed with the development of this expression, the two derivatives involving the delayed neutron emission spectrum need to be evaluated. Specifically, the following are obtained:

$$\frac{\partial \chi_{\rm ng}^{\rm d}}{\partial \chi_{\rm n'g'}^{\rm d}} = \delta_{\rm nn'} \left(\delta_{\rm gg'} - \chi_{\rm ng}^{\rm d} \right) \,, \tag{105}$$

for which Equation 73 for the spectrum derivative has been applied, and

$$\frac{\partial \chi_{\rm g}}{\partial \chi_{\rm n'\sigma'}^{\rm d}} = \beta_{\rm n'} \frac{\partial \chi_{\rm n'g}^{\rm d}}{\partial \chi_{\rm n'\sigma'}^{\rm d}} = \beta_{\rm n'} \left(\delta_{\rm gg'} - \chi_{\rm n'g}^{\rm d} \right) , \qquad (106)$$

where the first equality is obtained by considering the definition given in Equation 67 for the fission spectrum, along with the assumption that its prompt and delayed components are independent of each other.

By inserting these two relations into the recently derived Equation 104, the follow-

ing expression is obtained:

$$(\hat{\beta}_{\text{eff,n}})_{\chi_{n'h}^{d}} = \chi_{n'h}^{d} \left\{ \frac{\int_{V} d\vec{r} \sum_{g'=1}^{G} \phi_{g'}^{\dagger} \delta_{nn'} \left(\delta_{g'h} - \chi_{ng'}^{d} \right) \sum_{g=1}^{G} \beta_{n} \nu_{g} \sum_{f,g} \phi_{g}}{\langle \phi^{\dagger}, \mathbf{F} \phi \rangle} + \right. \\ \left. - \hat{\beta}_{\text{eff,n}} \frac{\int_{V} d\vec{r} \sum_{g'=1}^{G} \phi_{g'}^{\dagger} \beta_{n'} \left(\delta_{g'h} - \chi_{n'g'}^{d} \right) \sum_{g=1}^{G} \nu_{g} \sum_{f,g} \phi_{g}}{\langle \phi^{\dagger}, \mathbf{F} \phi \rangle} \right\} \\ = \chi_{n'h}^{d} \left\{ \delta_{nn'} \frac{\beta_{n} \int_{V} d\vec{r} \phi_{h}^{\dagger} \left(\sum_{g=1}^{G} \nu_{g} \sum_{f,g} \phi_{g} \right)}{\langle \phi^{\dagger}, \mathbf{F} \phi \rangle} - \delta_{nn'} \frac{\beta_{n} \int_{V} d\vec{r} \left(\sum_{g'=1}^{G} \phi_{g'}^{\dagger} \chi_{ng'}^{d} \right) \left(\sum_{g=1}^{G} \nu_{g} \sum_{f,g} \phi_{g} \right)}{\langle \phi^{\dagger}, \mathbf{F} \phi \rangle} + \\ - \hat{\beta}_{\text{eff,n}} \frac{\beta_{n'} \int_{V} d\vec{r} \phi_{h}^{\dagger} \left(\sum_{g'=1}^{G} \phi_{g'}^{\dagger} \chi_{n'g'}^{d} \right) \left(\sum_{g=1}^{G} \nu_{g} \sum_{f,g} \phi_{g} \right)}{\langle \phi^{\dagger}, \mathbf{F} \phi \rangle} + \\ + \hat{\beta}_{\text{eff,n}} \frac{\beta_{n'} \int_{V} d\vec{r} \left(\sum_{g'=1}^{G} \phi_{g'}^{\dagger} \chi_{n'g'}^{d} \right) \left(\sum_{g=1}^{G} \nu_{g} \sum_{f,g} \phi_{g} \right)}{\langle \phi^{\dagger}, \mathbf{F} \phi \rangle} \right\} \\ = \chi_{n'h}^{d} \left\{ \delta_{nn'} \frac{\beta_{n} \text{SIDP}_{h}}{V \text{IMPOR}} - \delta_{nn'} \frac{\beta_{n} V \text{IMPOR}_{n}^{d}}{V \text{IMPOR}} + \\ - \hat{\beta}_{\text{eff,n}} \frac{\beta_{n'} \text{SIDP}_{h}}{V \text{IMPOR}} + \hat{\beta}_{\text{eff,n}} \frac{\beta_{n'} V \text{IMPOR}_{n'}^{d}}{V \text{IMPOR}} \right\} ,$$

where the definitions given for the perturbation integrals introduced in Equation 59 (VIMPOR) and Equation 58 (SIDP) have been used, while Equation 66 has been rewritten in the following energy-discretized form:

$$VIMPOR_{n}^{d} = \int_{V} d\vec{r} \sum_{g'=1}^{G} \phi_{g'}^{\dagger} \chi_{ng'}^{d} \sum_{g=1}^{G} \nu_{g} \Sigma_{f,g} \phi_{g}.$$
 (108)

Hence, the direct term can be obtained finally by dividing this last Equation 107 by the value of the effective neutron fraction associated with the precursor family n, leading to the following expression:

$$\frac{(\hat{\beta}_{\text{eff,n}})_{\chi_{n'h}^{d}}}{\hat{\beta}_{\text{eff,n}}} = \chi_{n'h}^{d} \left\{ \left(\delta_{nn'} \frac{\beta_{n}}{\hat{\beta}_{\text{eff,n}}} - \beta_{n'} \right) \frac{\text{SIDP}_{h}}{\text{VIMPOR}} + \left(\hat{\beta}_{\text{eff,n'}} - \delta_{nn'} \right) \right\}. \tag{109}$$

The development of the indirect sensitivity terms is now undertaken, and they can

be expressed as follows:

$$\langle \tilde{\Psi}_{\mathbf{n}}^{\dagger}, (\mathbf{A} - \frac{\mathbf{F}}{k_{\text{eff}}})_{\chi_{\mathbf{n}'\mathbf{h}}^{d}} \phi \rangle = -\frac{\chi_{\mathbf{n}'\mathbf{h}}^{d}}{k_{\text{eff}}} \int_{V} d\vec{r} \sum_{\mathbf{g}'=1}^{\mathbf{G}} \tilde{\Psi}_{\mathbf{n}\mathbf{g}'}^{\dagger} \left(\frac{\chi_{\mathbf{g}'}}{\chi_{\mathbf{n}'\mathbf{h}}^{d}}\right) \sum_{\mathbf{g}=1}^{\mathbf{G}} \nu_{\mathbf{g}} \Sigma_{\mathbf{f},\mathbf{g}} \phi_{\mathbf{g}}$$

$$= -\frac{\chi_{\mathbf{n}'\mathbf{h}}^{d}}{k_{\text{eff}}} \int_{V} d\vec{r} \sum_{\mathbf{g}'=1}^{\mathbf{G}} \tilde{\Psi}_{\mathbf{n}\mathbf{g}'}^{\dagger} \beta_{\mathbf{n}'} \left(\frac{\chi_{\mathbf{n}'\mathbf{g}'}}{\chi_{\mathbf{n}'\mathbf{h}}^{d}}\right) \sum_{\mathbf{g}=1}^{\mathbf{G}} \nu_{\mathbf{g}} \Sigma_{\mathbf{f},\mathbf{g}} \phi_{\mathbf{g}}$$

$$= -\frac{\chi_{\mathbf{n}'\mathbf{h}}^{d}}{k_{\text{eff}}} \int_{V} d\vec{r} \sum_{\mathbf{g}'=1}^{\mathbf{G}} \tilde{\Psi}_{\mathbf{n}\mathbf{g}'}^{\dagger} \beta_{\mathbf{n}'} \left(\delta_{\mathbf{g}'\mathbf{h}} - \chi_{\mathbf{n}'\mathbf{g}'}^{d}\right) \sum_{\mathbf{g}=1}^{\mathbf{G}} \nu_{\mathbf{g}} \Sigma_{\mathbf{f},\mathbf{g}} \phi_{\mathbf{g}}$$

$$= -\frac{\beta_{\mathbf{n}'} \chi_{\mathbf{n}'\mathbf{h}}^{d}}{k_{\text{eff}}} \left\{ \int_{V} d\vec{r} \, \tilde{\Psi}_{\mathbf{n}\mathbf{h}}^{\dagger} \sum_{\mathbf{g}=1}^{\mathbf{G}} \nu_{\mathbf{g}} \Sigma_{\mathbf{f},\mathbf{g}} \phi_{\mathbf{g}} - \int_{V} d\vec{r} \, \sum_{\mathbf{g}'=1}^{\mathbf{G}} \tilde{\Psi}_{\mathbf{n}\mathbf{g}'}^{\dagger} \chi_{\mathbf{n}'\mathbf{g}'}^{d} \sum_{\mathbf{g}=1}^{\mathbf{G}} \nu_{\mathbf{g}} \Sigma_{\mathbf{f},\mathbf{g}} \phi_{\mathbf{g}} \right\}$$

$$= -\frac{\beta_{\mathbf{n}'} \chi_{\mathbf{n}'\mathbf{h}}^{d}}{k_{\text{eff}}} \left\{ \text{SIDP}_{\mathbf{h}}(\tilde{\Psi}_{\mathbf{n}}^{\dagger}, \phi) - \text{VIMPOR}_{\mathbf{n}'}^{d}(\tilde{\Psi}_{\mathbf{n}}^{\dagger}, \phi) \right\}$$

and

$$\begin{split} \langle \tilde{\Psi}_{\mathbf{n}}, (\mathbf{A}^{\dagger} - \frac{\mathbf{F}^{\dagger}}{k_{\mathrm{eff}}})_{\chi_{\mathbf{n}'\mathbf{h}}^{\mathrm{d}}} \phi^{\dagger} \rangle &= -\frac{\chi_{\mathbf{n}'\mathbf{h}}^{\mathrm{d}}}{k_{\mathrm{eff}}} \int_{V} d\vec{r} \sum_{\mathbf{g}'=1}^{\mathrm{G}} \phi_{\mathbf{g}'}^{\dagger} \left(\frac{\chi_{\mathbf{g}'}}{\chi_{\mathbf{n}'\mathbf{h}}^{\mathrm{d}}} \right) \sum_{\mathbf{g}=1}^{\mathrm{G}} \nu_{\mathbf{g}} \Sigma_{\mathbf{f},\mathbf{g}} \tilde{\Psi}_{\mathbf{n}\mathbf{g}} \\ &= -\frac{\chi_{\mathbf{n}'\mathbf{h}}^{\mathrm{d}}}{k_{\mathrm{eff}}} \int_{V} d\vec{r} \sum_{\mathbf{g}'=1}^{\mathrm{G}} \phi_{\mathbf{g}'}^{\dagger} \beta_{\mathbf{n}'} \left(\frac{\chi_{\mathbf{n}'\mathbf{g}'}}{\chi_{\mathbf{n}'\mathbf{h}}^{\mathrm{d}}} \right) \sum_{\mathbf{g}=1}^{\mathrm{G}} \nu_{\mathbf{g}} \Sigma_{\mathbf{f},\mathbf{g}} \tilde{\Psi}_{\mathbf{n}\mathbf{g}} \\ &= -\frac{\chi_{\mathbf{n}'\mathbf{h}}^{\mathrm{d}}}{k_{\mathrm{eff}}} \int_{V} d\vec{r} \sum_{\mathbf{g}'=1}^{\mathrm{G}} \phi_{\mathbf{g}'}^{\dagger} \beta_{\mathbf{n}'} \left(\delta_{\mathbf{g}'\mathbf{h}} - \chi_{\mathbf{n}'\mathbf{g}'}^{\mathrm{d}} \right) \sum_{\mathbf{g}=1}^{\mathrm{G}} \nu_{\mathbf{g}} \Sigma_{\mathbf{f},\mathbf{g}} \tilde{\Psi}_{\mathbf{n}\mathbf{g}} \\ &= -\frac{\beta_{\mathbf{n}'}\chi_{\mathbf{n}'\mathbf{h}}^{\mathrm{d}}}{k_{\mathrm{eff}}} \left\{ \int_{V} d\vec{r} \phi_{\mathbf{h}}^{\dagger} \sum_{\mathbf{g}=1}^{\mathrm{G}} \nu_{\mathbf{g}} \Sigma_{\mathbf{f},\mathbf{g}} \tilde{\Psi}_{\mathbf{n}\mathbf{g}} - \int_{V} d\vec{r} \sum_{\mathbf{g}'=1}^{\mathrm{G}} \phi_{\mathbf{g}'}^{\dagger} \chi_{\mathbf{n}'\mathbf{g}'}^{\mathrm{d}} \sum_{\mathbf{g}=1}^{\mathrm{G}} \nu_{\mathbf{g}} \Sigma_{\mathbf{f},\mathbf{g}} \tilde{\Psi}_{\mathbf{n}\mathbf{g}} \right\} \\ &= -\frac{\beta_{\mathbf{n}'}\chi_{\mathbf{n}'\mathbf{h}}^{\mathrm{d}}}{k_{\mathrm{eff}}} \left\{ \mathrm{SIDP}_{\mathbf{h}}(\phi^{\dagger}, \tilde{\Psi}_{\mathbf{n}}) - \mathrm{VIMPOR}_{\mathbf{n}'}^{\mathrm{d}}(\phi^{\dagger}, \tilde{\Psi}_{\mathbf{n}}) \right\}. \end{split}$$

Once again, no contributions to the indirect terms arise from the neutronic loss operator \mathbf{A} , as it does not exhibit any dependence on the considered input parameter. Finally, by combining the direct and indirect terms, the expression for the sensitivity

coefficient is obtained:

$$S\left(\hat{\beta}_{\text{eff,n}}, \chi_{\text{n'h}}^{\text{d}}\right) = \chi_{\text{n'h}}^{\text{d}} \left\{ \left(\delta_{\text{nn'}} \frac{\beta_{\text{n}}}{\hat{\beta}_{\text{eff,n}}} - \beta_{\text{n'}}\right) \frac{\text{SIDP}_{\text{h}}}{\text{VIMPOR}} + \left(\hat{\beta}_{\text{eff,n'}} - \delta_{\text{nn'}}\right) + \right.$$

$$\left. + \frac{\beta_{\text{n'}}}{k_{\text{eff}}} \left[\text{SIDP}_{\text{h}}(\tilde{\Psi}_{\text{n}}^{\dagger}, \phi) - \text{VIMPOR}_{\text{n'}}^{\text{d}}(\tilde{\Psi}_{\text{n}}^{\dagger}, \phi) + \right. \right.$$

$$\left. + \text{SIDP}_{\text{h}}(\phi^{\dagger}, \tilde{\Psi}_{\text{n}}) - \text{VIMPOR}_{\text{n'}}^{\text{d}}(\phi^{\dagger}, \tilde{\Psi}_{\text{n}}) \right] \right\}.$$

$$\left. (112)$$

The terms appearing in the expression of this type of sensitivity coefficients satisfy the requirement that they are obtainable exclusively through the use of functions provided by ERANOS, either directly or through combinations thereof.

4.1.4 Sensitivity Coefficients of the Effective Delayed Neutron Fraction $\hat{eta}_{\rm eff,n}$ to the Prompt Neutrons Emission Spectrum $\chi^{\rm p}_{\rm igz}$

The section is concluded by considering the case in which the perturbed parameter is the prompt neutron emission spectrum ($\nu^{\rm p}_{i'{\rm hz'}}$) of isotope i', evaluated at an energy corresponding to group h and in zone z' of the reactor core, which, when applied to the result obtained through GPT calculations in Equation 38, translates into the following expression for the respective sensitivity coefficient of the effective delayed neutron fraction:

$$S\left(\hat{\beta}_{\text{eff,n}}, \chi_{\text{i'hz'}}^{\text{p}}\right) = \frac{(\hat{\beta}_{\text{eff,n}})_{\chi_{\text{i'hz'}}^{\text{p}}}}{\hat{\beta}_{\text{eff,n}}} - \langle \tilde{\Psi}_{\text{n}}^{\dagger}, \left(\mathbf{A} - \frac{\mathbf{F}}{k_{\text{eff}}}\right)_{\chi_{\text{i'l,l}}^{\text{p}}} \phi \rangle - \langle \tilde{\Psi}_{\text{n}}, \left(\mathbf{A}^{\dagger} - \frac{\mathbf{F}^{\dagger}}{k_{\text{eff}}}\right)_{\chi_{\text{i'l,l}}^{\text{p}}} \phi^{\dagger} \rangle.$$
(113)

As in the previous cases, the derivation starts with the direct term, given by $\frac{\left(\hat{\beta}_{\mathrm{eff,n}}\right)_{\chi^{P}_{i'hz'}}}{\hat{\beta}_{\mathrm{eff,n}}}$,

whose numerator can be written as:

$$\begin{split} &(\hat{\beta}_{\mathrm{eff,n}})_{\chi_{\mathrm{i'hz'}}^{\mathrm{P}}} = -\hat{\beta}_{\mathrm{eff,n}} \frac{\chi_{\mathrm{i'hz'}}^{\mathrm{P}} \int_{V_{z}} d\vec{r} \sum_{g'=1}^{\mathrm{G}} \phi_{g'}^{\dagger} \left(\frac{d\chi_{g'}}{d\chi_{\mathrm{i'hz'}}^{\mathrm{P}}}\right) \sum_{\mathrm{g}=1}^{\mathrm{G}} \nu_{\mathrm{g}} \sum_{\mathrm{f,g}} \phi_{\mathrm{g}}}{\langle \phi^{\dagger}, \mathbf{F} \phi \rangle} \\ &= -\hat{\beta}_{\mathrm{eff,n}} \frac{\chi_{\mathrm{i'hz'}}^{\mathrm{P}} \int_{V_{z}} d\vec{r} \sum_{g'=1}^{\mathrm{G}} \phi_{g'}^{\dagger} (1-\beta) \left(\frac{d\chi_{\mathrm{i'g'z'}}^{\mathrm{P}}}{d\chi_{\mathrm{i'hz'}}^{\dagger}}\right) \sum_{\mathrm{g}=1}^{\mathrm{G}} \nu_{\mathrm{g}} \sum_{\mathrm{f,g}} \phi_{\mathrm{g}}}{\langle \phi^{\dagger}, \mathbf{F} \phi \rangle} \\ &= -\hat{\beta}_{\mathrm{eff,n}} \frac{\chi_{\mathrm{i'hz'}}^{\mathrm{P}} \int_{V_{z}} d\vec{r} \sum_{\mathrm{g'}=1}^{\mathrm{G}} \phi_{\mathrm{g'}}^{\dagger} (1-\beta) \left(\delta_{\mathrm{g'h}} - \chi_{\mathrm{i'g'z'}}^{\mathrm{P}}\right) \sum_{\mathrm{g}=1}^{\mathrm{G}} \nu_{\mathrm{g}} \sum_{\mathrm{f,g}} \phi_{\mathrm{g}}}{\langle \phi^{\dagger}, \mathbf{F} \phi \rangle} \\ &= -\hat{\beta}_{\mathrm{eff,n}} \chi_{\mathrm{i'hz'}}^{\mathrm{P}} (1-\beta) \frac{\int_{V_{z}} d\vec{r} \phi_{\mathrm{h}}^{\dagger} \left(\sum_{\mathrm{g}=1}^{\mathrm{G}} \nu_{\mathrm{g}} \sum_{\mathrm{f,g}} \phi_{\mathrm{g}}\right)}{\langle \phi^{\dagger}, \mathbf{F} \phi \rangle} + \\ &+ \hat{\beta}_{\mathrm{eff,n}} \chi_{\mathrm{i'hz'}}^{\mathrm{P}} (1-\beta) \frac{\int_{V_{z}} d\vec{r} \sum_{\mathrm{g'}=1}^{\mathrm{G}} \psi_{\mathrm{g'}} \sum_{\mathrm{f',g'z'}} \sum_{\mathrm{g}=1}^{\mathrm{G}} \nu_{\mathrm{g}} \sum_{\mathrm{f,g}} \phi_{\mathrm{g}}}{\langle \phi^{\dagger}, \mathbf{F} \phi \rangle} \\ &= -\hat{\beta}_{\mathrm{eff,n}} \chi_{\mathrm{i'hz'}}^{\mathrm{P}} (1-\beta) \left\{ \frac{\mathrm{SIDP}_{\mathrm{hz'}}}{\mathrm{VIMPOR}} - \frac{\mathrm{VIMPOR}_{\mathrm{i'z'}}^{\mathrm{P}}}{\mathrm{VIMPOR}} \right\}, \end{split}$$

where the following quantity, representing the fission source related exclusively to prompt neutrons, has been defined:

$$\begin{split} \text{VIMPOR}_{\text{iz}}^{\text{p}} &= \int_{V_{z}} d\vec{r} \sum_{\text{g}'=1}^{\text{G}} \phi_{\text{g}'}^{\dagger} \chi_{\text{ig}'\text{z}}^{\text{p}} \sum_{\text{g}=1}^{\text{G}} \nu_{\text{g}} \Sigma_{\text{f},\text{g}} \phi_{\text{g}} \\ &= \int_{V_{z}} d\vec{r} \sum_{\text{g}'=1}^{\text{G}} \phi_{\text{g}'}^{\dagger} \left(\frac{\chi_{\text{ig}'\text{z}} - \sum_{\text{n}} \beta_{\text{n}} \chi_{\text{ng}'}^{\text{d}}}{1 - \beta} \right) \sum_{\text{g}=1}^{\text{G}} \nu_{\text{g}} \Sigma_{\text{f},\text{g}} \phi_{\text{g}} \\ &= \frac{\text{VIMPOR}_{\text{iz}} - \hat{\beta}_{\text{eff},\text{z}} \text{VIMPOR}}{1 - \beta} \,, \end{split} \tag{115}$$

which in turn involves the effective delayed neutron fraction in zone z of the core ($\hat{\beta}_{\text{eff,z}}$), and the fission source associated with isotope i in the same zone z (conventionally denoted as $VIMPOR_{iz}$).

At this stage, the direct term is obtained by normalizing the previously inferred Equation 114 with respect to $\hat{\beta}_{\text{eff,n}}$, yielding:

$$\frac{(\hat{\beta}_{\text{eff,n}})_{\chi_{i'\text{hz'}}^{P}}}{\hat{\beta}_{\text{eff,n}}} = -\chi_{i'\text{hz'}}^{P} \left\{ (1-\beta) \frac{\text{SIDP}_{\text{hz'}}}{\text{VIMPOR}} - \left(\frac{\text{VIMPOR}_{i'\text{z'}}}{\text{VIMPOR}} - \hat{\beta}_{\text{eff,z'}} \right) \right\}, \quad (116)$$

in which $\mathrm{VIMPOR}^{\mathrm{p}}_{i'z'}$ has been expressed according to its definition given in Equation 115.

Regarding the indirect terms, the following expression is derived:

$$\begin{split} \langle \tilde{\Psi}_{\mathbf{n}}^{\dagger}, \left(\mathbf{A} - \frac{\mathbf{F}}{k_{\text{eff}}}\right)_{\chi_{i'\text{hz}'}^{P}} \phi \rangle &= \\ &= -\frac{\chi_{i'\text{hz}'}^{P}}{k_{\text{eff}}} \int_{V} d\vec{r} \sum_{g'=1}^{G} \tilde{\Psi}_{ng'}^{\dagger} \left(\frac{d\chi_{g'}}{d\chi_{i'\text{hz}'}^{P}}\right) \sum_{g'=1}^{G} \nu_{g'} \Sigma_{\mathbf{f},g'} \phi_{g'} \\ &= -\frac{\chi_{i'\text{hz}'}^{P}}{k_{\text{eff}}} \int_{V_{z'}} d\vec{r} \sum_{g'=1}^{G} \tilde{\Psi}_{ng'}^{\dagger} (1-\beta) \left(\frac{d\chi_{i'\text{hz}'}^{P}}{d\chi_{i'\text{hz}'}^{P}}\right) \sum_{g'=1}^{G} \nu_{g'} \Sigma_{\mathbf{f},g'} \phi_{g'} \\ &= -\frac{\chi_{i'\text{hz}'}^{P}}{k_{\text{eff}}} \int_{V_{z'}} d\vec{r} \sum_{g'=1}^{G} \tilde{\Psi}_{ng'}^{\dagger} (1-\beta) \left(\delta_{g'\text{h}} - \chi_{i'\text{g}'z'}^{P}\right) \sum_{g'=1}^{G} \nu_{g'} \Sigma_{\mathbf{f},g'} \phi_{g'} \\ &= -\frac{\chi_{i'\text{hz}'}^{P} (1-\beta)}{k_{\text{eff}}} \left\{ \int_{V_{z'}} d\vec{r} \tilde{\Psi}_{n\text{h}}^{\dagger} \left(\sum_{g'=1}^{G} \nu_{g'} \Sigma_{\mathbf{f},g'} \phi_{g'} \right) + \\ &- \int_{V_{z'}} d\vec{r} \sum_{g'=1}^{G} \tilde{\Psi}_{ng'}^{\dagger} \chi_{i'g'z'}^{P} \sum_{g'=1}^{G} \nu_{g'} \Sigma_{\mathbf{f},g'} \phi_{g'} \right\} \\ &= -\frac{\chi_{i'\text{hz}'}^{P} (1-\beta)}{k_{\text{eff}}} \left\{ \text{SIDP}_{\text{hz}'} (\tilde{\Psi}_{n}^{\dagger}, \phi) - \text{VIMPOR}_{i'z'}^{P} (\tilde{\Psi}_{n}^{\dagger}, \phi) \right\} \\ &= -\frac{\chi_{i'\text{hz}'}^{P}}{k_{\text{eff}}} \left\{ (1-\beta) \text{SIDP}_{\text{hz}'} (\tilde{\Psi}_{n}^{\dagger}, \phi) + \\ &- \left(\text{VIMPOR}_{i'z'} (\tilde{\Psi}_{n}^{\dagger}, \phi) - \hat{\beta}_{\text{eff},z'} \text{VIMPOR} (\tilde{\Psi}_{n}^{\dagger}, \phi) \right) \right\} \end{split}$$

and

$$\begin{split} \langle \tilde{\Psi}_{\mathbf{n}}, (\mathbf{A}^{\dagger} - \frac{\mathbf{F}^{\dagger}}{k_{\text{eff}}})_{\chi_{\text{l'hz'}}^{p}} \phi^{\dagger} \rangle &= \\ &= -\frac{\chi_{\text{l'hz'}}^{p}}{k_{\text{eff}}} \int_{V} d\vec{r} \sum_{\mathbf{g}'=1}^{G} \phi_{\mathbf{g}'}^{\dagger} \left(d\chi_{\mathbf{g}'} / d\chi_{\text{l'hz'}} \right) \sum_{\mathbf{g}'=1}^{G} \nu_{\mathbf{g}'} \Sigma_{\mathbf{f},\mathbf{g}'} \tilde{\Psi}_{\mathbf{n}\mathbf{g}'} \\ &= -\frac{\chi_{\text{l'hz'}}^{p}}{k_{\text{eff}}} \int_{V_{\mathbf{z}'}} d\vec{r} \sum_{\mathbf{g}'=1}^{G} \phi_{\mathbf{g}'}^{\dagger} (1-\beta) \left(d\chi_{\mathbf{l'g'z'}} / d\chi_{\mathbf{l'hz}} \right) \sum_{\mathbf{g}'=1}^{G} \nu_{\mathbf{g}'} \Sigma_{\mathbf{f},\mathbf{g}'} \tilde{\Psi}_{\mathbf{n}\mathbf{g}'} \\ &= -\frac{\chi_{\mathbf{l'hz'}}^{p}}{k_{\text{eff}}} \int_{V_{\mathbf{z}'}} d\vec{r} \sum_{\mathbf{g}'=1}^{G} \phi_{\mathbf{g}'}^{\dagger} (1-\beta) \left(\delta_{\mathbf{g}'\mathbf{h}} - \chi_{\mathbf{l'g'z'}} \right) \sum_{\mathbf{g}'=1}^{G} \nu_{\mathbf{g}'} \Sigma_{\mathbf{f},\mathbf{g}'} \tilde{\Psi}_{\mathbf{n}\mathbf{g}'} \\ &= -\frac{\chi_{\mathbf{l'hz'}}^{p} (1-\beta)}{k_{\text{eff}}} \left\{ \int_{V_{\mathbf{z}'}} d\vec{r} \phi_{\mathbf{h}}^{\dagger} \left(\sum_{\mathbf{g}'=1}^{G} \nu_{\mathbf{g}'} \Sigma_{\mathbf{f},\mathbf{g}'} \tilde{\Psi}_{\mathbf{n}\mathbf{g}'} \right) + \\ &- \int_{V_{\mathbf{z}'}} d\vec{r} \sum_{\mathbf{g}'=1}^{G} \phi_{\mathbf{g}'}^{\dagger} \chi_{\mathbf{l'g'z'}}^{p} \sum_{\mathbf{g}'=1}^{G} \nu_{\mathbf{g}'} \Sigma_{\mathbf{f},\mathbf{g}'} \tilde{\Psi}_{\mathbf{n}\mathbf{g}'} \right\} \\ &= -\frac{\chi_{\mathbf{l'hz'}}^{p} (1-\beta)}{k_{\text{eff}}} \left\{ \text{SIDP}_{\mathbf{hz'}} (\phi^{\dagger}, \tilde{\Psi}_{\mathbf{n}}) - \text{VIMPOR}_{\mathbf{l'z'}}^{p} (\phi^{\dagger}, \tilde{\Psi}_{\mathbf{n}}) \right\} \\ &= -\frac{\chi_{\mathbf{l'hz'}}^{p}}{k_{\text{eff}}} \left\{ (1-\beta) \text{SIDP}_{\mathbf{hz'}} (\phi^{\dagger}, \tilde{\Psi}_{\mathbf{n}}) - \hat{\beta}_{\text{eff},\mathbf{z}'} \text{VIMPOR} (\phi^{\dagger}, \tilde{\Psi}_{\mathbf{n}}) \right\}. \end{split}$$

Also in this case, it can be observed that the contribution of the loss operators ($\bf A$ and $\bf A^\dagger$) to the indirect component of the sensitivity is zero, being entirely accounted for by the neutron production operators ($\bf F$ and $\bf F^\dagger$) appearing in the forward and adjoint forms of the Boltzmann equation.

By combining the direct and indirect contributions, the resulting expression for the

sensitivity coefficient under investigation is obtained:

$$S(\hat{\beta}_{\text{eff,n}}, \chi_{i'\text{hz'}}^{\text{p}}) = \chi_{i'\text{hz'}}^{\text{p}} \left\{ \frac{1}{\text{VIMPOR}} \left[\left(\text{VIMPOR}_{i'\text{z'}} - \hat{\beta}_{\text{eff,z'}} \text{VIMPOR} \right) + \right. \right. \\ \left. - \left(1 - \beta \right) \text{SIDP}_{\text{hz'}} \right] + \\ \left. - \frac{1}{k_{\text{eff}}} \left[\left(\text{VIMPOR}_{i'\text{z'}} (\tilde{\Psi}_{n}^{\dagger}, \phi) - \hat{\beta}_{\text{eff,z'}} \text{VIMPOR} (\tilde{\Psi}_{n}^{\dagger}, \phi) \right) + \right. \\ \left. - \left(1 - \beta \right) \text{SIDP}_{\text{hz'}} (\tilde{\Psi}_{n}^{\dagger}, \phi) \right] + \\ \left. - \frac{1}{k_{\text{eff}}} \left[\left(\text{VIMPOR}_{i'\text{z'}} (\phi^{\dagger}, \tilde{\Psi}_{n}) - \hat{\beta}_{\text{eff,z'}} \text{VIMPOR} (\phi^{\dagger}, \tilde{\Psi}_{n}) \right) + \right. \\ \left. - \left(1 - \beta \right) \text{SIDP}_{\text{hz'}} (\phi^{\dagger}, \tilde{\Psi}_{n}) \right] \right\}$$

The analytical development of the direct and indirect terms carried out has allowed this latter type of sensitivity coefficients to be expressed through quantities calculable by functions provided by ERANOS. This calculation completes the set of sensitivity coefficients addressed in this thesis.

4.2 Implementation of the Quantities Entering Sensitivity Coefficient Expressions

The analytical formulations of the four selected sensitivity coefficients derived in the previous section were developed with the objective of fully exploiting the functionalities already available in ERANOS. While some of these quantities can be obtained directly as outputs of specific modules, others require the use of a combination of such quantities, complemented by dedicated procedures written in the LU language.

The portion of ERANOS code developed for this purpose constitutes the central part of the overall script, which also includes an initial section dedicated to the construction of the reactor model (the toy model developed for testing is presented below, in Section 5.2.1) and a final section focused on the actual computation of the various sensitivity coefficients (discussed later on this chapter, in Section 4.2.1). In the last two stages, particular emphasis was placed on coding flexibility, which is reflected in the ability for the user to freely select the multigroup energy discretization, the isotopes, and the precursor families to be included in the calculation. This versatility ensures that

the developed tools can be applied to different reactor configurations and benchmark cases without requiring structural modifications to the code.

In the following, the implementation strategies adopted for the various quantities involved in the analytical expressions of the sensitivity coefficients considered in this study are presented.

Flux and Importance (ϕ and ϕ^{\dagger})

Immediately after the cell calculation level is completed - leading to the generation of the MICRO, MACRO, and MEDIUM EDLs (as stated in Section 3.3.1) - the reference flux ϕ and importance ϕ^\dagger are evaluated. The setup of this calculation involves a sequence of logical blocks that specifies the geometric parameters, material properties, and numerical solution strategies. These can be categorized into three main steps, corresponding to the three ERANOS modules employed for this purpose :

- In the first step, the FD_DIFFUSION_MATRIX_COEFFICIENT module is responsible for generating the coefficients of the diffusion matrix for the neutron flux equation. These coefficients describe, for each volume in the discretized domain, the contribution of the flux exchanges with neighboring volumes, and form part of the coefficient matrix of the linear system governing the stationary flux distribution. A key option here concerns the treatment of neutron transport: either through a diffusive approximation or via an explicit transport model. In the present case, the transport model is adopted, providing higher accuracy in the evaluation of the coefficients.
- In the second step, the numerical method used to solve the neutron flux equation is specified, using coefficients computed previously, by means of the FD_DIFFUSION_METHOD module. The finite difference method is adopted (see Appendix A), which provides an efficient solution of the linear systems arising from the discretization of the transport equation.
- The final step, associated with the DIRECTION_COSINE_AND_WEIGHT_CREATION module, specifies the angular quadrature set for the discrete transport calculations. In the test cases considered, the symmetric S_4 quadrature set is employed, which discretizes the solid angle into a finite number of weighted directions while preserving symmetry with respect to the principal Cartesian planes.

Hence, the flux is computed as described in Section 3.4.3, providing access to both scalar and angular components. The only difference between the module used for flux (ϕ and Ψ) calculation and that used for importance (ϕ^{\dagger} and Ψ^{\dagger}) lies in the directive that specifies whether the module is performed in the forward or adjoint mode.

Effective multiplication factor (k_{eff})

The calculation of $k_{
m eff}$ was performed using the INTEGRALE_PERTURBATION_TRANSPORT

module (see Section 3.4.4). This module implements a perturbative methodology that allows the evaluation of $k_{\rm eff}$ based on a combination of forward and adjoint angular fluxes (defined in Section 3.4.3), macroscopic cross-sections, and the system geometry. As an alternative, used for verification purposes, the value of the effective multiplication factor can be retrieved from the module employed to compute the flux or the importance.

Average numbers of emitted neutrons (ν)

The average number of neutrons emitted per fission event is not explicitly stored in the MICRO and MACRO EDLs. However, this information is implicitly available in their NU_FISSION section, which contains the quantity $\nu\Sigma_{\rm f}$, representing the total neutron production rate per unit volume and per unit time due to fission. Since the EDLs also include a dedicated section for the fission cross section (FISSION), the average number of neutrons per fission event, ν , can be computed by taking the ratio of these two quantities – ensuring consistency in energy group, reactor zone, and (in the case of MICRO data) fissile isotope – according to the following relations:

$$\begin{cases} \nu_{\rm gz} = \frac{(\nu \Sigma_{\rm f})_{\rm gz}}{\Sigma_{\rm f,gz}} & \text{for MACRO data} \\ \nu_{\rm igz} = \frac{(\nu \sigma_{\rm f})_{\rm igz}}{\sigma_{\rm f,igz}} & \text{for MICRO data} \end{cases} \tag{120}$$

For the delayed component, the average number of delayed neutrons emitted per fission is directly provided by the original cross-sections evaluations. These values, denoted as $\nu_{\rm in}^d$, are given per isotope and per delayed neutron family. The prompt component is then obtained by subtracting the delayed contribution from the total average, as expressed by:

$$\nu_{\rm igz}^{\rm p} = \nu_{\rm igz} - \sum_{\rm n} \nu_{\rm in}^{\rm d} \,, \tag{121} \label{eq:energy_potential}$$

where the summation is carried out over all precursor families n to account for their cumulative contribution to the delayed neutron yield.

Fission sources

The quantity VIMPOR, representing the fission source weighted by the importance function, is computed using the same perturbative framework adopted for the calculation of $k_{\rm eff}$, namely the INTEGRALE_PERTURBATION_TRANSPORT module.

The sensitivity analysis of $\hat{\beta}_{eff}$ with respect to various input parameters requires the computation of fission sources constructed from different combinations of fluxes, generalized fluxes, and other nuclear quantities, often restricted to specific isotopes, reactor zones, or selected combinations thereof. These selections are configured through

the directives of the INTEGRALE_PERTURBATION_TRANSPORT module. In particular, isotope-specific contributions are obtained by providing the module with a MACRO EDL generated via the MACRO_CALCULATION module (Section 3.4.1), in which only the isotope of interest is retained.

Another frequently used fission source in these calculations is defined using the delayed neutron emission spectrum for each precursor family ($\chi_{\rm ng}^{\rm d}$) in place of the standard fission spectrum ($\chi_{\rm g}$). To enable this, the delayed spectra are inserted into the MACRO EDL passed as input to the INTEGRALE_PERTURBATION_TRANSPORT module. A dedicated procedure was implemented to overwrite the original fission spectrum in the EDL data structure with the delayed emission spectrum corresponding to the selected precursor family.

SIDP and SIAP

These quantities, being defined as perturbation integrals, are likewise computed using the INTEGRAL_PERTURBATION_TRANSPORT module. Following the same procedures adopted for the evaluation of fission sources, SIAP and SIDP can be computed with respect to specific isotopes and zones. This is achieved either by restricting the integration domain to selected core regions or by substituting the reference fluxes with appropriately constructed generalized fluxes.

Delayed Neutrons Fraction (β)

Defined in accordance with Equation 65, $\beta_{\rm in}$ represents the fraction of delayed neutrons originating from precursor family n of isotope i. This quantity is not directly provided by ERANOS and must therefore be computed by combining existing modules with additional operations implemented using the LU input language.

The first step consists in generating a source EDL using the IMPORTANCE_CALCULATION_ SOURCE_CREATION module (described in Section 3.4.2), which stores the fission production term $\nu\Sigma_{\rm f}$. By enabling the optional FUNCTIONAL directive, the functional (nufiss_phi_int) is also evaluated, representing the energy- and volume-integrated contribution of the product $\nu\Sigma_{\rm f}\cdot\phi$ over the entire reactor core. This functional is subsequently used as a normalization factor and corresponds to:

$${\tt nufiss_phi_int} = \sum_{\tt z} \left(\sum_{{\tt g,m}\in \tt z} (\nu \Sigma_{\tt f})_{\tt gz} \, \phi_{\tt g,m} \, V_{\tt m} \right) \, ,$$

Subsequently, the calculation of $\beta_{\rm in}$ requires the creation of a second source EDL, again using the IMPORTANCE_CALCULATION_SOURCE_CREATION module. As input, a MACRO EDL is provided that is constructed for the specific isotope i, in which the response cross sections are restricted to the fission cross section of the selected isotope ($\Sigma_{\rm f,i}$).

The associated response functions allow the evaluation of the functional fiss_phi, representing the isotope fission rate over the reactor core volume:

$$exttt{fiss_phi} = \sum_{ exttt{z}} \left(\sum_{ ext{g,m} \in exttt{z}} \Sigma_{ ext{f,igz}} \, \phi_{ ext{g,m}} \, V_{ ext{m}}
ight).$$
 (123)

This quantity is then multiplied by the average number of delayed neutrons emitted per fission event of isotope i in precursor family n, denoted by $\nu_{\rm in}^{\rm d}$, and subsequently normalized with respect to the functional nufiss_phi_int:

$$\frac{\nu_{\text{in}}^{\text{d}} \cdot \text{fiss_phi}}{\text{nufiss_phi_int}} = \frac{\sum_{z} \left(\sum_{g,m \in z} \nu_{\text{in}}^{\text{d}} \sum_{f,igz} \phi_{g,m} V_{m} \right)}{\sum_{z} \left(\sum_{g,m \in z} \nu_{gz} \sum_{f,gz} \phi_{g,m} V_{m} \right)} = \beta_{\text{in}}.$$
 (124)

The resulting expression is consistent with the definition of β_{in} given in Equation 65, and therefore represents the fraction of delayed neutrons per isotope and per family.

When the level of detail of the β information is increased by extending its evaluation to combinations defined by isotope, precursor family, energy group, and reactor zone ($\beta_{\rm ingz}$, which appears in the analytical expression of $S(\hat{\beta}_{\rm eff,n}, \nu_{\rm igz}^{\rm p})$), particular attention must be paid to the computational strategy adopted for the quantity previously referred to as fiss_phi. In this context, ERANOS does not allow for the direct extraction of the functional value using the IMPORTANCE_CALCULATION_SOURCE_CREATION module, as it lacks the capability to output quantities resolved by energy group.

It is therefore necessary to reconstruct the term fiss_phi as the product of the average neutron flux $\bar{\phi}_{gz}$ in the selected zone z and energy group g, and the corresponding macroscopic fission cross-section $\Sigma_{\rm f,gz}$:

$$\mbox{fiss_phi} \simeq \bar{\phi}_{\rm gz} \cdot \Sigma_{\rm f,gz} \,, \eqno(125)$$

which provides a sufficiently accurate approximation.

As a result, the delayed neutron fraction evaluated for a specific isotope, family, energy group, and zone can be expressed as:

$$\beta_{\rm ingz} = \frac{\nu_{\rm in}^{\rm d} \cdot \bar{\phi}_{\rm gz} \cdot \Sigma_{\rm f,gz}}{\rm nufiss~phi~int}.$$
 (126)

Notice that, by summing over the indices corresponding to isotope, precursor family, energy group, and reactor zone, the β parameter can be reconstructed in all forms required by the expressions used for the computation of the sensitivity coefficients. As discussed in Section 3.4.5, ERANOS provides a dedicated module for the calculation of the effective delayed neutron fraction, available both as a total value and resolved

by precursor family. The results produced by this module are used as a reference for the internal verification of the β implementations developed in the present work, by constructing an independent estimate of $\hat{\beta}_{\text{eff}}$ based on those values.

Generalized sources

The distinctive element of the variational approach in GPT lies in the Lagrange multipliers $\tilde{\Psi}$ and $\tilde{\Psi}^{\dagger}$, which, in the physical context under consideration, represent generalized fluxes (see Section 2.5.1). In accordance with this GPT framework, these two quantities are computed from their respective generalized sources, namely the forward generalized source (Equation 35) and the adjoint generalized source (Equation 34), which are reported below:

$$\begin{cases}
\left(\mathbf{A} - \frac{\mathbf{F}}{k_{\text{eff}}}\right) \tilde{\Psi}_{n} = \frac{\chi_{n}^{d} \left[\beta_{n} \nu \Sigma_{f} \phi\right]}{\langle \phi^{\dagger} \chi_{n}^{d}, \beta_{n} \nu \Sigma_{f} \phi\rangle} - \frac{\chi \left[\nu \Sigma_{f} \phi\right]}{\langle \phi^{\dagger} \chi, \nu \Sigma_{f} \phi\rangle} \\
\left(\mathbf{A}^{\dagger} - \frac{\mathbf{F}^{\dagger}}{k_{\text{eff}}}\right) \tilde{\Psi}_{n}^{\dagger} = \frac{\left[\phi^{\dagger} \chi_{n}^{d}\right] \beta_{n} \nu \Sigma_{f}}{\langle \phi^{\dagger} \chi_{n}^{d}, \beta_{n} \nu \Sigma_{f} \phi\rangle} - \frac{\left[\phi^{\dagger} \chi\right] \nu \Sigma_{f}}{\langle \phi^{\dagger} \chi, \nu \Sigma_{f} \phi\rangle}
\end{cases} (127)$$

These sources must therefore be computed in ERANOS, so that they can subsequently be used as inputs in the different calls of the RECTANGULAR_SN_TRANSPORT_ITERATION module, which is employed to compute the corresponding generalized flux values.

In what follows, the first and second terms on the right-hand side of each generalized source expression are referred to as the positive and negative components of the source, respectively. The procedures adopted to implement the necessary elements for reconstructing these source terms in ERANOS, within the framework of the perturbative problem under consideration, are described below, starting with the numerators.

• The numerator of the direct positive term (corresponding to the quantity $\chi_n^d \left[\beta_n \nu \Sigma_f \phi\right]$) is obtained by iterating over all energy groups and multiplying the functional representing $\nu \Sigma_f \phi$ (evaluated via the source generation module IMPORTANCE_CALCUL ATION_SOURCE_CREATION) by the previously computed parameter β_n . The delayed neutron emission spectrum χ_{ng}^d , which shares the same family index n as the parameter β_n , is then applied as a multiplicative factor at the end of the iteration, leading to:

$$\texttt{SOURCE_NUM_POS_DIR} = \left(\sum_{\mathbf{g}'} \beta_{\mathbf{n}} \left(\nu \Sigma_{\mathbf{f}}\right)_{\mathbf{g}'} \phi_{\mathbf{g}'}\right) \chi_{\mathbf{ng}}^{\mathbf{d}}; \tag{128}$$

• The numerator of the direct negative term (expressed as $\chi \left[\nu \Sigma_{\rm f} \phi \right]$) involves no delayed neutron contributions. It is computed by summing the functional $\nu \Sigma_{\rm f} \phi$ over

all energy groups, and multiplying the result by the fission spectrum $\chi_{\rm g}$ evaluated at the energy group of interest:

$$\texttt{SOURCE_NUM_NEG_DIR} = \left(\sum_{\mathbf{g}'} (\nu \Sigma_{\mathbf{f}})_{\mathbf{g}'} \phi_{\mathbf{g}'}\right) \chi_{\mathbf{g}} \,; \tag{129}$$

• The numerator of the adjoint positive term (represented by $\left[\phi^{\dagger}\chi_{n}^{d}\right]\beta_{n}\nu\Sigma_{f}$) is constructed by multiplying the fraction of delayed neutrons associated with family n (β_{n}), the fission neutron production coefficient $(\nu\Sigma_{f})_{g}$, and the sum over all energy groups of the product $\phi^{\dagger}\chi_{n}^{d}$:

$$\text{SOURCE_NUM_POS_ADJ} = \beta_{n} \left(\sum_{g'} \phi_{g'}^{\dagger} \chi_{ng'}^{d} \right) (\nu \Sigma_{f})_{g}; \tag{130}$$

• The numerator of the adjoint negative term (expressed as $\left[\phi^{\dagger}\chi\right]\nu\Sigma_{\rm f}$) consists of two factors: the summation over energy groups of the product of neutron importance and fission spectrum, and the fission neutron production coefficient $(\nu\Sigma_{\rm f})_{\rm g}$:

$${\tt SOURCE_NUM_NEG_ADJ} = \left(\sum_{\mathbf{g'}} \phi_{\mathbf{g'}}^\dagger \chi_{\mathbf{g'}}\right) (\nu \Sigma_{\mathbf{f}})_{\mathbf{g}} \,. \tag{131}$$

With regard to the denominators, only two distinct terms are required, as they appear identically in both the direct and adjoint source expressions:

• The normalization factor in the positive term corresponds to the numerator in the definition of the parameter $\hat{\beta}_{\rm eff,n}$, that is, $\langle \phi^\dagger \chi_{\rm n}^{\rm d}, \beta_{\rm n} \nu \Sigma_{\rm f} \phi \rangle$. In ERANOS, this is evaluated using the generalized linear integrals function (Section 3.4.4), with the reference flux ϕ as input and a source term composed of: (i) the sum over energy groups of the product $\phi^\dagger \chi_{\rm n}^{\rm d}$, (ii) the $\beta_{\rm n}$ value, and (iii) the neutron production coefficient from fission. The reconstructed expression in ERANOS is:

$$\text{NORM_FACTOR_POS}_n = \sum_{g\,z} \left(\sum_{m \in z} \left(\sum_{g'} \phi_{g'm}^\dagger \chi_n^d \right) \beta_n (\nu \Sigma_f)_{gz} \phi_{gm} V_m \right) \; ; \qquad \text{(132)}$$

• The normalization factor of the negative term corresponds to the total fission source $\langle \phi^\dagger \chi, \nu \Sigma_{\rm f} \phi \rangle$, i.e., the perturbation integral already defined as VIMPOR. Thus, it is expressed as:

$$NORM_FACTOR_NEG = VIMPOR$$
. (133)

Generalized fluxes calculation

A total of four generalized fluxes are generated, each corresponding to one of the numerator terms of the forward and adjoint generalized sources defined in Equation 127. Each flux is computed using the function RECTANGULAR_SN_TRANSPORT_ITERATION (see Section 3.4.3), which takes as input a source EDL containing the group-wise data associated with one of the four terms: SOURCE_NUM_POS_DIR (Equation 128), SOURCE_NUM_NEG_DIR (Equation 129), SOURCE_NUM_POS_ADJ (Equation 130), and SOURCE_NUM_NEG_ADJ (Equation 131).

The resulting generalized fluxes are denoted as $\tilde{\Psi}_{pos,n}$, $\tilde{\Psi}_{neg,n}$, $\tilde{\Psi}_{pos,n}^{\dagger}$, and $\tilde{\Psi}_{neg,n}^{\dagger}$, respectively. These fluxes do not directly match the generalized fluxes introduced in the analytical formulation (namely, $\tilde{\Psi}_n$ and $\tilde{\Psi}_n^{\dagger}$), and the associated quantities do not individually represent physically meaningful observables. This apparent discrepancy is resolved by recognizing that the desired generalized fluxes are obtained as linear combinations of the positive and negative components:

$$\begin{cases} \tilde{\Psi}_{n} = \frac{\tilde{\Psi}_{pos,n}}{\text{NORM_FACTOR_POS}_{n}} - \frac{\tilde{\Psi}_{neg,n}}{\text{NORM_FACTOR_NEG}} \\ \tilde{\Psi}_{n}^{\dagger} = \frac{\tilde{\Psi}_{pos,n}^{\dagger}}{\text{NORM_FACTOR_POS}_{n}} - \frac{\tilde{\Psi}_{neg,n}^{\dagger}}{\text{NORM_FACTOR_NEG}} \end{cases}$$
(134)

In the developed ERANOS modules, generalized fluxes are consistently managed in terms of their separate components. This practice, also recommended in the ERANOS user manual to mitigate pointwise convergence issues (as discussed in Section 3.4.3) and to improve computational efficiency by avoiding explicit summation of source terms, has a direct impact on the structure of the implemented procedures for computing sensitivity coefficients.

Prompt component of the fission spectrum (χ_{igz}^{p})

The derivation of the prompt fission spectrum is based on a rearrangement of Equation 64. The total delayed contribution to the fission spectrum, denoted as $\chi_{\rm g}^{\rm DELAYED}$, is obtained by summing over all precursor families n the product of the delayed neutron fraction and the corresponding delayed emission spectrum:

$$\chi_{\rm g}^{\rm DELAYED} = \sum_{\rm n} \beta_{\rm n} \chi_{\rm ng}^{\rm d} \,.$$
(135)

Given that the total fission spectrum values are stored in the MICRO EDL as a function of isotope, energy group, and spatial zone, the prompt component can be computed for each combination by applying the following relation:

$$\chi_{\text{igz}}^{\text{p}} = \frac{\chi_{\text{igz}} - \chi_{\text{g}}^{\text{DELAYED}}}{1 - \beta},$$
(136)

which, by definition, is already normalized to unity.

4.2.1 Implementation of Procedures for Sensitivity Coefficient Calculation Using the GPT Approach

Once all the quantities appearing in the expressions of the sensitivity coefficients have been computed within the developed ERANOS script, it becomes possible to implement the modules responsible for the actual calculation of the sensitivity coefficients. These modules combine the previously computed quantities according to the analytical definitions of the sensitivity coefficients, thereby enabling the evaluation of their numerical values.

A detailed description of the ERANOS modules is provided below, specifically implemented for the calculation of the four sensitivity coefficients analyzed so far.

The Sensitivity coefficient $S(\hat{eta}_{\mathrm{eff,n}}, u_{\mathrm{i'n'}}^{\mathrm{d}})$

The coefficient $S(\hat{\beta}_{\mathrm{eff,n}}, \nu_{i'n'}^{\mathrm{d}})$ represents the sensitivity of the effective delayed neutron fraction for family n, with respect to the average number of delayed neutrons of family n' emitted per fission event by isotope i'.

Its numerical evaluation requires the computation of some specific quantities, namely:

- the Kronecker delta between the precursor families involved in the parameter of interest and the perturbed parameter ($\delta_{nn'}$), which distinguishes whether the family n' associated with the perturbed parameter $\nu^d_{i'n'}$ is the same as, or different from, the family n to which the parameter $\hat{\beta}_{\text{eff,n}}$ refers;
- the $u^{\rm d}$ -dependent component of the fission spectrum, $\tilde{\chi}_{\rm gz}(\nu^{\rm d}_{{\rm i'n'}})$, as defined in Equation 86;
- the various fission source terms expressed as integrals over the full phase space, denoted using the Bra-Ket notation $\langle \cdot \rangle$.

While the implementation of $\delta_{nn'}$ in the LU language is straightforward – returning a value of one when the indices n and n' coincide, and zero otherwise – the same does not apply to the ν^d -dependent fission spectrum component and the fission source terms, which require dedicated procedures.

The analytical expression of $\tilde{\chi}_{\rm gz}(\nu_{\rm i'n'}^{\rm d})$, given in terms of quantities already inferred at

this stage of the calculation, can be retrieved starting from the following relations:

$$\begin{cases} \tilde{\chi}(\nu_{\rm in}^{\rm d}) = \nu_{\rm in}^{\rm d} \frac{\partial \chi}{\partial \nu_{\rm in}^{\rm d}} \\ \frac{\partial \chi}{\partial \nu_{\rm in}^{\rm d}} = \frac{\partial \beta}{\partial \nu_{\rm in}^{\rm d}} \chi^{\rm p} + \sum_{\rm n} \frac{\partial \beta_{\rm n}}{\partial \nu_{\rm in}^{\rm d}} \chi_{\rm n}^{\rm d} \\ \frac{\partial \beta_{\rm n}}{\partial \nu_{\rm in'}^{\rm d}} = \frac{\beta_{\rm in'}}{\nu_{\rm in'}^{\rm d}} (\delta_{\rm nn'} - \beta_{\rm n}) \\ \frac{\partial \beta}{\partial \nu_{\rm in}^{\rm d}} = \frac{\beta_{\rm in}}{\nu_{\rm in}^{\rm d}} (1 - \beta) \end{cases}$$

$$(137)$$

which summarizes the information encapsulated in Equation 86, Equation 81, Equation 82 and Equation 83. By performing the appropriate substitutions within the system and conveniently rearranging the terms of the resulting equation, the following expression is obtained for the component of the fission spectrum that depends on the parameter $\nu_{i'n'}^{d}$:

$$\tilde{\chi}_{\rm gz}(\nu_{\rm i'n'}^{\rm d}) = \beta_{\rm i'n'} (\beta - 1) \chi_{\rm gz}^{\rm p} - \sum_{\rm f} \left(\beta_{\rm i'n'} (\beta_{\rm f} - \delta_{\rm fn'}) \chi_{\rm fg}^{\rm d} \right) , \tag{138}$$

where the subscript index f is also used to indicate a given precursor family.

Regarding the various fission sources appearing in the expression for the sensitivity coefficient under consideration, all of them can be directly obtained using the modules dedicated to the computation of perturbative integrals. This requires that the necessary MACRO EDLs be first generated through the MACRO_CALCULATION procedure, and subsequently provided as input to the INTEGRAL_PERTURBATION_TRANSPORT module. However, this process must be preceded by the careful modification, within each MACRO, of the relevant quantities defining the specific fission source, in particular the appropriate components (prompt, delayed, or both) of the fission spectrum and the average number of emitted neutrons to be considered in each case. This step is performed by assigning the desired values in the sections of the MACRO EDL associated with the specific parameters to be changed, such as the fission spectrum $\chi_{\rm gz}$ or the product of the average number of neutrons emitted per fission event and the macroscopic fission cross section $(\nu \Sigma_{\rm f})_{\rm gz}$, using the LU language. Specifically, the fission sources that must be computed, as they appear in the direct term of $S(\hat{\beta}_{\rm eff,n}, \nu_{\rm in}^{\rm d})$, are the following:

• $\langle \phi^{\dagger} \chi, \nu^{\rm d}_{i'n'} \Sigma_{{\rm f},i'} \phi \rangle$ – obtained form a MACRO calculated for a given isotope i', where the delayed neutron source per unit flux $(\nu^{\rm d}_{i'n'} \Sigma_{{\rm f},i'})$, associated with precursor family n' of isotope i', is overwritten in the section containing the product of the average number of neutrons emitted per fission event and the macroscopic fission cross section;

- $\langle \phi^\dagger \chi_{\rm n}^{\rm d}, \nu_{{\rm i'n'}}^{\rm d} \Sigma_{{\rm f},{\rm i'}} \phi \rangle$ obtained from a MACRO calculated for a specific isotope i', in which both the delayed emission spectrum of family n ($\chi_{\rm n}^{\rm d}$) and the delayed neutron source per unit flux ($\nu_{{\rm i'n'}}^{\rm d} \Sigma_{{\rm f},{\rm i'}}$), associated with family n' and isotope i', are overwritten;
- $\langle \phi^\dagger \tilde{\chi}(\nu^d_{i'n'}), \nu \Sigma_f \phi \rangle$ obtained from a MACRO in which the reference fission spectrum is replaced by the component that depends exclusively on the parameter $\nu^d_{i'n'}$, previously denoted by the symbol $\tilde{\chi}(\nu^d_{i'n'})$.

The same approach is adopted for the evaluation of the fission sources contributing to the indirect terms, which involve generalized fluxes.

A key difference with respect to the analytical formulation of $S(\hat{\beta}_{\mathrm{eff,n}}, \nu_{\mathrm{i'n'}}^{\mathrm{d}})$ (as expressed in Equation 89) lies in the fact that, in the numerical implementation, each generalized flux must be decomposed into two distinct components: one corresponding to the positive contribution and the other to the negative contribution of the respective generalized source, as prescribed by the numerical approach outlined in Section 4.2. Therefore, for each invocation of the module used in the computation of perturbative integrals, it is necessary to explicitly specify which component of the generalized flux is being utilized. The correct normalization of these components – as defined in Equation 134 – is accounted for only in the final implementation of the sensitivity coefficient $S(\hat{\beta}_{\mathrm{eff,n}}, \nu_{\mathrm{i'n'}}^{\mathrm{d}})$, which ultimately assumes the following form:

$$S(\hat{\beta}_{\mathrm{eff,n}}, \nu_{\mathrm{i'n'}}^{\mathrm{d}}) = \frac{\beta_{\mathrm{i'n}}}{\beta_{\mathrm{n}}} \left[(\delta_{\mathrm{nn'}} - \beta_{\mathrm{n}}) + \frac{\beta_{\mathrm{n}}}{\hat{\beta}_{\mathrm{eff,n}}} \frac{\langle \phi^{\dagger} \chi_{\mathrm{n}}^{\mathrm{d}}, \nu_{\mathrm{i'n'}}^{\mathrm{d}} \Sigma_{\mathrm{f,i'}} \phi \rangle}{\mathrm{VIMPOR}} + \frac{-\langle \phi^{\dagger} \chi, \nu_{\mathrm{i'n'}}^{\mathrm{d}} \Sigma_{\mathrm{f,i'}} \phi \rangle}{\mathrm{VIMPOR}} - \frac{\langle \phi^{\dagger} \tilde{\chi}(\nu_{\mathrm{i'n'}}^{\mathrm{d}}), \nu \Sigma_{\mathrm{f}} \phi \rangle}{\mathrm{VIMPOR}} \right] + \\ + \frac{1}{k_{\mathrm{eff}} \cdot \mathrm{NORM_FACTOR_POS_{\mathrm{n}}}} \left\{ \langle \tilde{\Psi}_{\mathrm{pos,n}}^{\dagger} \tilde{\chi}(\nu_{\mathrm{i'n'}}^{\mathrm{d}}), \nu \Sigma_{\mathrm{f}} \phi \rangle + \langle \tilde{\Psi}_{\mathrm{pos,n}}^{\dagger} \chi, \nu_{\mathrm{i'n'}}^{\mathrm{d}} \Sigma_{\mathrm{f,i'}} \phi \rangle + \\ + \langle \phi^{\dagger} \tilde{\chi}(\nu_{\mathrm{i'n'}}^{\mathrm{d}}), \nu \Sigma_{\mathrm{f}} \tilde{\Psi}_{\mathrm{pos,n}} \rangle + \langle \phi^{\dagger} \chi, \nu_{\mathrm{i'n'}}^{\mathrm{d}} \Sigma_{\mathrm{f,i'}} \tilde{\Psi}_{\mathrm{pos,n}} \rangle \right\}$$

$$- \frac{1}{k_{\mathrm{eff}} \cdot \mathrm{NORM_FACTOR_NEG}} \left\{ \langle \tilde{\Psi}_{\mathrm{neg,n}}^{\dagger} \tilde{\chi}(\nu_{\mathrm{i'n'}}^{\mathrm{d}}), \nu \Sigma_{\mathrm{f}} \phi \rangle + \langle \tilde{\Psi}_{\mathrm{neg,n}}^{\dagger} \chi, \nu_{\mathrm{i'n'}}^{\mathrm{d}} \Sigma_{\mathrm{f,i'}} \phi \rangle + \\ + \langle \phi^{\dagger} \tilde{\chi}(\nu_{\mathrm{i'n'}}^{\mathrm{d}}), \nu \Sigma_{\mathrm{f}} \tilde{\Psi}_{\mathrm{neg,n}} \rangle + \langle \phi^{\dagger} \chi, \nu_{\mathrm{i'n'}}^{\mathrm{d}} \Sigma_{\mathrm{f,i'}} \tilde{\Psi}_{\mathrm{neg,n}} \rangle \right\}$$

The various terms involved in the expression of the sensitivity coefficient $S(\hat{\beta}_{\text{eff},n}, \nu^{\text{d}}_{i',n'})$ as implemented in ERANOS are summarized in Figure 7, where the approach adopted for obtaining each term is highlighted.

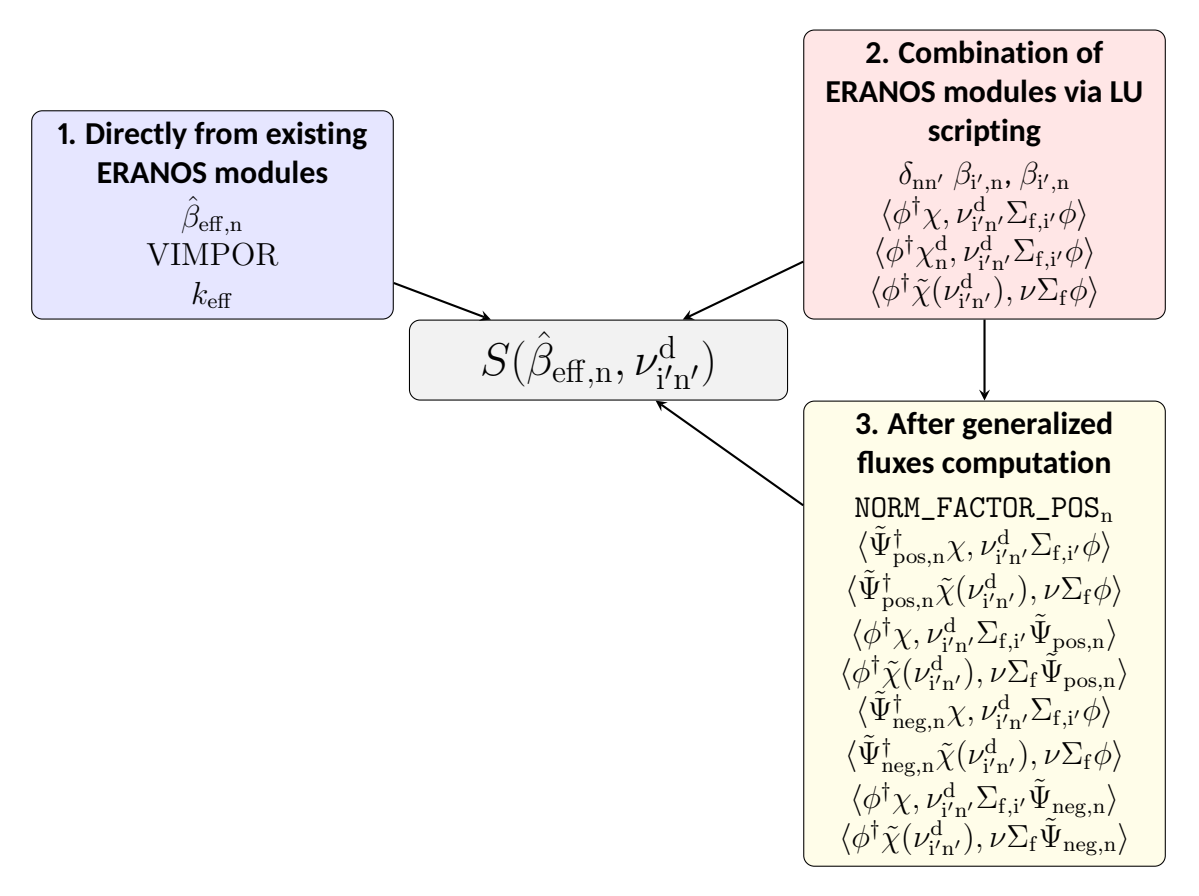


Figure 7: Diagram summarizing the terms contributing to the calculation of the sensitivity coefficient $S(\hat{\beta}_{\mathrm{eff,n}}, \nu^{\mathrm{d}}_{\mathrm{i'n'}})$ as implemented in ERANOS (see Equation 139). The contributing terms are grouped into three distinct categories: (1) quantities directly provided by existing ERANOS modules (notice that NORM_FACTOR_NEG coincides with VIMPOR); (2) derived terms constructed through a structured combination of ERANOS modules by means of the internal LU programming language; (3) hybrid terms requiring LU-based combination and the explicit use of generalized fluxes as input.

The Sensitivity coefficient $S(\hat{eta}_{\mathrm{eff,n}}, u^{\mathrm{p}}_{\mathrm{i'g'z'}})$

The analytical expression for the sensitivity of the effective delayed neutron fraction for family n to the average number of prompt neutrons emitted in energy group g' per fission event by isotope i' in core region z', is provided in Equation 102.

Accordingly, the quantities to be inferred in this context include:

- the component of the fission spectrum dependent on ν^p , denoted as $\tilde{\chi}_{gz}(\nu^p_{i'g'z'})$ and defined in Equation 99;
- the various fission terms represented by integrals extended over the entire phase space.

The analytical expression of $\tilde{\chi}_{gz}(\nu^p_{i'g'z'})$, given in terms of quantities already inferred at this stage of the calculation, can be retrieved starting from the following relations:

$$\begin{cases} \tilde{\chi}(\nu_{\rm igz}^{\rm p}) = \nu_{\rm igz}^{\rm p} \frac{\partial \chi}{\partial \nu_{\rm igz}^{\rm p}} \\ \frac{\partial \chi}{\partial \nu_{\rm igz}^{\rm p}} = \frac{\partial \beta}{\partial \nu_{\rm igz}^{\rm p}} \chi^{\rm p} + \sum_{\rm n} \frac{\partial \beta_{\rm n}}{\nu_{\rm igz}^{\rm p}} \chi_{\rm n}^{\rm d} \\ \frac{\partial \beta_{\rm n}}{\partial \nu_{\rm igz}^{\rm p}} = -\beta_{\rm n} \frac{\beta_{\rm ingz}}{\nu_{\rm in}^{\rm d}} \\ \frac{\partial \beta}{\partial \nu_{\rm igz}^{\rm p}} = -\sum_{\rm n} \beta_{\rm n} \frac{\beta_{\rm i'ng'z'}}{\nu_{\rm i'n}^{\rm d}} \end{cases}$$

$$(140)$$

which summarizes the information encapsulated in Equation 99, Equation 92, Equation 93 and Equation 95. By performing the appropriate substitutions within the system and conveniently rearranging the terms of the resulting equation, the following expression is obtained for the component of the fission spectrum that depends on the parameter $\nu_{i'g'g'g'}^{\rm p}$:

$$\tilde{\chi}_{\rm gz}(\nu_{\rm i'g'z'}^{\rm p}) = \left(\sum_{\rm f} \beta_{\rm f} \frac{\beta_{\rm i'fg'z'}}{\nu_{\rm i'f}^{\rm d}}\right) \nu_{\rm i'g'z'}^{\rm p} \chi_{\rm gz}^{\rm p} - \sum_{\rm f} \left(\beta_{\rm f} \frac{\beta_{\rm i'fg'z'}}{\nu_{\rm i'f}^{\rm d}} \chi_{\rm fg}^{\rm d}\right) \nu_{\rm i'g'z'}^{\rm p}, \tag{141}$$

where the subscript index f is also used to indicate a given precursor family.

The relevant fission terms are those appearing in the numerators of the components that constitute the indirect contribution to the sensitivity. Specifically, they all have the form $\langle \phi_a^\dagger \tilde{\chi}(\nu_{i'g'z'}^p), \nu \Sigma_f \phi_b \rangle$, where ϕ_a and ϕ_b denote generic fluxes. These terms are obtained modifying the reference MACRO so that the fission spectrum is replaced by its component depending exclusively on the parameter $\nu_{i'g'z'}^p$, previously denoted by $\tilde{\chi}(\nu_{i'g'z'}^p)$.

As in the previous case, each generalized flux is decomposed into two components (positive and negative), and their proper normalization is accounted for in the the final evalution of the sensitivity coefficient $S(\hat{\beta}_{\mathrm{eff,n}}, \nu^{\mathrm{p}}_{\mathrm{i'g'z'}})$, which ultimately takes the following expression:

$$\begin{split} S(\hat{\beta}_{\mathrm{eff,n}}, \nu_{\mathrm{i'g'z'}}^{\mathrm{p}}) &= -\nu_{\mathrm{i'g'z'}}^{\mathrm{p}} \frac{\beta_{\mathrm{i'ng'z'}}}{\nu_{\mathrm{i'n}}^{\mathrm{d}}} + \frac{\beta_{\mathrm{i'n}}}{\hat{\beta}_{\mathrm{eff,n}}} \frac{(\nu^{\mathrm{p}}\Sigma_{\mathrm{f}})_{\mathrm{i'g'z'}} \mathrm{SIAP}_{\mathrm{ng'z'}}^{\mathrm{d}}}{\mathrm{VIMPOR}} + \\ &- \frac{(\nu^{\mathrm{p}}\Sigma_{\mathrm{f}})_{\mathrm{i'g'z'}} \mathrm{SIAP}_{\mathrm{g'z'}}}{\mathrm{VIMPOR}} - \frac{\langle \phi^{\dagger}\tilde{\chi}(\nu_{\mathrm{i'g'z'}}^{\mathrm{p}}), \nu\Sigma_{\mathrm{f}}\phi \rangle}{\mathrm{VIMPOR}} + \\ &+ \frac{1}{k_{\mathrm{eff}} \cdot \mathrm{NORM_FACTOR_POS_{n}}} \bigg\{ \langle \tilde{\Psi}_{\mathrm{pos,n}}^{\dagger}\tilde{\chi}(\nu_{\mathrm{i'g'z'}}^{\mathrm{p}}), \nu\Sigma_{\mathrm{f}}\phi \rangle + \\ &+ (\nu^{\mathrm{p}}\Sigma_{\mathrm{f}})_{\mathrm{i'g'z'}} \mathrm{SIAP}_{\mathrm{g'z'}} (\tilde{\Psi}_{\mathrm{pos,n}}^{\dagger}, \phi) + \langle \phi^{\dagger}\tilde{\chi}(\nu_{\mathrm{i'g'z'}}^{\mathrm{p}}), \nu\Sigma_{\mathrm{f}}\tilde{\Psi}_{\mathrm{pos,n}} \rangle + \\ &+ (\nu^{\mathrm{p}}\Sigma_{\mathrm{f}})_{\mathrm{i'g'z'}} \mathrm{SIAP}_{\mathrm{g'z'}} (\tilde{\Psi}_{\mathrm{pos,n}}^{\dagger}, \phi) + \langle \phi^{\dagger}\tilde{\chi}(\nu_{\mathrm{i'g'z'}}^{\mathrm{p}}), \nu\Sigma_{\mathrm{f}}\tilde{\Psi}_{\mathrm{pos,n}} \rangle + \\ &+ (\nu^{\mathrm{p}}\Sigma_{\mathrm{f}})_{\mathrm{i'g'z'}} \mathrm{SIAP}_{\mathrm{g'z'}} (\tilde{\Psi}_{\mathrm{neg,n}}^{\dagger}, \phi) + \langle \phi^{\dagger}\tilde{\chi}(\nu_{\mathrm{i'g'z'}}^{\mathrm{p}}), \nu\Sigma_{\mathrm{f}}\tilde{\Psi}_{\mathrm{neg,n}} \rangle + \\ &+ (\nu^{\mathrm{p}}\Sigma_{\mathrm{f}})_{\mathrm{i'g'z'}} \mathrm{SIAP}_{\mathrm{g'z'}} (\tilde{\Psi}_{\mathrm{neg,n}}^{\dagger}, \phi) + \langle \phi^{\dagger}\tilde{\chi}(\nu_{\mathrm{i'g'z'}}^{\mathrm{p}}), \nu\Sigma_{\mathrm{f}}\tilde{\Psi}_{\mathrm{neg,n}} \rangle + \\ &+ (\nu^{\mathrm{p}}\Sigma_{\mathrm{f}})_{\mathrm{i'g'z'}} \mathrm{SIAP}_{\mathrm{g'z'}} (\tilde{\Psi}_{\mathrm{neg,n}}^{\dagger}, \phi) + \langle \phi^{\dagger}\tilde{\chi}(\nu_{\mathrm{i'g'z'}}^{\mathrm{p}}), \nu\Sigma_{\mathrm{f}}\tilde{\Psi}_{\mathrm{neg,n}} \rangle + \\ &+ (\nu^{\mathrm{p}}\Sigma_{\mathrm{f}})_{\mathrm{i'g'z'}} \mathrm{SIAP}_{\mathrm{g'z'}} (\tilde{\Psi}_{\mathrm{neg,n}}^{\dagger}, \phi) + \langle \phi^{\dagger}\tilde{\chi}(\nu_{\mathrm{i'g'z'}}^{\mathrm{p}}), \nu\Sigma_{\mathrm{f}}\tilde{\Psi}_{\mathrm{neg,n}} \rangle + \\ &+ (\nu^{\mathrm{p}}\Sigma_{\mathrm{f}})_{\mathrm{i'g'z'}} \mathrm{SIAP}_{\mathrm{g'z'}} (\tilde{\Psi}_{\mathrm{neg,n}}^{\dagger}, \phi) + \langle \phi^{\dagger}\tilde{\chi}(\nu_{\mathrm{i'g'z'}}^{\mathrm{p}}), \nu\Sigma_{\mathrm{f}}\tilde{\Psi}_{\mathrm{neg,n}} \rangle + \\ &+ (\nu^{\mathrm{p}}\Sigma_{\mathrm{f}})_{\mathrm{i'g'z'}} \mathrm{SIAP}_{\mathrm{g'z'}} (\tilde{\Psi}_{\mathrm{neg,n}}^{\dagger}, \phi) + \langle \phi^{\dagger}\tilde{\chi}(\nu_{\mathrm{i'g'z'}}^{\mathrm{p}}), \nu\Sigma_{\mathrm{f}}\tilde{\Psi}_{\mathrm{neg,n}} \rangle + \\ &+ (\nu^{\mathrm{p}}\Sigma_{\mathrm{f}})_{\mathrm{i'g'z'}} \mathrm{SIAP}_{\mathrm{g'z'}} (\tilde{\Psi}_{\mathrm{neg,n}}^{\dagger}, \phi) + \langle \phi^{\dagger}\tilde{\chi}(\nu_{\mathrm{i'g'z'}}^{\mathrm{p}}), \nu\Sigma_{\mathrm{f}}\tilde{\Psi}_{\mathrm{neg,n}} \rangle + \\ &+ (\nu^{\mathrm{p}}\Sigma_{\mathrm{f}})_{\mathrm{i'g'z'}} \mathrm{SIAP}_{\mathrm{g'z'}} (\tilde{\Psi}_{\mathrm{neg,n}}^{\dagger}, \phi) + \langle \phi^{\dagger}\tilde{\chi}(\nu_{\mathrm{i'g'z'}}^{\dagger}), \nu\Sigma_{\mathrm{f}}\tilde{\Psi}_{\mathrm{neg,n}} \rangle + \langle \psi^{\mathrm{p}}\tilde{\chi}(\nu_{\mathrm{i'g'z'}}^{\dagger}), \nu\Sigma_{\mathrm{f}}\tilde{\Psi}_{\mathrm{neg,n}} \rangle + \langle \psi^{\mathrm{p}}\tilde{\chi}(\nu_{\mathrm{i'g'z'}}^{\dagger}), \nu\Sigma_{\mathrm{f}}\tilde{\chi}(\nu_{\mathrm{i'g'}}^{\dagger}), \nu\Sigma_{\mathrm{f$$

The various terms involved in the expression of the sensitivity coefficient $S(\hat{\beta}_{\text{eff},n}, \nu^{\text{p}}_{\mathbf{i}'\mathbf{g}'\mathbf{z}'})$ as implemented in ERANOS are summarized in Figure 8, where the approach adopted for obtaining each term is highlighted.

The Sensitivity coefficient $S(\hat{eta}_{\mathrm{eff,n}},\chi_{\mathrm{n'}\sigma'}^{\mathrm{d}})$

The analytical formulation of the sensitivity coefficients of the parameter of interest, β_n , with respect to the delayed neutron emission spectrum, $\chi^d_{n'g'}$ – for each energy group g' and precursor family n' – is provided in Equation 112. The terms computed within the core of the code are sufficient to evaluate the sensitivity coefficients $S(\hat{\beta}_n,\chi^d_{n'g'})$, except for the Kronecker delta term $\delta_{nn'}$, which differentiates between the precursor family n considered in the effective delayed neutron fraction and the family n' associated with the delayed neutron emission spectrum.

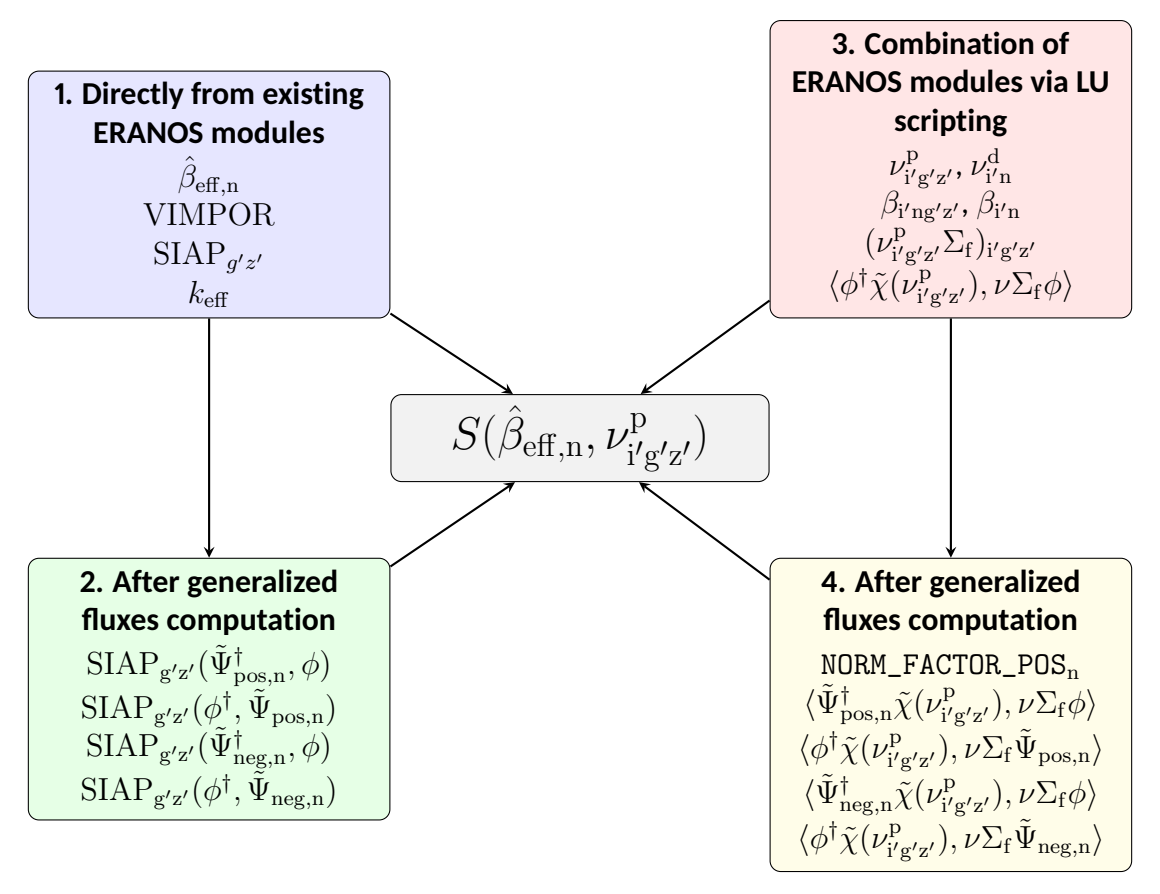


Figure 8: Diagram summarizing the terms contributing to the calculation of the sensitivity coefficient $S(\hat{\beta}_{\mathrm{eff,n}}, \nu^{\mathrm{p}}_{i'g'z'})$ as implemented in ERANOS (see Equation 142). The contributing terms are grouped into four distinct categories: (1) quantities directly provided by existing ERANOS modules (note that NORM_FACTOR_NEG coincides with VIMPOR); (2) quantities retrievable from the same modules when supplied with previously computed generalized fluxes; (3) derived terms constructed through a structured combination of ERANOS modules by means of the internal LU programming language; (4) hybrid terms requiring both LU-based combination and the explicit use of generalized fluxes as input.

For the computation of the generalized sources, the adopted approach requires decomposing the forward and adjoint generalized fluxes into positive and negative components. These components are then linearly combined – using the appropriate normalization factors – in the final expression of the sensitivity coefficient, presented below:

$$\begin{split} S\left(\hat{\beta}_{\mathrm{eff,n}},\chi_{\mathrm{n'g'}}^{\mathrm{d}}\right) &= \\ &= \chi_{\mathrm{n'g'}}^{\mathrm{d}} \left\{ \left(\delta_{\mathrm{n,n'}} \frac{\beta_{\mathrm{n}}}{\hat{\beta}_{\mathrm{eff,n}}} - \beta_{\mathrm{n'}}\right) \frac{\mathrm{SIDP_{g'}}}{\mathrm{VIMPOR}} + \left(\hat{\beta}_{\mathrm{eff,n'}} - \delta_{\mathrm{n,n'}}\right) \right\} + \\ &+ \frac{\beta_{\mathrm{n'}}}{k_{\mathrm{eff}} \cdot \mathrm{NORM_FACTOR_POS_{\mathrm{n}}}} \left\{ \mathrm{SIDP_{g'}}(\tilde{\Psi}_{\mathrm{pos,n}}^{\dagger}, \phi) - \mathrm{VIMPOR_{n'}^{\mathrm{d}}}(\tilde{\Psi}_{\mathrm{pos,n}}^{\dagger}, \phi) + \\ &+ \mathrm{SIDP_{g'}}(\phi^{\dagger}, \tilde{\Psi}_{\mathrm{pos,n}}) - \mathrm{VIMPOR_{n'}^{\mathrm{d}}}(\phi^{\dagger}, \tilde{\Psi}_{\mathrm{pos,n}}) \right\} + \\ &- \frac{\beta_{\mathrm{n'}}}{k_{\mathrm{eff}} \cdot \mathrm{NORM_FACTOR_NEG}} \left\{ \mathrm{SIDP_{g'}}(\tilde{\Psi}_{\mathrm{neg,n}}^{\dagger}, \phi) - \mathrm{VIMPOR_{n'}^{\mathrm{d}}}(\tilde{\Psi}_{\mathrm{neg,n}}^{\dagger}, \phi) + \\ &+ \mathrm{SIDP_{g'}}(\phi^{\dagger}, \tilde{\Psi}_{\mathrm{neg,n}}) - \mathrm{VIMPOR_{n'}^{\mathrm{d}}}(\phi^{\dagger}, \tilde{\Psi}_{\mathrm{neg,n}}) \right\} \end{split}$$

The various terms involved in the expression of the sensitivity coefficient $S(\hat{\beta}_{eff,n}, \chi^{d}_{n'g'})$ as implemented in ERANOS are summarized in Figure 9, where the approach adopted for obtaining each term is highlighted.

The Sensitivity coefficient $S(\hat{eta}_{\mathrm{eff,n}},\chi^{\mathrm{p}}_{\mathrm{i'g'z'}})$

All the terms derived within the core of the code are sufficient to evaluate the sensitivity coefficient $S(\hat{\beta}_{\mathrm{eff,n}},\chi^{\mathrm{p}}_{\mathrm{i'g'z'}})$, whose expression is derived in Equation 119. As in the previously described modules, the terms involving generalized fluxes are decomposed into their positive and negative components. These are then recombined within the final expression of the sensitivity coefficient, applying the appropriate normalization

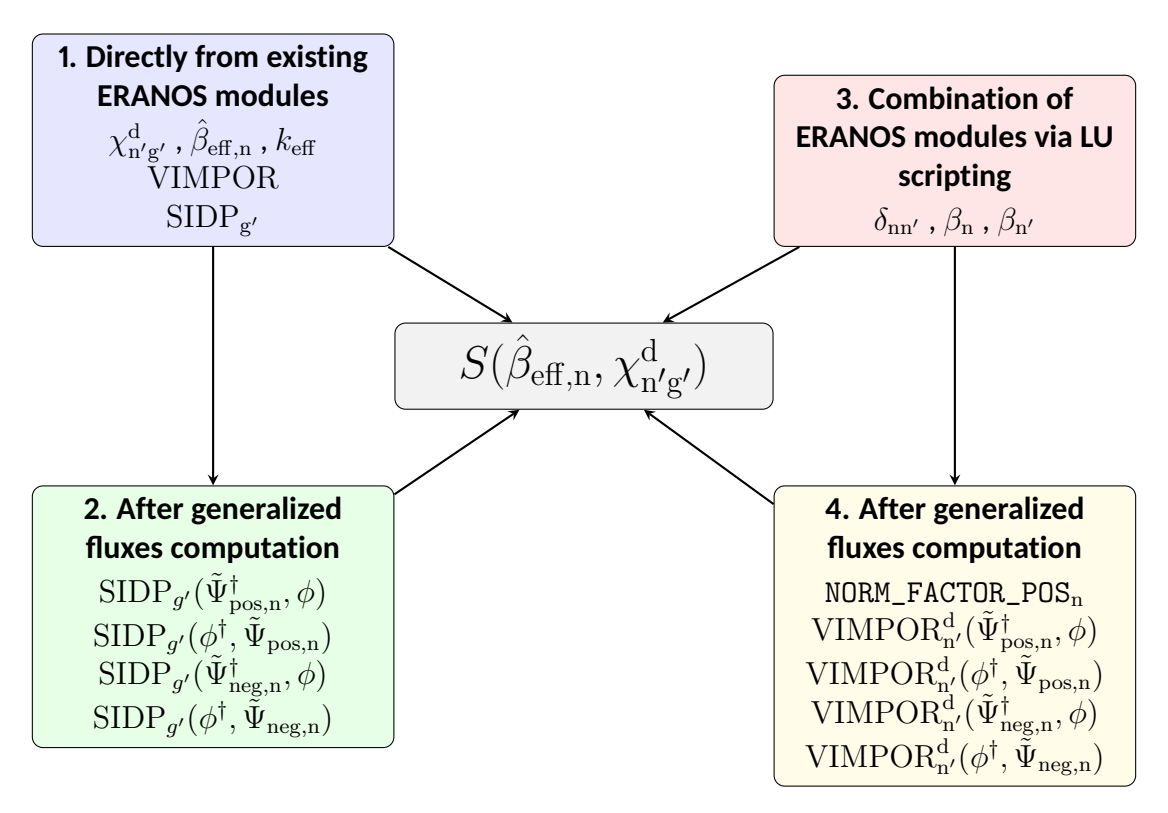


Figure 9: Diagram summarizing the terms contributing to the calculation of the sensitivity coefficient $S(\hat{\beta}_{\mathrm{eff,n}},\chi_{\mathrm{n'g'}}^{\mathrm{d}})$ as implemented in ERANOS (see Equation 143). The contributing terms are grouped into four distinct categories: (1) quantities directly provided by existing ERANOS modules (note that NORM_FACTOR_NEG coincides with VIMPOR); (2) quantities retrievable from the same modules when supplied with previously computed generalized fluxes; (3) derived terms constructed through a structured combination of ERANOS modules by means of the internal LU programming language; (4) hybrid terms requiring both LU-based combinations and the explicit use of generalized fluxes as input.

factors:

$$\begin{split} S(\hat{\beta}_{\text{eff,n}},\chi_{i'g'z'}^{\mathcal{P}}) &= \\ &= \chi_{i'g'z'}^{\mathcal{P}} \bigg\{ \bigg[\bigg(\frac{\text{VIMPOR}_{i'z'}}{\text{VIMPOR}} - \hat{\beta}_{\text{eff,z'}} \bigg) - (1-\beta) \frac{\text{SIDP}_{g'z'}}{\text{VIMPOR}} \bigg] + \\ &+ \frac{1}{k_{\text{eff}} \cdot \text{NORM_FACTOR_POS}_{n}} \bigg[(1-\beta) \text{SIDP}_{g'z'} (\tilde{\Psi}_{\text{pos,n}}^{\dagger}, \phi) + \\ &- \text{VIMPOR}_{i'z'} (\tilde{\Psi}_{\text{pos,n}}^{\dagger}, \phi) - \hat{\beta}_{\text{eff,z'}} \text{VIMPOR} (\tilde{\Psi}_{\text{pos,n}}^{\dagger}, \phi) + \\ &+ (1-\beta) \text{SIDP}_{g'z'} (\phi^{\dagger}, \tilde{\Psi}_{\text{pos,n}}) - \text{VIMPOR}_{i'z'} (\phi^{\dagger}, \tilde{\Psi}_{\text{pos,n}}) + \\ &- \hat{\beta}_{\text{eff,z'}} \text{VIMPOR} (\phi^{\dagger}, \tilde{\Psi}_{\text{pos,n}}) \bigg] + \\ &+ \frac{1}{k_{\text{eff}} \cdot \text{NORM_FACTOR_NEG}} \bigg[(1-\beta) \text{SIDP}_{g'z'} (\tilde{\Psi}_{\text{neg,n}}^{\dagger}, \phi) + \\ &- \text{VIMPOR}_{i'z'} (\tilde{\Psi}_{\text{neg,n}}^{\dagger}, \phi) - \hat{\beta}_{\text{eff,z'}} \text{VIMPOR} (\tilde{\Psi}_{\text{neg,n}}^{\dagger}, \phi) + \\ &+ (1-\beta) \text{SIDP}_{g'z'} (\phi^{\dagger}, \tilde{\Psi}_{\text{neg,n}}) - \text{VIMPOR}_{i'z'} (\phi^{\dagger}, \tilde{\Psi}_{\text{neg,n}}) + \\ &- \hat{\beta}_{\text{eff,z'}} \text{VIMPOR} (\phi^{\dagger}, \tilde{\Psi}_{\text{neg,n}}) \bigg] \bigg\} \end{split}$$

The various terms involved in the expression of the sensitivity coefficient $S(\hat{\beta}_{\mathrm{eff,n}},\chi^{\mathrm{d}}_{\mathrm{n'g'}})$ as implemented in ERANOS are summarized in Figure 10, where the approach adopted for obtaining each term is highlighted.

The results obtained through the four modules specifically developed within the ERA-NOS framework reflect the progress achieved thus far toward the main objective pursued in this thesis.

4.2.2 Implementation of Procedures for Sensitivity Coefficient Calculation Using the Direct Perturbation (DP) Approach

The numerical values of the sensitivity coefficients derived usign the variational GPT method are verified through by comparison with the results of selected sensitivity coefficients obtained using the Direct Perturbation (DP) approach.

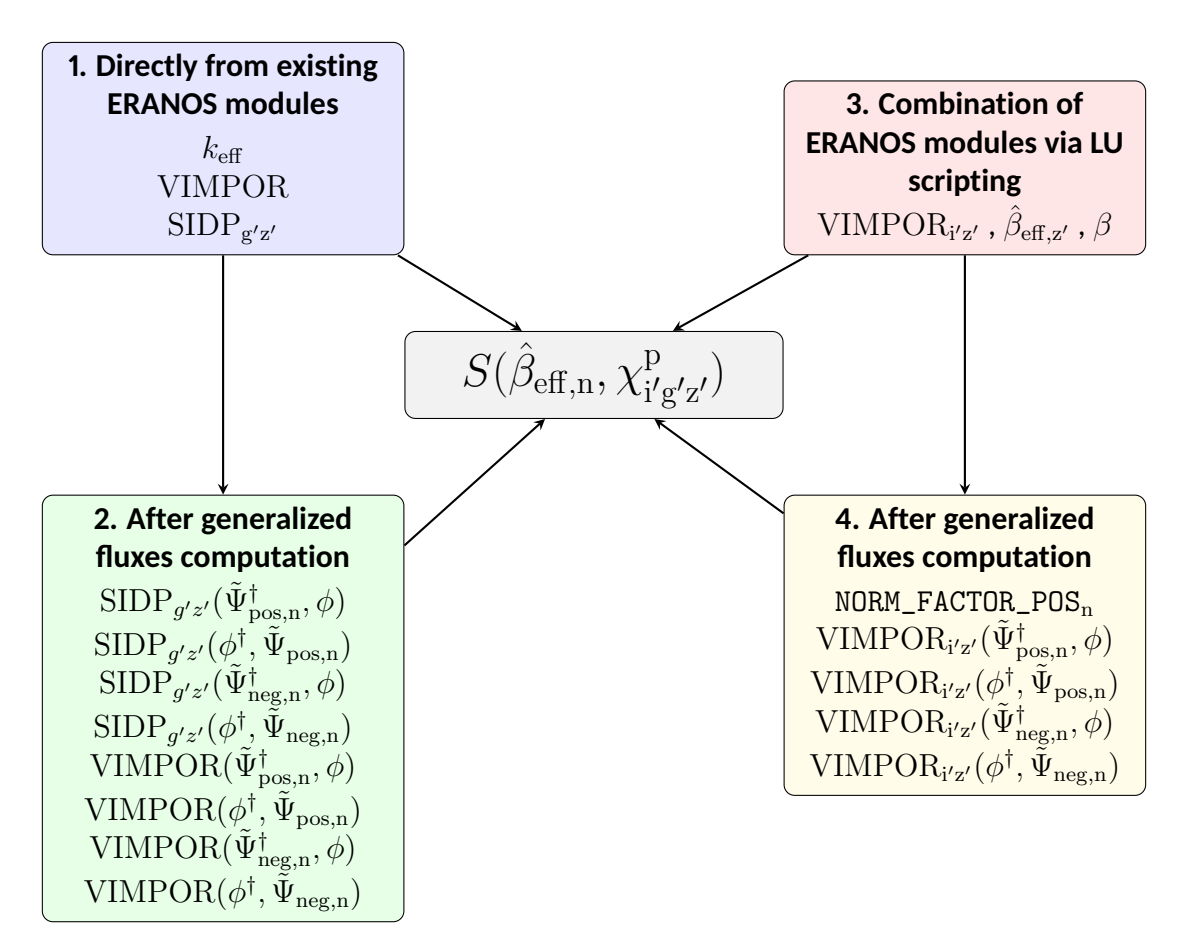


Figure 10: Diagram summarizing the terms contributing to the calculation of the sensitivity coefficient $S(\hat{\beta}_{\mathrm{eff,n}},\chi^p_{i'g'z'})$ as implemented in ERANOS (see Equation 144). The contributing terms are organized into four distinct categories: (1) quantities directly provided by existing ERANOS modules (note that NORM_FACTOR_NEG coincides with VIMPOR); (2) quantities retrievable from the same modules when supplied with previously computed generalized fluxes; (3) derived terms constructed through a structured combination of ERANOS modules by means of the internal LU programming language; (4) hybrid terms requiring both LU-based combination and the explicit use of generalized fluxes as input.

The DP method consists in modifying a selected microscopic parameter α involved in the physical model – such as the average number of delayed neutrons emitted per fission, $\nu^{\rm d}$ – by a small relative amount, set to 1% in the context of this work, and computing the resulting variation in the integral response of interest (e.g., $\hat{\beta}_{\rm eff}$).

In the present analysis, the DP technique is employed to evaluate the sensitivity coefficients $S(\hat{\beta}_{\mathrm{eff,n}},\alpha)$, quantifying the response of the effective delayed neutron fraction for precursor family n to perturbations in the input parameter α . The sensitivity is then evaluated by the following finite-difference expression:

$$S(\hat{\beta}_{n}, \alpha) = \frac{1}{\hat{\beta}_{n}} \frac{\hat{\beta}_{n}^{\text{pert}} - \hat{\beta}_{n}}{\alpha^{\text{pert}} - \alpha}, \tag{145}$$

which constitutes a numerical approximation of the first derivative of the response function $(\hat{\beta}_n)$ to the perturbed parameter (α) . The normalization with respect to $\hat{\beta}_n$ produces a relative sensitivity coefficient. This allows for a direct comparison with the results previously obtained using the variational GPT-based method (examined in detail in Section 2.5).

It is worth recalling that the main strength of the DP approach lies in the transparency of its formulation. This method allows perturbations to be applied directly to the physical quantities of interest, making both the implementation and the verification of the procedure more accessible (in contrast, variational methods often involve complex analytical expressions that include multiple interdependent terms of different physical nature, whose derivation and coding require additional care). For this reason, it proves to be an effective verification tool for the results obtained through GPT, despite allowing comparison of only a limited subset of coefficients – selected as a sample among the possible combinations of isotope, reaction type, energy group, and spatial zone – due to its lower computational efficiency compared to GPT.

As simple as this approach to obtaining sensitivity coefficients may seem, the selective introduction of the perturbation at specific stages of the calculation process makes it possible to derive the contributions of the individual components of sensitivity, namely the direct and the indirect terms.

The flexibility that allows one to evaluate a single component of the sensitivity, rather than only its total value, lies in how the perturbed value of the parameter of interest, $\hat{\beta}_n^{\rm pert}$ is treated computationally. In practice, while the developed modules requires no significant modifications, the perturbed value must be consistently associated with a perturbation arising either from direct effects(caused directly by the variation of an input parameter), from indirect effects (caused exclusively by the resulting variation in the neutron fluxes ϕ and ϕ^\dagger appearing in the Boltzmann Equation), or from a combination of both, depending on the stage at which the perturbation is introduced:

Total Sensitivity is obtained by perturbing the input parameter α at the very beginning of the computational chain. All the ERANOS modules are then executed with the

perturbed value, naturally yielding a perturbed value $\hat{\beta}^{\text{pert}}$ in which all quantities appearing in Equation 14 are affected;

Direct Sensitivity can be obtained using the DP method by applying the perturbation to the input parameter after the direct (ϕ) and adjoint (ϕ^{\dagger}) neutron fluxes were computed. Thus, in the evaluation of $\hat{\beta}^{\mathrm{pert}}$, the fluxes provided as input to the BETA_EFFECTIVE_CALCULATION module remain fixed at their nominal values;

Indirect Sensitivity in contrast to the previous case, the perturbation to the input parameter is introduced before the calculation of the reference neutron fluxes, and then removed (restoring the nominal value) once the flux calculations are completed. In this way, the difference between $\hat{\beta}^{\text{pert}}$ and the unperturbed value arises exclusively from the neutron fluxes used in the calculation.

The DP method for calculating the sensitivity coefficients relies on the perturbation of the selected input parameter. However, it is important to emphasize that this step should not be treated as straightforward. In fact, due to the absence of a ν -only section in the section-based structure of the MICRO and MACRO EDLs, as well as the normalization constraint imposed on the fission spectra (Equation 67), specific precautions must be taken depending on the type of input parameter being perturbed:

• in the case of the average number of delayed neutrons emitted per fission event $(\nu_{\rm in}^{\rm d})$, the perturbation must be applied to the value originally provided by ERANOS for a specific isotope i and precursor family n. At the level of the MICRO EDL corresponding to the selected isotope, the relevant information is extracted from the appropriate sections: the neutron source term (given by the product $\nu_{\rm igz}\sigma_{\rm f,igz}$) and the microscopic fission cross-section $(\sigma_{\rm f,igz})$.

Their ratio, yields the average number of neutrons emitted per fission event (ν_{igz}). The perturbation of its delayed component is then introduces through the following:

$$\nu_{\mathrm{igz}}^{\mathrm{pert}} = \nu_{\mathrm{igz}} + 1\%\nu_{\mathrm{in}}^{\mathrm{d}}\,,\tag{146}$$

where the percentage represents the imposed variation with respect to the nominal value. After multiplying again by $\sigma_{\rm f,igz}$, the resulting value is overwritten in the corresponding section of the MICRO EDL, and from this, a new MACRO EDL is computed, which is subsequently used for the calculation of the perturbed effective delayed neutron fraction;

• with regard to the average number of prompt neutrons emitted per fission event (ν_{igz}^p) , the perturbation procedure is analogous to the previous case, except that the perturbed value is associated with the prompt component. This component is obtained by subtraction, according to $\nu_{igz}^p = \nu_{igz} - \sum_n \nu_{in}^d$. Following the same

steps within the MICRO EDL corresponding to the selected isotope i, the value of $\nu_{\rm igz}$ is first retrieved, after which the perturbation is applied to its prompt component as:

$$\nu_{\rm igz}^{\rm pert} = \nu_{\rm igz} + 1\%\nu_{\rm igz}^{\rm p} \,. \tag{147}$$

The resulting value is then multiplied by $\sigma_{\rm f,igz}$ and overwritten in the corresponding section of the MICRO EDL. This updated MICRO EDL is subsequently used as input for the module that generates the perturbed MACRO EDL, consistently reflecting this specific modification.;

• when perturbing of the delayed neutron emission spectrum, $\chi_{\rm ng}^{\rm d}$, associated with a given precursor family n and energy group g, the main complication lies in enforcing the unit normalization constraint of the emission spectra. The data provided by ERANOS for this parameter are only available at macroscopic level (i.e. delayed neutron emission spectra for individual isotopes are not resolved). consequently, the perturbation is applied directly at the level of the MACRO EDL.

This data structure contains the values of the total fission spectrum for each energy group and reactor zone ($\chi_{\rm gz}$). The perturbation imposed on $\chi_{\rm ng}^{\rm d}$ is introduced into the total spectrum at group g across all core zones according to:

$$\chi_{\rm gz}' = \chi_{\rm gz} + 1\% \beta_{\rm n} \chi_{\rm ng}^{\rm d} , \qquad (148)$$

where the primed quantity denotes an unnormalized spectrum, and the delayed neutron fraction β_n is kept at its nominal value, since it depends solely on fission yields and delayed neutron emission probabilities (thus excluding any indirect perturbation resulting from the modification of the fission spectrum).

The next step is the normalization of the perturbed spectrum, which is carried out for each core zone z as:

$$\chi_{\rm gz}^{\rm pert} = \frac{\chi_{\rm gz}'}{\sum_{\rm g'} \chi_{\rm g'z}'}.$$
 (149)

This procedure is repeated independently for every zone z, and the resulting normalized values are then overwritten in the corresponding MACRO EDL;

• Lastly, the DP applied to the prompt component of the fission spectrum, $\chi_{\text{igz}}^{\text{p}}$, associated with a specific isotope i, energy group g, and core zone z, is derived in ERANOS according to the relation given in Equation 136.

Since this parameter is isotope-dependent, the perturbation must be carried out at the MICRO EDL level, specifically in the section associated to the selected isotope i.

Once the value of the total fission spectrum (χ_{igz}) for the group g and zone z is retrived from this MICRO, it is modified by perturbing the prompt component, according to:

$$\chi'_{igz} = \chi_{igz} + 1\%(1 - \beta)\chi^{p}_{igz},$$
 (150)

where the primed quantity denotes the unnormalized spectrum, and the delayed neutron fraction β is kept at its nominal value.

As in the previous case, normalization is then applied using a similar relation to that expressed in Equation 149:

$$\chi_{\text{igz}}^{\text{pert}} = \frac{\chi_{\text{igz}}'}{\sum_{\text{g'}} \chi_{\text{ig'z}}'},$$
(151)

which is performed for each energy group within each zone. The resulting normalized values are overwritten in the MICRO EDL section corresponding to the fission spectrum of isotope i. From this modified MICRO, a new MACRO EDL is subsequently generated using the dedicated ERANOS module.

5 Preliminary Results from the Implemented Sensitivity Analysis Modules

In the previous chapter, the methodological framework for evaluating sensitivity coefficients was established, encompassing both the variational (GPT-based) and Direct Perturbation (DP) approaches which were both implemented within the ERANOS environment.

This chapter presents preliminary numerical results obtained with these newly developed ERANOS modules. The aim is to provide a preliminary verification of the procedures and to test their internal consistency by comparing the sensitivity estimates derived from the GPT and DP approaches.

It should be emphasized that sensitivity coefficients, are deterministic quantities. They are defined as the functional derivative of a reactor response (such as $k_{\rm eff}$, power distribution, or $\hat{\beta}_{\rm eff}$) with respect to an infinitesimal variation of a nuclear data parameter (e.g. cross sections, neutron multiplicities, or spectra). In the context of deterministic codes, sensitivity coefficients are not subject to statistical uncertainty: they are computed exactly – within the limits of the adopted numerical approximations – through the solution of adjoint-based transport equations. Accordingly, they should not be regarded as statistical estimators, but rather as analytical tools that quantify how local perturbations in nuclear data propagate to integral reactor responses.

The verification process adopted to assess the correctness and logical robustness of the new ERANOS implementations follows a progressive strategy. The developed numerical modules were first applied to simplified test configurations – where this term refers both to the core model and the number of isotopes, delayed neutron precursor families, and energy groups considered. Starting from configurations characterized by minimal complexity, the procedures were then gradually extended to increasingly realistic configurations. The ultimate goal is to apply the sensitivity evaluation modules for the delayed neutron fraction with respect to parameters other than cross sections (i.e., coefficients referred to in previous chapters as $S(\hat{\beta}_{\mathrm{eff}},\alpha)$) to the full ALFRED reactor core model.

Notice that the ALFRED core model was originally based on a three-dimensional hexagonal geometry. However, for the purposes of S/U analysis, it is transformed into a two-dimensional cylindrical (RZ) representation (see Appendix B for further details). This transformation is necessary not primarily due to geometric support limitations of the perturbative modules, but rather because these modules currently accept only fluxes computed via finite difference methods, as implemented in the BISTRO code (more information about BISTRO can be found in Appendix A). Since BISTRO does not

support hexagonal geometry calculations, the core model must be reformulated in RZ geometry to ensure compatibility with the employed numerical solvers.

The progressive verification approach makes it possible to determine the level of computational complexity – both in core modeling and execution parameters – at which the developed ERANOS modules are still capable of generating accurate and consistent sensitivity estimates. It also facilitates debugging and testing, since significant discrepancies in the computed results can more easily be traced back to specific sections of the code.

Moreover, the strategy keeps the execution time short during the initial stages of verification, thereby enabling rapid testing of potential fixes for identified issues.

5.1 Verification with a Minimal Core Configuration and Comparison with Analytical Benchmarks

Following the progressive validation strategy, the verification process was initially conducted using a minimal configuration, chosen both to allow for analytical benchmarking and to facilitate early-stage debugging. This minimal configuration is characterized by the following features:

- cylindrical geometry,
- a single isotope,
- one delayed neutron precursor family,
- a single energy group (i.e. no energy resolution),
- one spatial zone corresponding to an infinitely large mesh element.

These simplifications make it possible to derive analytical expressions for the sensitivity coefficients, which then serve as benchmarks for verifying the results obtained with both the GPT- and DP-based modules.

Under these conditions, the general expression of the sensitivity coefficient $S(\hat{\beta}_{\text{eff},n},\alpha)$, reported in Equation 37, reduces to the following simplified form of the relative sensitivity of the parameter β :

$$S(\beta, \alpha) = \frac{\alpha}{\beta} \frac{\partial \beta}{\partial \alpha}, \tag{152}$$

in which only the direct sensitivity contribution is present.

The reduction of the general formulation (Equation 37) to this simplified expression is justified by the following considerations:

• The generalized importances $\tilde{\Psi}$ and $\tilde{\Psi}^{\dagger}$ vanish due to the orthogonality conditions imposed on them (Equation 26), which, in this minimal case, reduce to:

$$\tilde{\Psi}^* F \phi = 0$$
 and $\tilde{\Psi} F^* \phi^* = 0$, (153)

where all quantities are scalars and spatially independent. Assuming the flux ϕ and the adjoint flux ϕ^* are non-zero, the only way to satisfy the conditions in Equation 153 is to have $\tilde{\Psi}=0$ and $\tilde{\Psi}^\dagger=0$.

• Under the assumptions of the minimal configuration, the effective delayed neutron fraction $\hat{\beta}_{\text{eff,n}}$ reduces to the delayed neutron fraction β . This equivalence holds as a direct consequence of the following relation:

$$\hat{\beta}_{\text{eff,n}} = \hat{\beta}_{\text{eff}} = \frac{\phi^* \chi \beta \nu \Sigma_{\text{f}} \phi}{\phi^* \chi \nu \Sigma_{\text{f}} \phi} = \beta , \qquad (154)$$

where $\chi^{\rm p}=\chi^{\rm d}=\chi=1$, as imposed by the spectrum normalization condition in Equation 67.

The values obtained from this configuration provide a robust reference for validating the sensitivity coefficients computed by the new ERANOS modules. Despite its extreme simplicity, this test framework is specifically designed to preserve the essential physical and numerical features required to meaningfully assess correctness and internal consistency.

The analytical evaluation of the sensitivity coefficients of the delayed neutron fraction $\hat{\beta}_{\rm eff,n}$ yielded the following results, derived from Equation 152 and developed for each input parameter considered:

ullet Sensitivity to the average number of delayed neutrons emitted per fission event $u_{
m in}^{
m d}$ The reference analytical expression is:

$$S(\beta, \nu^{\rm d}) = \frac{\nu^{\rm d}}{\beta} \frac{\partial \beta}{\partial \nu^{\rm d}} = 1 - \beta$$
, (155)

where the derivative term is derived as shown in Equation 83.

Since $\beta \ll 1$, the expected reference value for numerical verification is:

$$S(\beta, \nu^{\rm d}) \approx 1.$$
 (156)

This expectation was successfully confirmed by both the GPT-based and DP-based modules implemented in ERANOS .

ullet Sensitivity to the average number of prompt neutrons emitted per fission event $u_{\mathrm{igz}}^{\mathrm{p}}$ The corresponding analytical expression is:

$$S(\beta, \nu^{\mathrm{p}}) = \frac{\nu^{\mathrm{p}}}{\beta} \frac{\partial \beta}{\partial \nu^{\mathrm{p}}} = -\frac{\nu^{\mathrm{p}}}{\nu^{\mathrm{d}}} \beta = -\frac{\nu^{\mathrm{p}}}{\nu^{\mathrm{d}}} \frac{\nu^{\mathrm{d}}}{\nu} = -\frac{\nu^{\mathrm{p}}}{\nu}, \tag{157}$$

where the derivative is justified by Equation 95, and the final form follows from applying the minimal configuration assumption $\beta = \nu^{\rm d}/\nu^{\rm p}$.

Since the contribution of delayed neutrons to the total number of neutrons per fission is negligible compared to prompt neutrons, i.e., $\nu \approx \nu^{\rm p}$, and in the absence of associated uncertainty evaluation, the expected reference value is

$$S(\beta, \nu^{\mathbf{p}}) \approx -1. \tag{158}$$

This was confirmed independently by both GPT and DP approaches.

ullet Sensitivity to the shape of the neutron emission spectra $\chi_{ m ng}^{ m d}$ and $\chi_{ m igz}^{ m p}$

In the minimal configuration, the emission spectra cannot be distinguished, as they are discretized into a single energy group. Consequently, no shape perturbation can be introduced, and the corresponding sensitivity coefficients necessarily vanish:

$$S(\beta, \chi^{\rm d}) = S(\beta, \chi^{\rm p}) = 0$$
. (159)

The results obtained with the ERANOS modules were indeed consistent with zero, within negligible numerical fluctuations, for both the GPT- and DP-based implementations.

The application of the ERANOS sensitivity modules to this minimal executive configuration yielded results in excellent agreement with the analytical reference values. The outcome of this preliminary verification step is concisely summarized in Table 4.

Table 4: Numerical verification of the ERANOS sensitivity modules against analytical reference values for $S(\beta,\alpha)$, with $\alpha=\nu^{\rm d},\,\nu^{\rm p},\,\chi^{\rm d},\,\chi^{\rm p}$, under the minimal configuration assumptions. Results are presented for both GPT- and DP-based implementations.

Input parameter	$S_{\mathrm{GPT}}\left(\beta,\alpha\right)$	$S_{\mathrm{DP}}\left(eta,lpha ight)$	$S_{ m analytical}\left(eta,lpha ight)$
$\alpha = \nu^{\mathrm{d}}$	1	1	1
$\alpha = \nu^{\mathrm{p}}$	-1	-1	-1
$\alpha = \chi^{d}$	0	0	0
$\alpha = \chi^{\mathrm{p}}$	0	0	0

This confirms the correct implementation of the underlying sensitivity formulations in both the GPT and DP modules, as well as their consistent behaviour under minimal configuration assumptions. The verification carried out in this simplified context provides a robust foundation for subsequent analyses involving more complex models and input dependencies.

5.2 Verification of Sensitivity Modules by GPT and DP Approaches Using a Simplified Core Model

In accordance with the progressive methodology adopted in this work, the verification process was subsequently extended to an intermediate level of complexity, with the aim of bridging the gap between the analytical benchmarks and the full ALFRED core model.

To this end, a simplified yet sufficiently representative core model (Toy Model) was developed, designed to capture key physical behaviors while avoiding the complexities of a full-core reactor simulation. The model employs a cylindrical geometry, with a computational setup featuring increased resolution in the parameters governing the number of isotopes, precursor families, energy groups, and spatial zones, relative to the minimal configuration introduced in Section 5.1.

5.2.1 Computational Testbed for the Newly Developed Sensitivity Analysis Modules

Given the complexity of the target system (ALFRED) for which the sensitivity modules were originally developed, the Toy Model mentioned in the introduction to this section was integrated into the ERANOS workflow as a computational testbed. This allows for a thorough testing phase following the initial verification step described in Section 5.1.

Although computationally inexpensive, the model was deliberately designed to retain a representative level of complexity – featuring multiple isotopes, delayed neutron precursor families, energy groups, and spatial zones – so as to effectively exercise the full range of implemented functionalities.

This choice served a dual purpose:

- to reduce the computational burden, thereby enabling faster verification and debugging cycles;
- to isolate and expose potential numerical or structural issues such as GPT-DP discrepancies, iterative convergence instabilities, spectrum normalization pitfalls, or unintended input sensitivities that could otherwise remain concealed in a full-core simulation, as may occur in the case of the detailed ALFRED core model.

In this context, particular attention was devoted to achieving comprehensive *code-path coverage*, whereby the test cases were designed not only to confirm correct execution but also to systematically activate all logical branches within the modules (e.g. conditionals, loop iterations, fallback procedures, etc.), thereby increasing confidence in the robustness and generality of the implementation.

The Toy Model implemented in the ERANOS workflow developed in this work consists of a cylindrical geometry entirely filled with fuel, subdivided into two spatial regions characterized by different material densities.

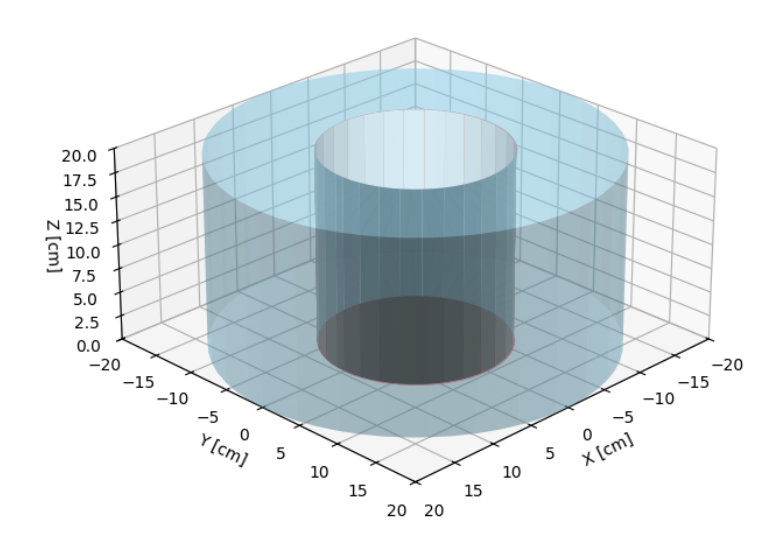


Figure 11: 3D representation of the simplified reactor configuration (Toy Model) employed for intermediate-level numerical verification. The geometry consists of two concentric cylindrical regions: an inner region (zone_A, with a composition of 80% fuel and 20% void) and an outer region (zone_B, with a composition of 90% fuel and 10% void). Both regions extend vertically for 20 cm, with inner and outer radii of 9.47 cm and 20 cm, respectively.

Both the radius and height of the cylinder are set to 20 cm. The cylindrical volume is radially partitioned into two concentric regions, as illustrated in Figure 11:

- the inner region, extending $\sim 9.47\,\mathrm{cm}$ from the central axis, is designated as zone_A;
- the outer annular region, spanning the remaining $\sim 10.53\,\mathrm{cm}$ of the radius, is designated to zone_B.

The radius at which the interface between the two concentric regions is positioned is defined in ERANOS with reference to the spatial lattice used for mesh-based volume discretization. Specifically, the interface is placed at a given mesh point within this lattice. By converting the corresponding lattice coordinate into centimeters, one obtains the radius value reported in the text.

The fuel is assumed to consist solely of enriched uranium, composed exclusively of 235 U (20%) and 238 U (80%). The two zones differ in their homogenized medium composition: <code>zone_A</code> contains 80% fuel and 20% void by volume, while <code>zone_B</code> contains 90% fuel and 10% void.

This zonal distinction serves not only to verify the internal logical structure of the implemented code – particularly its ability to manage the assignment of material properties to distinct spatial regions – but also to reproduce the two-region volumetric sub-

division characteristic of the ALFRED reference core model implemented in ERANOS. Indeed, if the implemented procedures demonstrate robustness when applied to this simplified zonal partitioning, analogous behavior can be anticipated when addressing the more complex full-core configuration of the ALFRED reactor.

The simulation was set up to include only the isotopes ²³⁵U and ²³⁸U, two delayed neutron precursor families, a six-group energy discretization, and the presence of the two distinct fuel zones (see Table 5 for a comparison with the limiting cases defined by the minimal configuration and the full ALFRED core model adopted in a previous S/U analysis study [40]). These modeling choices were made with the same objectives discussed above: to preserve a representative level of physical and numerical complexity sufficient to exercise the logic and data structures of the implemented code while at the same time avoiding the computational burden associated with a full-core simulation.

Table 5: Main features of the core configurations considered in this work, with a progressive increase in model complexity. Specifically, the values reported in the table for the ALFRED core model correspond to those adopted in a previous S/U analysis study [40].

Feature	Minimal	Тоу	ALFRED (S/U analysis implementation)
Geometry	Cylindrical	Cylindrical	Cylindrized from 3D hexagonal
Number of Isotopes	1	2	22
Precursor Families	1	2	8
Energy Groups	1	6	33
Spatial Zones	1	2	25
Spectral Data	None	Physically consistent fixed values	Generated by ERANOS procedure

Moreover, this approach facilitates the identification and isolation of potential sources of discrepancies between the sensitivity coefficients computed using the GPT and DP methods, since such deviations can be more readily traced to specific sections of the code. Conducting analogous diagnostics in a full-core configuration would be considerably more challenging, since numerical deviations may become entangled with model-scale effects and thus harder to interpret.

The emission spectra associated with the two delayed neutron precursor families $(\chi_1^{\rm d}$ and $\chi_2^{\rm d})$ were initialized without relying on the dedicated ERANOS procedures, which typically generate these data based on nuclear libraries. At this development stage, the primary objective is to verify the functionality of the sensitivity analysis modules, and it is therefore sufficient to initialize the delayed neutron spectra provided that fundamental physical constraints are satisfied. These constraints can be summarized as follows:

- each delayed neutron spectrum must be normalized to unity, as expressed in Equation 67;
- the resulting prompt fission spectrum χ^p must remain strictly positive in all energy groups. This condition is essential because χ^p is computed by subtraction,

according to Equation 136, which, in the case of two precursor families, takes the following form:

$$\chi_{\rm igz}^{\rm p} = \frac{\chi_{\rm igz} - \sum_{\rm n=1}^{2} \beta_{\rm n} \chi_{\rm ng}^{\rm d}}{1 - \beta}.$$
(160)

5.2.2 Analysis of Sensitivity Results on the Simplified Core Model

As a follow-up to the preliminary tests conducted on the minimal configuration (Section 5.1), an additional verification step was carried out by applying the methodology outlined in Chapter 4 to the more advanced testbed configuration described above, and by analyzing the resulting sensitivity coefficients.

This verification relies on a systematic comparison between the direct and indirect components of the considered sensitivity coefficient, as obtained using the ER-ANOS modules developed within the GPT framework and from those based on the DP method. The two contributions – the direct term and the indirect term – are examined separately to identify any potential discrepancies between the results produced by the two approaches.

The verification campaign conducted at this intermediate level of complexity enabled the identification and correction of several issues that had remained hidden in the minimal benchmark case. In particular, this step revealed implementation weaknesses in the sensitivity module related to handling the variable number of elements defining the executive configuration's parameters (i.e., the number of isotopes, precursor families, energy groups, and spatial zones considered), which had not been sufficiently exercised under the simplified conditions of the minimal configuration.

The most substantial progress, in terms of numerical verification, was achieved in the implementation of the module for computing the sensitivity coefficients $S(\hat{\beta}_{\mathrm{eff,n}}, \nu_{\mathrm{in}}^{\mathrm{d}})$. Among the four input parameters investigated in this work, the average number of delayed neutrons emitted per fission event, $\nu_{\mathrm{in}}^{\mathrm{d}}$, was deliberately addressed first. This prioritization was motivated by two main considerations:

- $u_{\rm in}^{\rm d}$ is a fundamental parameter known a priori, as it is directly available from the input data. In contrast, $u_{\rm igz}^{\rm p}$ is obtained by subtracting $u_{\rm in}^{\rm d}$ from the total average number of neutrons per fission, $u_{\rm igz}$, which must first be computed through dedicated processing routines (see Section 4.2).
- unlike spectral parameters such as $\chi^{\rm d}_{\rm ng}$ and $\chi^{\rm p}_{\rm igz}$, the parameter $\nu^{\rm d}_{\rm in}$ is not subject to additional constraints such as the normalization condition of Equation 67 or the positivity requirement across the energy domain imposed by the present Toy Model (see the discussion at the end of Section 5.2.1) which would otherwise increase the structural complexity of the newly implemented ERANOS modules and require additional development effort and verification time.

The resulting sensitivity coefficients $S(\hat{\beta}_{\mathrm{eff,n}}, \nu_{\mathrm{in}}^{\mathrm{d}})$ are discussed below, with the individual contributions from the direct and indirect terms considered separately. Since the direct term provides the dominant contribution to the total sensitivity, its verification is addressed first. Any inconsistency detected at this stage would immediately question the reliability of the newly implemented modules, whereas the indirect term, by construction, is expected to play only a secondary role. The discussion therefore begins with the analysis of the direct component, summarized in Table 6.

It should be noted that the numerical results generated by the ERANOS modules are originally provided with a precision of up to ten decimal digits. In this thesis, however, only the first five significant figures are reported. This level of precision is deemed sufficient for the purposes of the present analysis, as additional digits would not provide meaningful improvements in accuracy and would have no significant impact on the interpretation of the results or the conclusions drawn.

Table 6: Direct term's contributions to the sensitivity of the delayed neutron fraction associated with a specific precursor family, $\hat{\beta}_{\rm eff,fam}$, with respect to the average number of delayed neutrons emitted per fission event for a given isotope i and precursor family n, i.e. $\nu_{\rm in}^{\rm d}$, as represented by the coefficients $S^{\rm dir}(\hat{\beta}_{\rm eff,fam},\nu_{\rm in}^{\rm d}).$ Results are obtained using the newly implemented ERANOS sensitivity modules, based either on the GPT framework, $S^{\rm dir}_{\rm GPT}(\hat{\beta}_{\rm eff,fam},\nu_{\rm in}^{\rm d}),$ or on direct perturbation techniques, $S^{\rm ind}_{\rm GPT}(\hat{\beta}_{\rm eff,fam},\nu_{\rm in}^{\rm d}),$ applied to the simplified reactor model described in Section 5.2.1. The last column reports the relative discrepancies between the two methods, where the quantity $\Delta S^{\rm dir} = S^{\rm dir}_{\rm GPT} - S^{\rm dir}_{\rm DP}$ has been introduced.

Executive Variables		$S_{ ext{GPT}}^{ ext{dir}}(\hat{eta}_{ ext{eff,fam}}, u_{ ext{in}}^{ ext{d}})$	$S_{\mathrm{DP}}^{\mathrm{dir}}(\hat{eta}_{\mathrm{eff,fam}}, u_{\mathrm{in}}^{\mathrm{d}})$	$\Delta S^{ m dir}/S^{ m dir}_{ m DP}$	
fam = 1 $i = {}^{235}U$ $i = {}^{238}U$	n=1	9.0172×10^{-1}	9.0164×10^{-1}	9.0210×10^{-5}	
	$\iota = 0$	n=2	-1.3222×10^{-3}	-8.4513×10^{-4}	5.6456×10^{-1}
	n = 1	9.8141×10^{-2}	9.8149×10^{-2}	-8.4002×10^{-5}	
	$\iota = 0$	n=2	-6.1359×10^{-4}	-2.5818×10^{-4}	1.3766×10^{0}
	$i = {}^{235}$ U	n=1	-1.3746×10^{-4}	-1.8779×10^{-4}	-2.6804×10^{-1}
$\int_{-\infty}^{\infty} fam = 2$	$\iota = 0$	n=2	7.6454×10^{-1}	7.6515×10^{-1}	-7.8411×10^{-4}
	$i = {}^{238}\mathrm{U}$	n = 1	-2.5941×10^{-5}	-2.0442×10^{-5}	2.6900×10^{-1}
		n=2	2.3342×10^{-1}	2.3374×10^{-1}	-1.3715×10^{-3}

As shown in Table 6, the results demonstrate good agreement between the direct components of the sensitivity coefficients of the delayed neutron fraction with respect to the average number of delayed neutrons emitted per fission event, $S^{\rm dir}(\hat{\beta}_{\rm eff,fam}, \nu_{\rm in}^{\rm d})$. A detailed examination of the values produced by the newly implemented ERANOS

modules – based on either the GPT approach or the DP technique – confirms the expected physical behavior.

The most significant sensitivity coefficients for the response parameter $\hat{\beta}_{\rm eff,fam}$ are those in which the perturbed input parameter $\nu_{\rm in}^{\rm d}$ – the average number of delayed neutrons emitted per fission event – belongs to the same precursor family fam associated with the response. In these cases (n=fam), the sensitivity is positive, as an increase in the emission of delayed neutrons from a given family directly increases the delayed neutron fraction attributed to that family.

Conversely, when the perturbed parameter $\nu_{\rm in}^{\rm d}$ refers to a different precursor family ($n \neq fam$), the effect is of a different nature: increasing the number of delayed neutrons emitted by family n slightly reduces the relative contribution of the analyzed family fam to the effective delayed neutron fraction. As a result, the sensitivity becomes slightly negative. In these cases, the absolute value of the sensitivity is at least two orders of magnitude smaller than in the corresponding n = fam case, which confirms the physical consistency of the result.

From the standpoint of numerical verification, the most relevant aspect is the analysis of the relative discrepancies between the sensitivity coefficients computed with the GPT-based modules and the corresponding reference values obtained via DP methods. These discrepancies are expressed in Table 6 as the ratio $\Delta S^{\rm dir}/S_{\rm DP}^{\rm dir}$, where

$$\Delta S^{\rm dir} = S^{\rm dir}_{\rm GPT} - S^{\rm dir}_{\rm DP} \,. \tag{161} \label{eq:dirac}$$

Here, S_{GPT}^{dir} and S_{DP}^{dir} denote the contributions of the direct term to the sensitivity, as evaluated using the GPT-based module and the DP approach, respectively.

In the physically dominant cases, where both the response and the input parameter refer to the same precursor family (i.e. n=fam), the observed relative discrepancies are small and can be considered negligible. By contrast, in the cases where $n \neq fam$ the relative differences can be significantly larger. For example, the coefficient $S(\hat{\beta}_{\mathrm{eff},1},\nu_{i2}^{\mathrm{d}})$ for isotope ²³⁸U exhibits a relative deviation of

$$\frac{\Delta S^{\text{dir}}}{S_{\text{DP}}^{\text{dir}}} \approx 1.3766 \tag{162}$$

between the two methods. Nevertheless, these large discrepancies do not have physical relevance, as they correspond to absolute sensitivity values no greater than $\mathcal{O}(10^{-3})$.

Shifting the focus to the indirect component of the sensitivity coefficients (see Table 7), additional considerations arise concerning the outcome of the numerical verification. In particular, beyond the large relative discrepancies observed between the values computed using the two types of approach (GPT-based and DP-based) there are indications of potential issues in the code sections responsible for evaluating the indirect sensitivity term of the delayed neutron fraction with respect to the average number of delayed neutrons emitted per fission event, denoted as $S^{\rm ind}(\hat{\beta}_{\rm eff,fam}, \nu_{\rm in}^{\rm d})$.

Table 7: Indirect contributions to the sensitivity of the delayed neutron fraction associated with a given precursor family, $\hat{\beta}_{\rm eff,fam}$, with respect to the average number of delayed neutrons emitted per fission event for a given isotope i and precursor family n ($\nu_{\rm in}^{\rm d}$), represented by the coefficients $S^{\rm ind}(\hat{\beta}_{\rm eff,fam},\nu_{\rm in}^{\rm d})$. Results are obtained using the newly implemented ERANOS sensitivity modules, based on either the GPT framework (leading to the coefficients $S^{\rm ind}_{\rm GPT}(\hat{\beta}_{\rm eff,fam},\nu_{\rm in}^{\rm d}))$ or direct perturbation techniques ($S^{\rm ind}_{\rm DP}(\hat{\beta}_{\rm eff,fam},\nu_{\rm in}^{\rm d})$), and applied to the simplified reactor model described in Section 5.2.1 (the Toy Model). The last column reports the relative discrepancies between the two methods, where the quantity $\Delta S^{\rm ind} = S^{\rm ind}_{\rm GPT} - S^{\rm ind}_{\rm DP}$ has been introduced.

Ехеси	ıtive Variab	les	$S_{\mathrm{GPT}}^{\mathrm{ind}}(\hat{eta}_{\mathrm{eff,fam}}, u_{\mathrm{in}}^{\mathrm{d}})$	$S_{\mathrm{DP}}^{\mathrm{ind}}(\hat{eta}_{\mathrm{eff,fam}}, u_{\mathrm{in}}^{\mathrm{d}})$	$\Delta S^{ m ind}/S^{ m ind}_{ m DP}$
i _ 23511	$i = {}^{235}\mathrm{U}$	n=1	-1.2015×10^{-6}	5.7313×10^{-6}	-1.2096×10^{0}
fam = 1		n=2	-6.7652×10^{-6}	2.1256×10^{-5}	-1.3183×10^{0}
$i = {}^{238}\mathrm{U}$	n=1	-3.2507×10^{-6}	-1.4833×10^{-6}	1.1916×10^{0}	
		n=2	-4.0694×10^{-5}	-3.1806×10^{-5}	2.7945×10^{-1}
	$i = {}^{235}$ U	n = 1	5.5531×10^{-6}	-1.1914×10^{-6}	-5.6610×10^{0}
$\int_{-\infty}^{\infty} \int_{-\infty}^{\infty} \int_{-\infty}^{\infty$		n=2	2.6353×10^{-5}	-4.1704×10^{-6}	-7.3190×10^{0}
	$i = {}^{238}U$	n=1	1.1580×10^{-6}	1.8701×10^{-7}	5.1924×10^{0}
		n=2	1.4904×10^{-5}	5.9368×10^{-6}	1.5104×10^{0}

This hypothesis is supported by the inconsistent sign pattern exhibited by the indirect contributions when comparing the results from the GPT- and DP-based results. In the GPT-based implementation, the sign of the indirect term appears to depend primarily on the response index fam, with no clear isotope dependence. Conversely, the DP results suggest a systematic behavior: the indirect contribution is positive for isotope ²³⁵U and negative for ²³⁸U when the response parameter $\hat{\beta}_{\rm eff,fam}$ is evaluated for the first precursor family (fam=1), and this trend reversing for the second family (fam=2).

Despite these inconsistencies, the physical impact of the indirect term is limited. In fact, in most cases its contribution is negligible compared to the overall sensitivity – defined as the sum of the direct and indirect components of the coefficient $S(\hat{\beta}_{\rm eff,fam}, \nu_{\rm in}^{\rm d})$. The maximum contribution of the indirect term does not exceed approximately 6.2% of the total sensitivity, observed in the specific case fam=1, $i=\frac{238}{4}$ U, n=2.

The limited significance of the discrepancies observed so far – whether in the direct or indirect components of the sensitivity of the family-wise delayed neutron fraction $\hat{\beta}_{\rm eff,fam}$ with respect to the average number of delayed neutrons emitted per fission event $\nu^{\rm d}$ – becomes even more evident when analyzing the total delayed neutron fraction sensitivity. In particular, the coefficients $S(\hat{\beta}_{\rm eff},\nu^{\rm d}_{\rm in})$, which refer to the global

quantity $\hat{\beta}_{\text{eff}}$, are reported in Table 8.

Table 8: Sensitivity of the total delayed neutron fraction, $\hat{\beta}_{\rm eff}$, with respect to the average number of delayed neutrons emitted per fission event for a given isotope i and precursor family n, i.e. $\nu_{\rm in}^{\rm d}$, represented by the coefficients $S(\hat{\beta}_{\rm eff}, \nu_{\rm in}^{\rm d})$. Results are obtained using the newly implemented ERANOS sensitivity modules, based on either the GPT framework (leading to the coefficients $S_{\rm GPT}(\hat{\beta}_{\rm eff}, \nu_{\rm in}^{\rm d})$) or direct perturbation techniques ($S_{\rm DP}(\hat{\beta}_{\rm eff}, \nu_{\rm in}^{\rm d})$), and applied to the simplified reactor model described in Section 5.2.1 (the Toy Model). DP results serve as reference values for the numerical verification of the GPT-based implementation. The last column reports the relative discrepancies between the two methods, where the quantity $\Delta S = S_{\rm GPT} - S_{\rm DP}$ has been introduced.

Executive Variables		$S_{\mathrm{GPT}}(\hat{\beta}_{\mathrm{eff}}, \nu_{\mathrm{in}}^{\mathrm{d}})$	$S_{\mathrm{DP}}(\hat{eta}_{\mathrm{eff}}, u_{\mathrm{in}}^{\mathrm{d}})$	$\Delta S/S_{ m DP}$
$i = {}^{235}\mathrm{U}$	n=1	1.4305×10^{-1}	1.4299×10^{-1}	4.1841×10^{-4}
	n=2	6.4297×10^{-1}	6.4353×10^{-1}	-8.6899×10^{-4}
$i = {}^{238}\mathrm{U}$	n=1	1.5560×10^{-2}	1.5566×10^{-2}	-3.4682×10^{-4}
	n=2	1.9627×10^{-1}	1.9659×10^{-1}	-1.6276×10^{-3}

The sensitivity coefficients reported in Table 8 are derived using the expression shown in Equation 38, which, when applied to the specific case of the parameter $\nu^{\rm d}$, takes the form:

$$S(\hat{\beta}_{\text{eff}}, \nu_{\text{in}}^{\text{d}}) = \sum_{\text{fam}} \frac{\hat{\beta}_{\text{eff,fam}}}{\hat{\beta}_{\text{eff}}} S(\hat{\beta}_{\text{eff,fam}}, \nu_{\text{in}}^{\text{d}}).$$
 (163)

The results show that the overall sensitivity – i.e. namely that of the total delayed neutron fraction, which represents the primary response parameter of interest in this sensitivity analysis – confirms the validity of this verification step. The focus on this integral parameters is particularly significant in light of the broader objective of this study, which is to identify the design features required to optimize the safety margins required for the licensing of the ALFRED reactor.

None of the coefficients $S(\hat{\beta}_{\mathrm{eff}}, \nu_{\mathrm{in}}^{\mathrm{d}})$ obtained with the newly implemented ERANOS modules based on the GPT approach exhibit physically significant discrepancies when compared with the benchmark values computed via the DP techniques. Even in the worst-case scenario, the relative differences remain below 0.2%. This outcome confirms the successful completion of this intermediate stage and preliminary and provides preliminary evidence of the reliability of the GPT-based sensitivity module using ν^{d} as the input parameter, thereby supporting its application in more advanced sensitivity analyses involving increasingly complex core configurations.

6 Conclusions and Perspectives

6.1 Conclusions

The evolution of global energy systems is increasingly shaped by the dual imperative of accommodating rising demand while achieving profound decarbonization. In this context, ensuring a sustainable and secure energy mix is both urgent and complex, particularly amid geopolitical tensions and the continued reliance on fossil fuels. Nuclear energy is therefore positioned to play a strategic role, providing low-emission, dispatchable power that complements variable renewables and enhances system resilience.

However, current nuclear technologies face structural challenges related to sustainability, waste management, and long-term flexibility. Overcoming these limitations requires a fundamental rethinking of reactor design and deployment, as envisioned by Generation IV systems. These advanced reactors aim to enhance fuel utilization, minimize waste production, and provide greater operational flexibility.

Among them, Lead-cooled Fast Reactors (LFRs) are distinguished for their favorable safety features, high thermal efficiency, and compatibility with closed fuel cycles. Their development is actively supported by international collaborations and national programs; in Europe, particularly through ENEA's commitment to the Advanced Lead-cooled Fast Reactor European Demonstrator (ALFRED), conceived as the European reference project for LFR technology.

ALFRED is noteworthy not only for its technological innovation but also for its advanced safety philosophy. As a Generation IV reactor, it is expected not merely to comply with, but to surpass IAEA safety objectives, in accordance with the more ambitious targets set for this class of systems. These includes minimizing core damage risk, ensuring intrinsic reliability, and avoiding off-site emergency measures under extreme conditions. Achieving goals requires robust safety margins across all operational states, including Design Extension Conditions (DECs). To this end, ALFRED adopts the Best Estimate Plus Uncertainty (BEPU) methodology, which explicitly incorporates uncertainties in models, data, and boundary conditions. This provides a more realistic and comprehensive safety evaluation, advancing beyond traditional deterministic analyses and embodying a broader paradigm shift in the design and licensing of advanced reactors.

* * *

The present thesis has been conducted within the framework of neutronic design activities for the ALFRED reactor, at the Laboratory for Design and Analysis of Nuclear Systems of ENEA, in Bologna. The work has primarily focused on extending the capabilities of the ERANOS code system through the development and integration of novel

computational modules for the sensitivity analysis of the effective delayed neutron fraction $\hat{\beta}_{\text{eff}}$, with respect to parameters beyond nuclear cross-sections.

These functionalities are not currently available within the standard ERANOS toolkit and have been developed as an original contribution aimed at advancing the physical understanding of reactor core behavior and improving the precision and accuracy of safety evaluations. In particular, the sensitivity analysis of a key reactor parameters, such as $\hat{\beta}_{\rm eff}$, enables a detailed quantification of its dependence on nuclear data, design parameters, and structural features. This, in turn, enables reactor design optimization by systematically identifying which parameters must be determined with high precision to meet safety margin requirements, and which, due to their limited impact on the integral quantity of interest, allow for more flexible design choices that can reduce overall construction costs.

Moreover, sensitivity analysis constitutes a fundamental prerequisite for rigorous uncertainty quantification, wherein the propagation of input uncertainties to reactor-level integral quantities is systematically evaluated. The resulting insights are essential for the application of BEPU methodologies, and provide a robust foundation for safety assessments and reactor licensing processes conducted by regulatory authorities.

The methodological advancements developed in this work directly support the AL-FRED licensing framework and contribute to its alignment with the safety objectives established for Generation IV nuclear systems.

The approach relies on the application of Generalized Perturbation Theory (GPT) to the integral parameter $\hat{\beta}_{\text{eff}}$, representing the effective delayed neutron fraction. Starting from analytically derived formulations, explicit expressions were found for the sensitivity coefficients $S(\hat{\beta}_{\text{eff,n}},\alpha)$, where the response function corresponds to the delayed neutron fraction associated with a specific precursor family, $\hat{\beta}_{\text{eff,n}}$, and α denotes a generic input parameter.

Specifically, the analysis considered the average number of prompt ($\nu^{\rm p}$) and delayed ($\nu^{\rm d}$) neutrons emitted per fission, as well as the prompt ($\chi^{\rm p}$) and delayed ($\chi^{\rm d}$) neutron emission spectra.

The theoretical formulations for the sensitivity coefficients $S(\hat{\beta}_{\text{eff}}, \alpha)$ (Equation 37) were consequently developed for each of the selected nuclear parameters. Particular care was taken to recast each expression in a form that would enable the most effective exploitation of the computational functionalities embedded within ERANOS.

These functionalities are acknowledged for their established reliability, being derived from extensively validated computational codes that have undergone rigorous numerical verification and physical benchmarking procedures.

Following the analytical formulation developed in this work, the corresponding sensitivity expressions were systematically implemented within the ERANOS code suite. The new coefficients were therefore derived exclusively by leveraging functionalities already embedded in ERANOS, either through direct use of the relevant computational

modules, where applicable, or through their integration into custom procedures developed in LU, the proprietary programming language of the ERANOS system.

In this way, no external or ad-hoc formulations were introduced, thereby preserving consistency – at least in the first instance – with the validated framework of the code. The resulting computational strategy enables the evaluation of all four categories of sensitivity coefficients addressed in this study, each associated with a specific input parameter. While this approach was designed to remain fully integrated within the existing ERANOS infrastructure, dedicated verification and validation efforts remain necessary to rigorously assess the accuracy and reliability of the implemented methods. In particular, verification ensures that the developed algorithms correctly reproduce the underlying mathematical and numerical models, whereas validation is required to confirm that the results are consistent with experimental data or with trusted reference benchmarks.

The verification strategy adopted in this work follows a progressive approach, starting from a minimal configuration and incrementally increasing the level of complexity – ultimately targeting the ALFRED model developed for S/U analysis. This progressive strategy serves a dual purpose: it avoids the computational burden of full-core simulations in the early stages and facilitates the debugging process by allowing easier localization of potential implementation issues.

The initial verification phase employed a minimal setup comprising a single isotope, one precursor family, a single energy group (i.e., no energy resolution), and an infinitely extended homogeneous volume represented by a cylindrical geometry. All sensitivity coefficients developed in this work were successfully verified against analytical reference values, which are available only for such highly simplified model configurations.

The progressive verification approach was subsequently extended through a systematic exploration of increasing levels of multiplicity in the configurational variables, with the aim of achieving a plurality of variable states. This process culminated in the first intermediate configuration that enabled comprehensive path coverage of the code. The configuration was based on a simplified core representation (Toy Model) with finite cylindrical geometry, subdivided into two concentric cylindrical regions with distinct fuel compositions. Such geometry reflects the structure adopted in the ERANOS model of ALFRED, which employs a cylindrically symmetric representation to ensure compatibility with the specific requirements of the ERANOS computational modules used for sensitivity and uncertainty analyses.

For this setup, which included two different isotopes (235 U and 238 U), two precursor families, and an energy domain discretized into six groups, the verification process focused primarily on the sensitivity of the delayed neutron fraction per family with respect to the average number of delayed neutrons emitted per fission event, i.e., $S(\hat{\beta}_{\text{eff.n}}, \nu^{\text{d}})$.

Accordingly, this particular sensitivity coefficient was prioritized for two main rea-

sons:

- $\bullet\,$ The parameter $\nu_{\rm in}^{\rm d}$ is known a priori from nuclear data libraries;
- $\nu_{\rm in}^{\rm d}$ is not subject to constraints that would otherwise complicate the implementation of the sensitivity modules, thereby avoiding the need for additional development and verification efforts.

The verification process consisted in evaluating the direct, $S^{\rm dir}(\hat{\beta}_{\rm eff,n},\nu^{\rm d})$, the indirect, $S^{\rm ind}(\hat{\beta}_{\rm eff,n},\nu^{\rm d})$, and the total, $S(\hat{\beta}_{\rm eff},\nu^{\rm d})$, sensitivity coefficients. In each case, the results were benchmarked against reference values obtained with dedicated ERANOS modules developed within the framework of this work, which implement the Direct Perturbation (DP) approach. The DP method is based on the explicit calculation of the effect induced by a small (1%) perturbation of the input parameter. Thanks to its conceptual simplicity and numerical robustness, it enables the evaluation of both direct and indirect contributions, thus providing a reliable reference standard for verification.

The results show that the direct sensitivity components computed using the GPT and DP approaches do not exhibit any physically significant discrepancies, despite relative deviations spanning up to five orders of magnitude:

$$\frac{S_{\text{GPT}}^{\text{dir}}(\hat{\beta}_{\text{eff,fam}}, \nu_{\text{in}}^{\text{d}}) - S_{\text{DP}}^{\text{dir}}(\hat{\beta}_{\text{eff,fam}}, \nu_{\text{in}}^{\text{d}})}{S_{\text{DP}}^{\text{dir}}(\hat{\beta}_{\text{eff,fam}}, \nu_{\text{in}}^{\text{d}})} \in [10^{-5}, 10^{0}].$$
(164)

The largest deviations are associated with sensitivity coefficients of limited physical significance, specifically those involving a response and input belonging to different precursor families. For a given isotope i and response family index fam, the following relation holds:

$$\frac{S^{\text{dir}}(\hat{\beta}_{\text{eff,fam}}, \nu_{\text{i,n}}^{\text{d}})}{S^{\text{dir}}(\hat{\beta}_{\text{eff,fam}}, \nu_{\text{i,fam}}^{\text{d}})} = \mathcal{O}(10^{-2}),$$
(165)

indicating that contributions with $n \neq fam$, which correspond to the largest discrepancies, are of negligible relevance within the context of the direct sensitivity analysis.

In such cases, a small negative sensitivity is observed, reaching a maximum value of $S_{\mathrm{GPT}}^{\mathrm{dir}}(\hat{\beta}_{\mathrm{eff,fam}}, \nu_{\mathrm{in}}^{\mathrm{d}}) = -1.3222 \times 10^{-3}$ in the Toy Model. This behavior is consistent with expectations: increasing the number of delayed neutrons emitted by family n slightly reduces the relative contribution of the analyzed family fam to the effective delayed neutron fraction.

Further evidence of physical consistency is provided by the fact that, whenever the input $\nu^{\rm d}$ and the response refer to the same family, the sensitivity remains positive – as expected, since an increase in delayed neutron emission from a given family increases the corresponding delayed neutron fraction.

Conversely, the investigation of the indirect sensitivity component revealed substantial discrepancies between GPT- and DP-based results. In some cases, relative deviations exceeded a factor of seven, largely due to the very small magnitude of the reference values. Notably, the sign behavior of $S^{\rm ind}(\hat{\beta}_{\rm eff,fam},\nu_{\rm in}^{\rm d})$ differed between methods: the GPT implementation showed dependence primarily on the response index fam, whereas the DP method exhibited a more systematic trend involving both isotope and precursor family. These inconsistencies point to possible inaccuracies or limitations in the current implementation of the indirect term.

The physical impact of these discrepancies is, however, marginal. Even in the most extreme case ($S^{\rm ind}_{\rm GPT}(\hat{\beta}_{\rm eff,1}, \nu^{\rm d}_{^{238}{\rm U},2}) = -4.0694 \times 10^{-5}$), the indirect contribution represents $\sim 6.2\%$ of the total sensitivity – defined as the sum of direct and indirect terms – thus preserving the overall reliability of the sensitivity analysis.

This limited significance becomes even more evident when analyzing the total sensitivity of $\hat{\beta}_{\rm eff}$ with respect to $\nu^{\rm d}$. The coefficients $S(\hat{\beta}_{\rm eff}, \nu^{\rm d}_{\rm in})$, obtained with the newly developed GPT-based modules and benchmarked against DP results, show strong agreement for all isotopes and precursor families considered.

The computed relative deviations remain below approximately 0.16%, thereby confirming the numerical accuracy and stability of the GPT implementation within the scope of this verification study. This outcome is particularly relevant, as $\hat{\beta}_{\rm eff}$ is the primary response quantity in this work and a key parameter in reactor safety analyses. The strong consistency observed between the two perturbative approaches reinforces confidence in the developed GPT-based framework and provides a robust foundation for its extension to advanced sensitivity studies in realistic and complex reactor models. In turn, this contributes directly to the overarching objective of supporting safety-oriented design optimization for the ALFRED reactor.

With regard to the sensitivity coefficients associated with the other nuclear input parameters considered in this work – namely, the average number of prompt neutrons emitted per fission event (ν^p) , the delayed neutron spectrum (χ^d) , and the prompt component of the fission spectrum (χ^p) – the corresponding modules have been successfully implemented and verified within a simplified model configuration. Ongoing activities are focused on extending this verification to more representative core models, as part of a broader refinement and consolidation process aimed at increasing the overall maturity and applicability of the developed tools.

6.2 Perspectives

This study presents the development and implementation of novel ERANOS modules for evaluating sensitivity coefficients of the delayed neutron fraction $\hat{\beta}_{\rm eff}$ with respect to input parameters beyond cross-sections. In particular, the focus is placed on the average number of delayed ($\nu^{\rm d}$) and prompt ($\nu^{\rm p}$) neutrons emitted per fission event, as well as on the delayed ($\chi^{\rm d}$) and prompt ($\chi^{\rm p}$) emission spectra.

The objective has been substantially achieved through the development of a robust theoretical framework and the implementation of a reliable benchmarking strategy based on simplified models. However, further verification steps are necessary to ensure that the methodology yields accurate and consistent results when extended to more complex geometries.

The most significant progress achieved thus far concerns the development of the module for computing the sensitivity coefficient $S(\hat{\beta}_{\text{eff}}, \nu^{\text{d}})$, for which two immediate lines of advancement are envisaged:

- benchmarking in full-core configurations, by applying the ALFRED core model already developed for S/U analysis;
- debugging and refinement of the indirect sensitivity term $S^{\mathrm{ind}}(\hat{\beta}_{\mathrm{eff}}, \nu^{\mathrm{d}})$, to be performed in controlled computational environments such as the Toy Model or other reduced-complexity setups so as to ensure stability and correctness prior to full-core application.

In the first case, a preliminary numerical verification at the full-core level remains both meaningful and justified, since the inconsistencies observed in the indirect contribution (initially highlighted in the Toy Model analysis) were shown to be physically negligible. This next verification level is therefore expected to support the robustness of the implemented computational framework, and to further reinforce the conclusion that such discrepancies have no substantial impact on the overall verification process.

In the second case, efforts will be directed toward revising and refining the routines responsible for the indirect sensitivity calculation. This refinement is motivated by the identification of specific numerical inconsistencies that, although limited in scope, may affect the accuracy of the total sensitivity estimation.

It is important to emphasize that the numerical inconsistencies highlighted in this work should not be mistaken for the intrinsic approximations associated with the perturbative methods employed. In fact, within the framework of the variational GPT, such approximations naturally stem from the first-order character of the formulation, whereas the DP method remains exact by construction. The discrepancies discussed here could be of a different nature. Rather than reflecting a theoretical limitation, they were identified during the verification phase and could plausibly be attributed to artifacts introduced by the computational implementation.

More specifically, these inconsistencies are considered potentially detrimental because they may originate from inaccuracies within certain algorithmic routines developed in the course of this work. In particular, their source could lie in the handling and processing of data matrices extracted from the Evaluated Data Libraries (EDLs) by the newly implemented ERANOS modules for sensitivity evaluation. This distinction is of particular importance: while theoretical approximations are expected and quantifiable,

the numerical issues identified here are unintended and therefore call for targeted debugging and refinement to ensure both the stability and the accuracy of the sensitivity estimates.

Addressing these issues forms an integral part of the consolidation of the computational framework and is essential to ensure the robustness and reliability of the overall sensitivity analysis methodology.

With regard to the other sensitivity coefficients of the delayed neutron fraction $\hat{\beta}_{\rm eff}$ considered in this work, the next phase will focus on the refinement and correction of the corresponding code sections. The goal is to obtain satisfactory results in intermediate-level verifications, particularly within executable configurations based on the Toy Model.

Once one of the newly developed GPT-based ERANOS modules attains sufficient numerical maturity to be regarded as verified in configurations representative of the ALFRED core, subsequent efforts will be directed toward a structured, multi-level validation strategy. Since sensitivities with respect to the parameters under consideration are not directly measurable, physical validation against experimental data is not immediately feasible. Nevertheless, the availability of existing ERANOS modules – whose correctness has already been established – provides a solid reference for ensuring the internal consistency and credibility of the newly developed formulations. The validation process can also be extended to include cross-code benchmarking against results obtained from other reference codes, such as SERPENT [62] or MCNP [54], operated in direct perturbation mode. Although these comparisons cannot be considered equivalent to full experimental validation, they offer an important numerical verification: the agreement between independently developed implementations not only increases confidence in the obtained results, but also helps to reveal potential code-specific inconsistencies.

An additional line of development concerns the metrological evaluation of the methodology through uncertainty propagation. The sensitivities computed using the new GPT-based modules can be combined with nuclear data covariances from evaluated libraries to estimate the overall uncertainty in $\hat{\beta}_{\text{eff}}$. Comparison with analogous studies available in literature would serve as an indirect form of validation, allowing both the plausibility of the calculated uncertainty magnitudes and the ability of the newly developed modules to properly quantify and assess safety margins in reactor simulations to be verified.

On a broader scale, once the four ERANOS modules developed in this have been fully verified and subjected to the multi-level validation strategy described above, a comprehensive sensitivity analysis of the delayed neutron fraction will become feasible. This, in turn, will enable a robust uncertainty analysis with respect to $\hat{\beta}_{\rm eff}$, a parameter of fundamental importance for the core design of ALFRED. Carrying out such an analysis will provide essential insights into the design criteria necessary to comply with regulatory requirements, thereby supporting the licensing process by the competent

nuclear safety authorities.

Acknowledgements

I would like to express my sincere gratitude to Donato Maurizio Castelluccio and Matteo Stanzani for their continuous support and guidance throughout the development of this work. Their technical insights and unwavering availability have been fundamental in deepening my understanding and shaping the outcome of this study.

I am also thankful to Professor Paolo Finelli for offering me the opportunity to carry out this thesis project and for his trust in my work.

A Neutron Flux Evaluation with the Discrete Ordinates Method: The BISTRO Solver

The flux calculations involved in this work are performed using the BISTRO code, which solves the neutron transport equation in its integro-differential form (see Equation 2), both in one-dimensional and two-dimensional configurations, by means of the discrete ordinates method. It is therefore necessary to provide a conceptual overview of what is meant by this method. To this end, a set of simplifying assumptions will be adopted to facilitate the discussion (for a complete exposition of BISTRO, refer to its manual [63]).

Accordingly, the Boltzmann transport equation is here considered under the following set of assumptions:

- steady-state,
- monoenergetic,
- one-dimensional,
- related to an isotropic medium (i.e. with isotropic scattering and fission source).

The $S_{\rm N}$ method allows the Boltzmann equation to be solved by discretizing the angular variable into a finite number N of directions. The equation to be addressed, subject to the assumptions stated above, is as follows:

$$\mu \frac{\partial \phi(x,\mu)}{\partial x} + \Sigma_{\rm t}(x)\phi(x,\mu) = \frac{1}{2} \left(\Sigma_{\rm s}(x) + \frac{\nu \Sigma_{\rm f}(x)}{k_{\rm eff}} \right) \int_{-1}^{+1} d\mu' \, \phi(x,\mu') + S_{\rm ext} \,, \quad (166)$$

where the variable $\mu = \cos \theta$ has been introduced, with θ being the polar angle of the neutron flight direction in the laboratory reference frame.

The discretization of the flight directions into N elements leads to the definition of a corresponding set of constants μ_n and weighting coefficients w_n (with $n=1\dots N$). The purpose of these weights is to approximate the integral in Equation 166 using the quadrature formula:

$$\int_{-1}^{+1} d\mu' \, \phi(x, \mu') \approx \sum_{n=1}^{N} w_n \phi(x, \mu_n) \,. \tag{167}$$

As a result of the discretization process, the original equation involving two continuous variables (x, μ) is transformed into a set of N equations in a single variable (x),

each characterized by a constant μ_n :

$$\mu_{j} \frac{\partial \phi(x, \mu_{j})}{\partial x} + \Sigma_{t}(x)\phi(x, \mu_{j}) =$$

$$= \frac{1}{2} \left(\Sigma_{s}(x) + \frac{\nu \Sigma_{f}(x)}{k_{eff}} \right) \sum_{n=1}^{N} w_{n}\phi(x, \mu_{n}) + S_{ext}(x, \mu_{j}),$$
(168)

with $j=1\dots N$. It is worth noting that the number N of discrete directions is typically chosen to be even. By indexing the directions such that $n=1\dots N/2$ and $\mu_n>0$, the following symmetry relations can be expressed [64]:

$$\begin{cases} \mu_{\rm N+1-n} = -\mu_{\rm n} \\ w_{\rm N+1-n} = w_{\rm n} \end{cases} \tag{169}$$

provided that the flight directions μ_n are symmetric with respect to $\mu=0$, i.e. the direction defined by the vertical axis. This choice is motivated by the physical notion that neutrons arriving from symmetric radial directions carry equal importance. Furthermore, restricting the discretization to an even number of elements avoids the possibility of having a $\mu_n=0$, which would nullify the flux derivative appearing as the first term in Equation 168.

Despite these constraints, there remains considerable freedom in the selection of admissible directions. A commonly adopted choice is the Wick–Chandrasekhar scheme [65], in which the values of $\mu_{\rm m}$ are taken as the M zeros of the Legendre polynomial of order M:

$$P_{\rm M}(\mu_{\rm m}) = 0 \,, \quad m = 1 \dots M \,.$$
 (170)

This approach offers a significant advantage for computing the integral term in Equation 168, as Legendre polynomials are symmetric with respect to zero and can be integrated exactly up to a certain order.

Based on the above considerations, the boundary condition for the flux in a one-dimensional planar slab, defined over the domain $x \in [0,a]$ and enclosed by a vacuum, is formulated as follows:

$$\phi(0, \mu_{\rm j}) = \phi(a, -\mu_{\rm j}) = 0$$
 with $j = 1 \dots \frac{N}{2}$. (171)

Before proceeding with the solution of the system represented by Equations 168, it is convenient to group the right-hand side terms into a single parameter, specifically:

$$Q(x, \mu_{\rm j}) = \frac{1}{2} \left(\Sigma_{\rm s}(x) + \frac{\nu \Sigma_{\rm f}(x)}{k_{\rm eff}} \right) \sum_{\rm n=1}^{N} w_{\rm n} \phi(x, \mu_{\rm n}) + S_{\rm ext}(x, \mu_{\rm j}) \,. \tag{172}$$

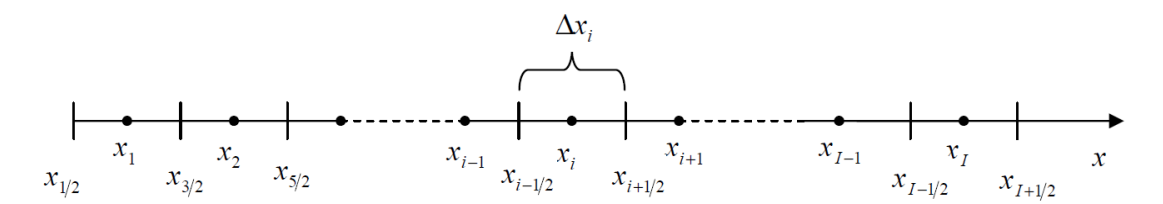


Figure 12: Spatial discretization for the discrete ordinates method in the one-dimensional case

The next step consists in performing the spatial discretization of the slab, which involves dividing it into I intervals (as shown in Figure 12), within each of which the material properties are assumed to be constant. As a consequence, each of the N equations from the system introduced in Equation 168 is further expanded into a system of I equations, whose unknowns correspond to the flux values $\phi(x_i, \mu_j)$, with $i=1\ldots I$, evaluated at the center of each spatial interval. The resulting global system can be compactly written as:

$$\mu_{\rm j} \frac{\phi_{\rm i+\frac{1}{2},j}-\phi_{\rm i-\frac{1}{2},j}}{\Delta x_{\rm i}} + \Sigma_{\rm t,i} \phi_{\rm ij} = Q_{\rm i,j} \,, \quad \text{with} \quad j=1\dots N \quad \text{and} \quad i=1\dots I \,, \quad \text{(173)}$$

where the discrete variables $\Delta x_i = x_{i+1/2} - x_{i-1/2}$ represent the width of each spatial interval, and a compact notation has been adopted such that $(i, j) = (x_i, \mu_i)$.

It should be noted, however, that the choice to approximate the derivative using a finite difference introduces into the equation flux values evaluated at the spatial mesh nodes. Therefore, additional information is required in order to proceed with the computation. One such piece of information is provided either by the solution at an adjacent node (which is assumed to have already been computed) or by a boundary condition, which typically supplies the flux value at one of the domain boundaries.

Elimination of the remaining unknown is achieved through application of the Diamond Difference scheme [66]. This rule assumes that the flux evaluated at the center of each spatial interval can be expressed as the arithmetic mean of the fluxes at the two interfaces:

$$\phi_{ij} = \frac{\phi_{i+\frac{1}{2},j} - \phi_{i-\frac{1}{2},j}}{2}.$$
 (174)

The solution algorithm applies the Diamond Difference differently depending on whether the equation corresponds to a discrete flight direction with $\mu_{\rm j}>0$ or $\mu_{\rm j}<0$. Specifically:

 $\mu_{
m j}>0$: The computation proceeds sequentially from left to right, that is, calculating the flux for increasing values of x, starting from the value of $\phi_{\frac{1}{2},{
m j}}$, which is assumed to be known from a specified boundary condition. The terms of the Diamond Rule are rearranged to express the interface flux as:

$$\phi_{i+\frac{1}{2},j} = 2\phi_{ij} - \phi_{i-\frac{1}{2},j}, \qquad (175)$$

which, when substituted into Equation 173, allows to compute the cell-centered flux value:

$$\phi_{ij} = \frac{\phi_{i-\frac{1}{2},j} + \frac{\Delta x_i}{2\mu_j} Q_{ij}}{1 + \frac{\Delta x_i}{2\mu_i} \Sigma_{t,i}}.$$
 (176)

Once this value is obtained, $\phi_{i+\frac{1}{2},j}$ can be evaluated using Equation 175, which in turn becomes the starting point for computing the flux in the next interval.

 $\mu_{\rm j} < 0$: The procedure mirrors the steps of the previous case, with the difference that the flux propagation (as well as the neutron direction, since $\mu_{\rm j} = \cos\theta_{\rm j} < 0$ in contrast to the previous case) proceeds from right to left. In this case, the equation used to compute the flux at the center of the interval is:

$$\phi_{i-\frac{1}{2},j} = 2\phi_{ij} - \phi_{i+\frac{1}{2},j}, \qquad (177)$$

which leads to the following relation:

$$\phi_{ij} = \frac{\frac{\Delta x_i}{2\mu_j} Q_{ij} - \phi_{i+\frac{1}{2},j}}{\frac{\Delta x_i}{2\mu_j} \Sigma_{t,i} - 1}.$$
 (178)

As in the previous scenario, once the central flux value is obtained, it is used to compute the flux at the adjacent node, which serves as the basis for the subsequent calculation.

Although the discussion so far has focused solely on forward fluxes, it is worth noting that BISTRO is also capable of solving the adjoint transport equation in the pseudo-steady-state regime (see Equation 7), thereby yielding the neutronic importance function ϕ^{\dagger} as a solution.

B ERANOS Implementation of the ALFRED Core for Sensitivity and Uncertainty Studies

The ALFRED reactor core is originally modeled with a three-dimensional hexagonal geometry, reflecting its real physical configuration characterized by a high degree of spatial symmetry. This hexagonal lattice structure is fundamental in accurately representing the arrangement of fuel assemblies and other core components.

However, to carry out S/U analyses using the ERANOS computational suite, it is necessary to adopt a two-dimensional cylindrical (RZ) representation of the reactor core. This requirement arises from the fact that the ERANOS modules dedicated to sensitivity evaluation rely on neutron flux distributions computed through finite difference methods, specifically those implemented in the BISTRO code (refer to Appendix A for further details). Since BISTRO does not support calculations on hexagonal geometries, the original three-dimensional hexagonal core model must be reformulated in RZ geometry to ensure compatibility with the employed numerical solvers.

The process begins with the definition of each hexagonal element – corresponding to a single assembly – as shown in the radial core map in Figure 4. Each assembly is further characterized axially according to its type (e.g., Inner Fuel, Outer Fuel, Control Rods), as illustrated in Figure 13. This step provides a full spatial discretization of the core, allowing differentiation of regions within each assembly that exhibit distinct neutronic properties.

Building upon this detailed 3D description, the "cylindrization" process is applied to convert the hexagonal lattice into a set of concentric cylindrical zones (Figure 14). This transformation involves subdividing the core volume into annular regions whose volumes are preserved exactly, thereby ensuring consistency in the representation of material and neutronic characteristics. The main degree of freedom remaining after volume preservation is the selection of the radii defining the interfaces between fuel zones, control rods, and safety devices.

The optimal placement of these cylindrical interfaces is chosen to maintain neutron flux profiles – both direct and adjoint – as close as possible to those of the original three-dimensional model [37]. This approach ensures that the cylindrical model accurately reproduces the core's neutronic behavior despite its geometric simplification.

The final cylindrical representation of the ALFRED core consists of 25 homogenized cylindrical zones. These zones, processed using the ECCO module (see Section 3.3), collectively represent the active core regions and surrounding structures in the simplified two-dimensional geometry used for the S/U analyses.

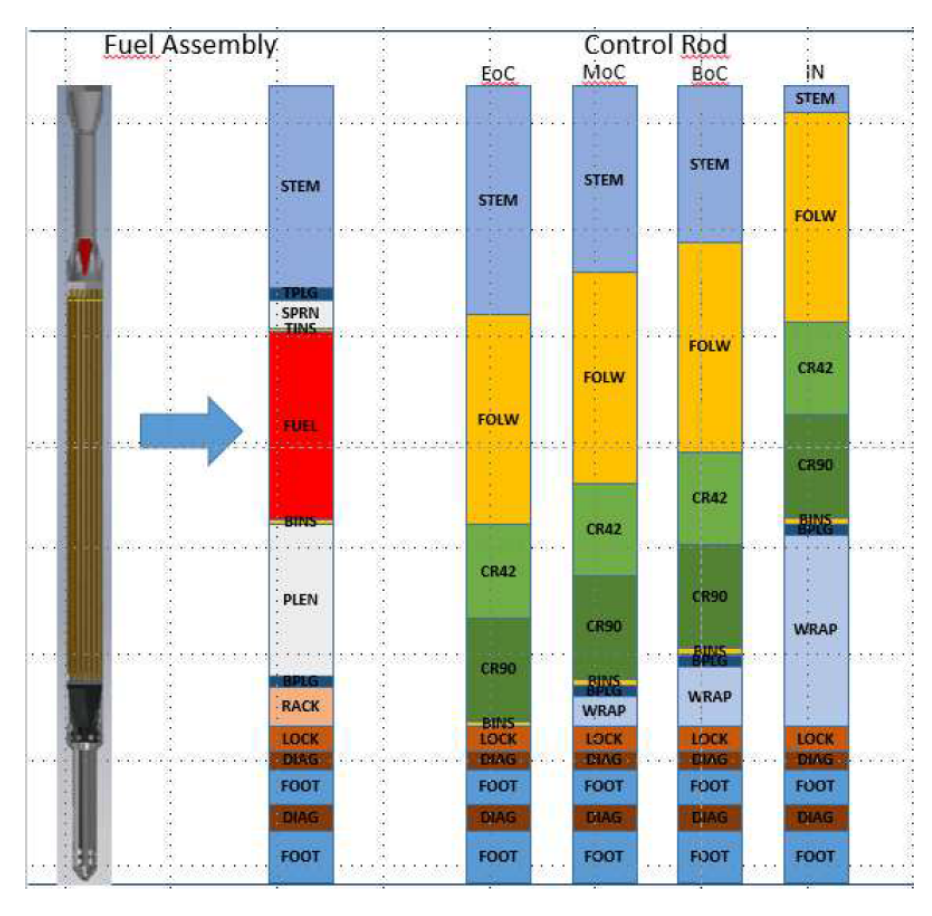


Figure 13: Schematic representation of the axial characterization process. The left side of the figure illustrates the conceptual transition from the physical fuel assembly to its computational representation, in which regions exhibiting distinct neutronic behavior are homogenized for simulation purposes. The right side highlights the necessity for multiple axial characterizations of a single assembly type – in this case, control rod assemblies – in order to accurately represent their varying configurations throughout the reactor operating cycle, including Beginning of Cycle (BoC), Middle of Cycle (MoC), End of Cycle (EoC), and fully inserted (IN) states. [37]

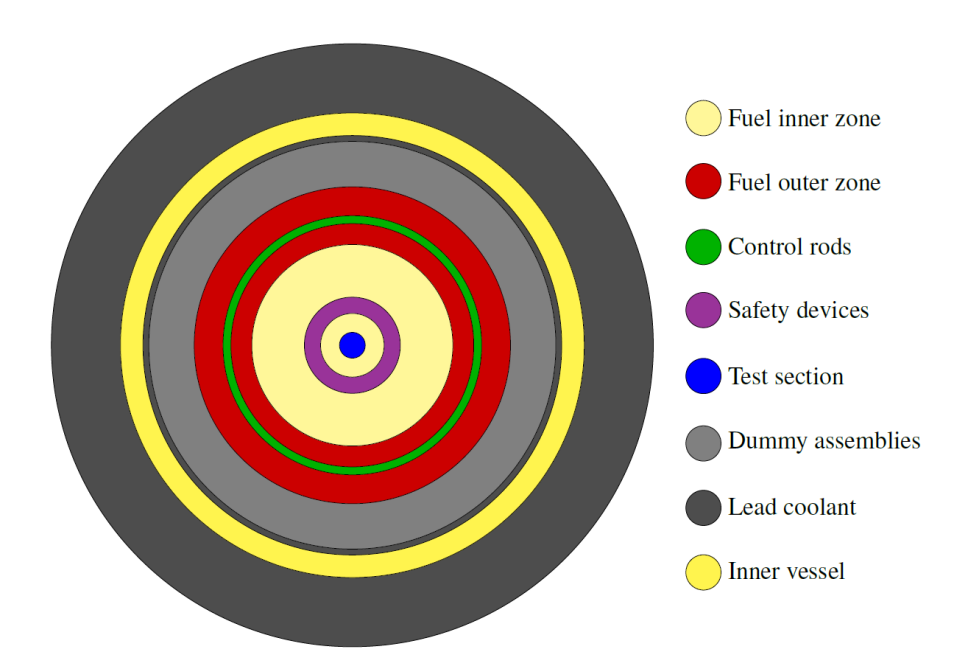


Figure 14: Cylindrized representation of the ALFRED core. The volume of each zone is preserved, and the placement of the annular interfaces reflects the average distance between the absorber devices and the axis passing through the reactor center. [37]

References

- [1] OECD. Environment at a Glance Indicators. OECD Publishing, Paris, 2025. Accessed on July 25, 2025.
- [2] International Energy Agency (IEA). Global energy review 2025, 2025. Licence: CC BY 4.0.
- [3] International Energy Agency (IEA). World energy outlook 2024, 2024. Licence: CC BY 4.0 (report); CC BY-NC-SA 4.0 (Annex A).
- [4] United Nations Framework Convention on Climate Change (UNFCCC). Paris agreement. Adopted in Paris on 12 December 2015. Depositary: United Nations Secretary-General. Official publication in: OJ L 282, 19 October 2016, pp. 4–18, 2015. Entered into force on 4 November 2016. No end date specified.
- [5] International Energy Agency (IEA). Global ev outlook 2024; net zero emissions by 2050 scenario. https://www.iea.org/reports/global-ev-outlook-2024, 2024. Accessed: 2025-07-25.
- [6] World Nuclear Association. Outline of nuclear energy history. https://world-nuclear.org/information-library/current-and-future-generation/outline-history-of-nuclear-energy, 2025. Accessed: 2025-07-25.
- [7] International Energy Agency (IEA). Electricity information 2024. https://www.iea.org/reports/electricity-information-2024, 2024. Accessed: 2025-07-25.
- [8] Ember. Global electricity source trends, 2024.
- [9] International Energy Agency. *The Path to a New Era for Nuclear Energy*. International Energy Agency, Paris, 2025.
- [10] International Energy Agency. Nuclear power in a clean energy system, 2019. Accessed: 2025-07-31.
- [11] International Energy Agency (IEA). The path to a new era for nuclear energy status of nuclear energy. https://www.iea.org/reports/the-path-to-a-new-era-for-nuclear-energy/status-of-nuclear-energy, 2024. Accessed: 2025-07-25.

- [12] International Atomic Energy Agency (IAEA). Statement to international conference on chernobyl: Twenty-five years on safety for the future, 2011. Details formation of WANO, IAEA safety standards, and global regulatory frameworks after Chernobyl.
- [13] Nuclear Energy Agency, OECD. Impacts of the fukushima daiichi accident on nuclear development policies, 2017. Presents regulatory reforms and policy shifts in the wake of Fukushima.
- [14] J Portugal-Pereira, P Ferreira, Jorge Cunha, A Szklo, R Schaeffer, and M Araújo. Better late than never, but never late is better: Risk assessment of nuclear power construction projects. *Energy Policy*, 120:158–166, 2018.
- [15] Stanley Dunlap, Georgia Recorder. Plant vogtle delays and ballooning costs since 2012 unveiling like 'groundhog day', 2022.
- [16] Deutsche Welle (DW). Finland's much-delayed olkiluoto-3 nuclear reactor connected to grid after 12 years of delay. https://www.dw.com/en/finlands-much-delayed-nuclear-plant-launches/a-61108015, 2022. Olkiluoto 3 connected to grid in 2022; originally planned for 2009; cost ballooned to €11bn.
- [17] Igor L Pioro and Gilles H Rodriguez. Generation iv international forum (gif). In Handbook of Generation IV Nuclear Reactors, pages 111–132. Elsevier, 2023.
- [18] WooHyun Jung. Gas-cooled fast reactor. In *Nuclear Power Reactor Designs*, pages 245–257. Elsevier, 2024.
- [19] Alessandro Alemberti, Valery Smirnov, Craig F Smith, and Minoru Takahashi. Overview of lead-cooled fast reactor activities. *Progress in Nuclear Energy*, 77:300–307, 2014.
- [20] Jérôme Serp, Michel Allibert, Ondřej Beneš, Sylvie Delpech, Olga Feynberg, Véronique Ghetta, Daniel Heuer, David Holcomb, Victor Ignatiev, Jan Leen Kloosterman, et al. The molten salt reactor (msr) in generation iv: overview and perspectives. Progress in Nuclear Energy, 77:308–319, 2014.
- [21] Pan Wu, Yanhao Ren, Min Feng, Jianqiang Shan, Yanping Huang, and Wen Yang. A review of existing supercritical water reactor concepts, safety analysis codes and safety characteristics. *Progress in Nuclear Energy*, 153:104409, 2022.
- [22] Hiroyuki Ohshima and Shigenobu Kubo. Sodium-cooled fast reactors (sfrs). In Handbook of Generation IV Nuclear Reactors, pages 173–194. Elsevier, 2023.

- [23] Xing L Yan. Very high temperature reactor. In *Handbook of generation IV nuclear reactors*, pages 133–165. Elsevier, 2023.
- [24] Nuclear Engineering International. Reactor defuelling completed at uk wylfa site. https://www.neimagazine.com/news/reactor-defuelling-completed-at-uk-wylfa-site-7421026/, 2021. Defueling enables transition to care and maintenance; decommissioning stages described.
- [25] K. W. Hesketh. Power Reactors. Oxford University Press, 1996.
- [26] Stephen Goldberg and Robert Rosner. Nuclear reactors: Generation to generation. American academy of arts and sciences Cambridge, MA, 2011.
- [27] Giorgio Locatelli, Chris Bingham, and Mauro Mancini. Small modular reactors: A comprehensive overview of their economics and strategic aspects. *Progress in Nuclear Energy*, 73:75–85, 2014.
- [28] Nicholas R Brown. A review of in-pile fuel safety tests of triso fuel forms and future testing opportunities in non-htgr applications. *Journal of Nuclear Materials*, 534:152139, 2020.
- [29] Mariano Tarantino, Massimo Angiolini, Serena Bassini, Sebastiano Cataldo, Chiara Ciantelli, Carlo Cristalli, Alessandro Del Nevo, Ivan Di Piazza, Dario Diamanti, Marica Eboli, et al. Overview on lead-cooled fast reactor design and related technologies development in enea. *Energies*, 14(16):5157, 2021.
- [30] European Commission, Directorate-General for Research, and Innovation. *Euratom Research and Training Programme 2021–2025*. Publications Office of the European Union, 2021.
- [31] D Jaramillo-Sierra, G Grasso, E Dorval, A Magni, A Cammi, and A Del Nevo. Alfred-burner: Core design, safety and performance. *Nuclear Engineering and Design*, 432:113826, 2025.
- [32] Giacomo Grasso, Francesco Lodi, and Donato Maurizio Castelluccio. Advanced nuclear reactors r&d: Enea's activities on core design. Presentation, Department of Physics, University of Bologna, November 2024. Presented on November 26, 2024.
- [33] Alessandro Alemberti. Status of the alfred project. In ESNII Biennial conference, pages 17–19, 2021.

- [34] G. Grasso, M. Sarotto, F. Lodi, and D. M. Castelluccio. An improved design for the alfred core. In *Proceedings of the International Congress on Advances in Nuclear Power Plants (ICAPP 2019)*, pages 12–15, Juan-les-Pins, France, May 2019. Paper ID: 000378.
- [35] World Health Organization et al. Fundamental safety principles. safety fundamentals. 2007.
- [36] M Dusic. Safety margins of operating reactors: Analysis of uncertainties and implications for decision making. International Atomic Energy Agency, 2003.
- [37] Donato M Castelluccio. Assessment of the impact of nuclear data uncertainties on the core design of alfred. 2020.
- [38] Alessandro Alemberti, Marco Caramello, Michele Frignani, Giacomo Grasso, Fabio Merli, Giulia Morresi, and Mariano Tarantino. Alfred reactor coolant system design. Nuclear engineering and design, 370:110884, 2020.
- [39] Ivan A Kodeli. Beta-effective sensitivity and uncertainty analysis of myrrha reactor for possible use in nuclear data validation and improvement. *Annals of Nuclear Energy*, 113:425–435, 2018.
- [40] Donato M Castelluccio, Giacomo Grasso, Francesco Lodi, Vincenzo Giuseppe Peluso, and Alberto Mengoni. Nuclear data target accuracy requirements for advanced reactors: The alfred case. *Annals of Nuclear Energy*, 162:108533, 2021.
- [41] Karolina Kolos, Vladimir Sobes, Ramona Vogt, Catherine E Romano, Michael S Smith, Lee A Bernstein, David A Brown, Mary T Burkey, Yaron Danon, Mohamed A Elsawi, et al. Current nuclear data needs for applications. *Physical Review Research*, 4(2):021001, 2022.
- [42] David A Brown, Mark Benjamin Chadwick, R Capote, AC Kahler, A Trkov, MW Herman, AA Sonzogni, Y Danon, AD Carlson, M Dunn, et al. Endf/b-viii. 0: the 8th major release of the nuclear reaction data library with cielo-project cross sections, new standards and thermal scattering data. *Nuclear Data Sheets*, 148:1–142, 2018.
- [43] A Santamarina, Dea Bernard, P Blaise, M Coste, A Courcelle, TD Huynh, C Jouanne, P Leconte, O Litaize, S Mengelle, et al. The jeff-3.1. 1 nuclear data library. *JEFF report*, 22(10.2):2, 2009.
- [44] E Dupont, MB Chadwick, Y Danon, C De Saint Jean, M Dunn, U Fischer, RA Forrest, T Fukahori, Z Ge, Hiroshi Harada, et al. Working party on international nuclear data evaluation cooperation (wpec). *Nuclear data sheets*, 120:264–267, 2014.

- [45] John Lilley. Nuclear physics: principles and applications. John Wiley & Sons, 2013.
- [46] Enzo De Sanctis, Stefano Monti, and Marco Ripani. Nuclear reactions and fission. In Energy from Nuclear Fission: An Introduction, pages 89–143. Springer, 2016.
- [47] Bahram Houchmandzadeh, Eric Dumonteil, Alain Mazzolo, and Andrea Zoia. Neutron fluctuations: The importance of being delayed. *Physical Review E*, 92(5):052114, 2015.
- [48] J Tommasi. Eranos user's manual-applications of perturbation theory with finite difference diffusion and sn transport flux solvers'. SPRC/LEPh, pages 07-003, 2007.
- [49] Hiroshi Mitani. Higher order perturbation method in reactor calculations. *Nuclear Science and Engineering*, 51(2):180–188, 1973.
- [50] David McMahon and Adam Pierson. A taylor series solution of the reactor point kinetics equations. *arXiv preprint arXiv:1001.4100*, 2010.
- [51] Ramadan M Kuridan. Neutron transport—the variational methods. In *Neutron Transport: Theory, Modeling, and Computations*, pages 203–226. Springer, 2023.
- [52] C De Saint Jean, P Blaise, J Tommasi, and Augusto Gandini. The heuristically-based generalized perturbation theory. *EPJ-Nuclear Sciences & Technologies*, 7, 2021.
- [53] RT Chiang and J Dorning. Diffusion equations as asymptotic approximations to the neutron transport equation. 1977.
- [54] Joel A Kulesza, Terry R Adams, Jerawan Chudoung Armstrong, Simon R Bolding, Forrest B Brown, Jeffrey S Bull, Timothy Patrick Burke, Alexander Rich Clark, Robert Arthur Art Forster III, Jesse Frank Giron, et al. Mcnp® code version 6.3. 0 theory & user manual. Technical report, Los Alamos National Laboratory (LANL), Los Alamos, NM (United States), 2022.
- [55] Gérald Rimpault, Danièle Plisson, Jean Tommasi, Robert Jacqmin, Jean-Marie Rieunier, Denis Verrier, and Didier Biron. The eranos code and data system for fast reactor neutronic analyses. In PHYSOR 2002-International Conference on the New Frontiers of Nuclear Technology: Reactor Physics, Safety and High-Performance Computing, 2002.
- [56] J Ch Sublet, Ch Dean, Daniele Plisson-Rieunier, et al. Eccolib-jeff-3.1 libraries. Technical report, CEA Cadarache, 13-Saint-Paul-lez-Durance (France). Dept. d'Etudes des Reacteurs, 2006.

- [57] Wim Haeck, Nathan Gibson, Patrick Talou, and Colin Josey. The road to a modernized njoy. In EPJ Web of Conferences, volume 302, page 07013. EDP Sciences, 2024.
- [58] Wim Haeck, Andrej Trkov, et al. Nuclear data processing. summary report of the technical meeting. Technical report, International Atomic Energy Agency, International Nuclear Data Committee ..., 2018.
- [59] G Rimpault et al. Physics documentation of eranos: the ecco cell code. CEA Technical Note RT-SPRC-LEPh-97-001, 1997.
- [60] William L Oberkampf and Timothy G Trucano. Verification and validation benchmarks. *Nuclear engineering and Design*, 238(3):716–743, 2008.
- [61] Yasunobu Nagaya, Ivan Kodeli, Go Chiba, and Makoto Ishikawa. Evaluation of sensitivity coefficients of effective multiplication factor with respect to prompt fission neutron spectrum. Nuclear Instruments and Methods in Physics Research Section A: Accelerators, Spectrometers, Detectors and Associated Equipment, 603(3):485-490, 2009.
- [62] Jaakko Leppänen, Ville Valtavirta, Antti Rintala, and Riku Tuominen. Status of serpent monte carlo code in 2024. *EPJ Nuclear Sciences & Technologies*, 11:3, 2025.
- [63] CJ Gho and G Palmiotti. Bistro: Bidimensionnel sn transport optimisé. un programme bidimensionnel de transport sn aux différences finies. *Note*, (1):84, 1984.
- [64] Bruno Montagnini. Lezioni sul trasporto dei neutroni.
- [65] Clarence E Lee. *The discrete Sn approximation to transport theory*, volume 2595. Los Alamos Scientific Laboratory of the University of California, 1962.
- [66] Yingchi Yu, Xin He, Maosong Cheng, and Zhimin Dai. Review of the discrete-ordinates method for particle transport in nuclear energy. *Energies*, 18(11):2880, 2025.